Development and Characterization of Oxyfunctionalized Boron Nitride Catalysts for the Oxidative Dehydrogenation of Light Alkanes to Olefins

By

Theodore Osaremen Agbi

A dissertation submitted in partial fulfillment of
the requirements for the degree of

Doctor of Philosophy
(Chemical Engineering)

at the
University of Wisconsin – Madison
2022

Date of final oral examination: 08/24/2022

This dissertation is approved by the following members of the Final Oral Committee:

Ive Hermans, Professor, Chemical & Biological Engineering, Chemistry
James Dumesic, Professor, Chemical & Biological Engineering
Thatcher Root, Professor, Chemical & Biological Engineering
George Huber, Professor, Chemical & Biological Engineering
Eric Shusta, Professor, Chemical & Biological Engineering, Biomedical Engineering

Abstract

Light olefins like ethylene and propylene are platform chemicals integral to the chemical industry. Production of polymers, oxygenates, and other important chemical intermediates demand global production volumes that top 100 million metric tons per year. Production of these light olefins, traditionally through steam cracking, is one of the most energy intensive processes in petrochemical sector. Changing refinery feedstocks (i.e., increased availability of natural gas) have created both necessity and opportunity for 'On-Purpose' propylene technologies to meet propylene demands. The oxidative dehydrogenation of propane to propylene (ODHP) is an attractive alternative process to produce propylene. ODHP enables lower process temperatures and avoids coke deactivation of the catalyst, and has the potential to significantly ease energy, capital, and material intensities of industrial propylene production. To-date, metal oxide ODHP catalysts like vanadia-based catalysts—the previous state of the art ODHP catalyst—do not achieve competitive propylene yields to make them industrially viable.

The pioneering work of our research group has identified BN—a material renowned for its chemical inertness—as a highly reactive, selective, and stable ODHP catalyst. Since this discovery, we have worked to understand the fundamental reaction mechanisms present and identify structure-performance relationships that may further develop this class of catalyst. To-date, we have developed extensive spectroscopic characterization capabilities to identify the oxyfunctionalized boron layer formed *in situ* which contains highly dynamic active species responsible for the high reactivity and selectivity observed. Understanding the activation of molecular O_2 and functionality of the oxyfunctionalized layer has been a highly collaborative process requiring a myriad of complimentary spectroscopic and reaction studies to develop fundamental insights. As such, I will provide a comprehensive context of our evolving knowledge in this collaborative project that have since been published where possible and will focus mainly on the recent insights made in this work.

The work presented in this dissertation characterizes and probes the reactivity of the highly dynamic oxyfunctionalized surface layer that has been correlated with the reactivity and selectivity observed on this catalyst. Herein, the coordination environment of B and extent of oxyfunctionalization were analyzed via X-ray Photoelectron Spectroscopy (XPS), X-ray Absorption Spectroscopy (XAS), and Attenuated Total Reflectance IR (ATR-IR) as a function of the reaction progress. Corresponding reaction studies show direct correlation between the development of tri-coordinated oxygenated B networks and the increasing reactivity and selectivity of the reaction during the catalyst's activation period. The significance of a set of reaction parameters was then examined to identify process levers conducive to oxyfunctionalization quantified by XPS.

The acid–base activity of these surface tri-coordnated B networks in the oxyfunctionalized layer are examined via two prototypical reactions: (1) isopropanol decomposition and (2) formic acid decomposition. Catalytic reaction via flow through reactor and temperature programmed decomposition (TPD) studies using Diffuse Reflectance Infrared Fourier Transform IR spectroscopy (DRIFTs) and Mass Spectrometry (MS) are used to extract insights for the adsorption modes of alkoxides and formates and their decomposition pathways. Observed surface reactions of isopropoxy intermediates under these conditions are used to understand possible surface reaction pathways available under ODHP conditions.

The role of O_2 in specific homogeneous pathways of the mixed hetero-homogeneous mechanism previously proposed by us and for supported boron oxide materials are examined. A simplified model for the surface-initiated radical oxidation chemistry pathways, was then used to probe a selectivity descriptor based on the different reactivities of propyl radicals. Using this knowledge, we design, and test model 3D printed BN based monoliths that optimize homogeneous reaction pathways. These catalysts are shown to be highly active and selective and stable for ~2.5wks. The results also suggest that oxygenates may be relevant products from homogeneous reactions.

“The Boron Project,” as we so lovingly called it, has seen several PhD students matriculate as we contributed diligently to uncovering the behavior of this material. The goal of this work is to highlight new avenues through which we can further understand surface reactivity, new tools through which we can probe gas phase radical chemistries, and new catalyst design approaches.

Acknowledgements

To Pearl Landis.

To the woman who left Jamaica to ask for me by name. I promised you I'd become a doctor to take care of you. I pray you are looking down on me. I pray I have taken care of your memory.

You no dey carry last.

Friends and Family

I am exceedingly grateful to God, my mentors, my friends, and my family who sacrificed to create the man I am today. I am thankful for the late-night phone calls, the unwavering grace, and the unconditional support you all have offered me. Your prayers and patience have forged a scientist, community organizer, and leader out of me, and I am forever in your debts. I only hope that the chapters of my life beyond this dissertation are able to give back to you all and the world around me in a profound way. To my mothers and fathers and brothers and sisters, both chosen and unchosen—I could not imagine a more encouraging and kinder tribe to have by my side. To Tiffany Oche, Devon Betts, Chiamaka Okorie, Mitchell Barrows, and Alessia Alexander—Thank you. There is no version of this PhD journey that could've existed without your care, perspective, and love. To Dr. William Morton, my loving and supportive partner, I genuinely could not have asked for a better soul to cross my path and spend the last 3.5yrs with. As I write this now, in tears, I am reminded of the number of times you have come into the office to remind me that I can do this. I love you.

Dr. Ive Hermans & Hermans Research Group

Thank you to Dr. Ive Hermans. Thank you for pushing me to be my best self. Your firm and compassionate approach brings a unique human spirit to research. You have made space to discuss both science and all the other important elements of my life always over a tiny complimentary glass of espresso. I'd like to think that some of your keen sense for business, goodness, and intellectual curiosity have rubbed off on me. I take with me a deep sense of courage and honesty which you have fostered in me. You taught me to be creative, to break things, to fail early, and to win with humility. Thank you, and Gretchen, for helping me find my way.

Thank you all for the support, compassion, and expertise of the last 5yrs. You all have helped me grow as a problem solver, how to learn, and how to have fun along the way. Special thanks to Natalie Altvater (and Leida Vazquez) who have been sources of unconditional understanding, conversation, and comradery. Thank you to Dr. Juan Venegas and Dr. Will McDermott for your guidance through the early parts of my PhD. You both have supported my growth from a clueless first year in the reactor lab to one of the point people for all things reactor lab. I would also like to thank Dr. Melissa Cendejas, Dr. Alyssa Love, Dr. Sarah Specht, and Dr. Lesli Mark for great personal investment you all have made in training, supporting, or just laughing with me.

Research Institutions and Collaborators

I acknowledge the support of the research synchrotron scientists at the Advanced Light Source at the Lawrence Berkely National Lab who offered experimental advice and technical

support for variety experiments we performed there. I greatly appreciate the collaborative work of Zisheng Zhang and Dr. Anastassia Alexandrova of UCLA, Dr. Fateme Rezaei and Khaled Baamran of Missouri University of Science & Technology, and Dr. Yomaira J. Pagan Torres and Edgar Pinilla of the University of Puerto-Rico Mayaguez.

Academic Support and Administrative Staff
I am extremely grateful for the rigorous academics of UW-Madison and the incredible teaching and research faculty. The expertise and passion for this work is palpable and have shaped me forever as a lifelong student. I would specifically like to thank Dr. James Dumesic and Dr. Siddarth Krishna who taught me graduate level kinetics. This was my very first class at UW-Madison and James and Siddarth brought a warmth to the classroom that I greatly appreciated as a nervous first year. I would also like to thank the Kate Fanis, Kathy Heinzen, and Kristi Heming (Graduate Student Coordinators) who have worked extremely hard to support my education, research travel, and financial needs throughout my PhD.

Technical, Experimental, and Instrumental Support
I appreciate the expertise and timely hard work of the staff in the Department of Chemical and Biological Engineering and Department of Chemistry. Specifically, I would like to thank Tracy Drier (Chemistry glass shop), Kendall Schneider and Steve Myers (Chemistry instrument shop), Blaze Thompson (Electronics shop), and John Jacobs (Material Science XPS Technician). All of whom supported the research goals of the Hermans group through complex experimentation designs.

Academic Fellowships and Research Financial Support
I acknowledge the financial support of the National GEM Consortium for providing funding for the first year of my PhD and my associated internship under the guidance of Dr. Susan Habas at the National Renewable Energy Laboratory. I acknowledge the financial support of the Graduate Engineering Research Scholars fellowship for providing funding for the second year of my PhD and for the hard work and passionate support of Kelly Burton throughout my degree. I acknowledge the financial support of the National Science Foundation Graduate Research Fellowship Program for funding the final three years of my PhD. This material is based upon work supported by the National Science Foundation Graduate Research Fellowship Program under Grant No. DGE-1747503. Any opinions, findings, and conclusions or recommendations expressed in this material are those of the author(s) and do not necessarily reflect the views of the National Science Foundation. I acknowledge the financial support of the U.S. Department of Energy, Office of Science, Office of Basic Energy Sciences, under award DE-SC0017918, which has funded the ongoing research on novel boron-based catalysts.

Last but not least.
I am incredibly grateful for the compassion and guidance of Dr. Matthew Rottnek who fostered a deep sense of personal responsibility, humanism, and soulfulness within me. Darius Weil, thank you for the hours long discussion on history, societal structures, and culture. You were instrumental in my development as an active and engaged member of my communities.

Table of Contents

List of Figures

List of Schemes

List of Tables

Chapter 1 – Introduction: Oxidative Dehydrogenation of Propane to Propylene as a Possible Energy Saving Alternative to Direct Dehydrogenation Technologies.

1.1 Bridging the Propylene Gap via "On-Purpose" Production Technologies

The U.S. chemical industry—the largest globally—is a keystone market of the U.S. economy, contributing nearly 2% of the U.S. GDP ($226 bn) in 2010.[1] This industry contributes to an ever-improving standard of living, but is also a significant energy consumer, consuming nearly 24% of the total energy in U.S. manufacturing sector (2010). This is accompanied by growing CO_2 output to sustain our current way of life. The last few decades have produced diagnostic and prescriptive tools to promote industry-wide changes through market-based and regulatory solutions. The petrochemical sector, which derives necessary primary chemicals from petroleum and natural gas feedstocks, is of particular concern. Primary chemicals like ammonia, ethylene, propylene, and methanol are essential feedstocks to value-added products across several industries and accounts for nearly 2/3 of the energy consumed in the petrochemical sector.[2,3] Rightor *et. al.* illustrated the energy required to produce refinery olefins like ethylene and propylene in comparison to ammonia—infamous for its energy intensive production—and the other top 15 chemicals in 2010 (figure 1.1). [3,4]

Light olefins are essential raw materials with applications across several end-use industries like automobile manufacturing, coating, packaging, plastics, and more.[5] Increasing demand for derivatives like polyethylene, cumene, ethyl benzene, and

polypropylene drive the global market growth of ethylene and propylene. Behind ethylene, propylene is the second most important petrochemical building block. Blue Wave Consulting reports a volumetric global propylene market size of 90.6 MT for 2021 with projected growth to 132.1 MT by 2028 (6% CAGR).[6] PMI reported a revenue market size of $3.67bn in 2020 with projected growth to $5.66bn by 2030 (4.5% CAGR).[7] Propylene production has clear implications for several markets, and the technologies necessary to meet demand are of significant interest. The largest share of propylene's global production volume is achieved as a by-product from refinery naphtha cracking or steam cracking in ethylene production.[8–10] However, increasing shale gas availability has motivated the retrofitting of Steam Crackers (SC) to process shale gas—rich in light alkanes—as a feedstock in the pursuit of cheaper ethylene.[9] The reduction in by-produced propylene has been met by technological innovations to increase propylene capacity or 'On-Purpose' Technologies (OPT) (figure 1.1b).[11]

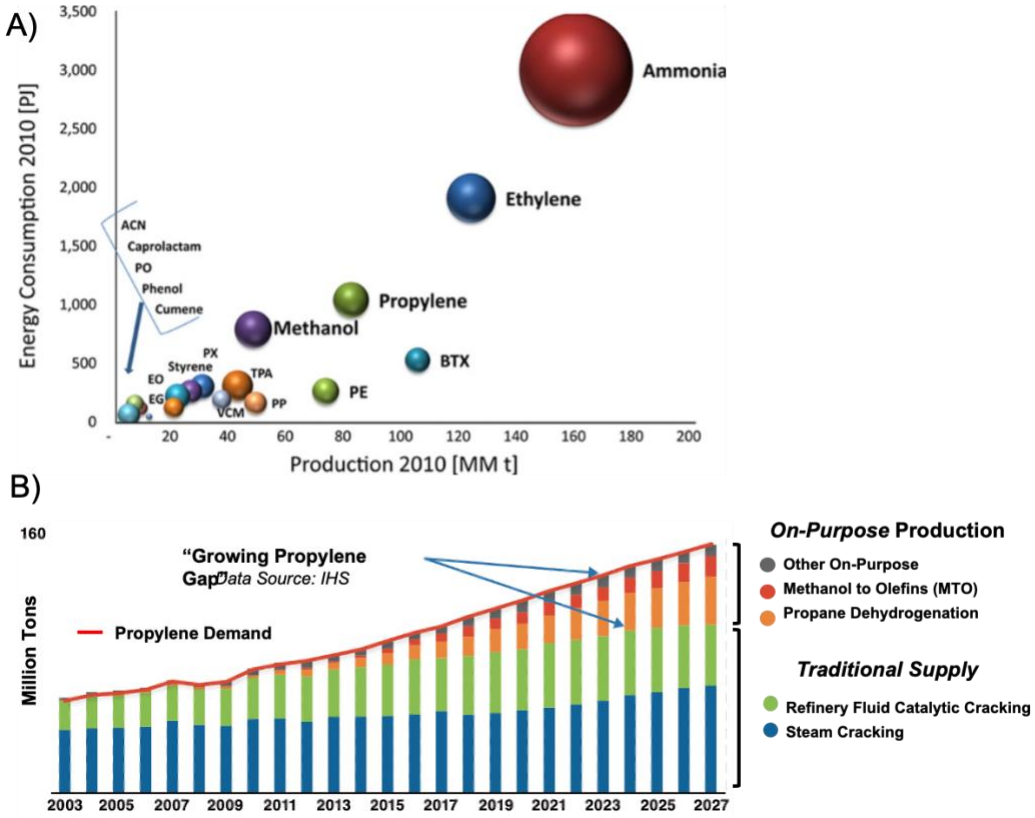

Figure 1.1. a) Energy consumption for production of top 18 chemicals. (ref. 3) b) Historical propylene production trends and the supply–demand gap bridged by "On–Purpose" technologies. (ref. 4)

Propane Dehydrogenation (PDH), reaction 1 (table 1.1), is the primary OPT for propylene production at commodity scale. PDH is industrially implemented by CB&I Catofin, Uhde STAR, and DOW Oleflex processes.[12] These processes achieve 30–40% olefin yield, which is economically viable considering the cost differential between propane and propylene. Although PDH is high yielding, it consumes a significant amount of energy in the dehydrogenation of the alkane. The endothermic and equilibrium–limited reaction pathway requires energy and capital–intensive high–temperature furnace operations (>700 ºC) and low–pressure reactor systems to drive the reaction. Industrial PDH catalysts are often Cr (carcinogenic) or Pt (expensive)

based catalysts. These materials suffer from coke deactivation and can involve complex regeneration schemes or a series of reactors to sustain olefin yields. Comparatively, the oxidative dehydrogenation of propane (ODHP) is an attractive alternative pathway to propylene, reaction 2. This non-equilibrium limited, non-deactivating, and highly exothermic pathway overcomes many of the challenges posed in PDH but suffers from low olefin yield.[13] The primary challenge in ODHP is the facile overoxidation of the alkene or the direct combustion of the alkane to unselective and thermodynamically stable combustion products like CO and CO_2 (i.e. CO_x), shown in reactions 3 and 4 respectively. So, while some 40 PDH plants have been issued sine 2011, extensive research into ODH alternatives have also increased in pace.[14]

Table 1.1. Oxidative and direct dehydrogenation reactions of propane to propylene with corresponding heats of reaction.

Reaction		ΔH / $\frac{kJ}{mol}$	Ref.
1	$C_3H_8 \rightleftharpoons C_2H_6 + H_2$	124	[15]
2	$2\ C_3H_8 + O_2 \rightarrow 2\ C_3H_6 + 2\ H_2O$	−236	[15]
3	$C_3H_6 + 3\ O_2 \rightarrow 3\ CO + 3\ H_2O$	−1077	[15]
4	$C_3H_6 + 4.5\ O_2 \rightarrow 3\ CO_2 + 3\ H_2O$	−1926	[15]

1.2 Oxidative Dehydrogenation of Light Alkanes to Olefins

Traditionally, transition metal oxides have been the most promising ODHP catalysts. Supported vanadium oxides (VO_x) are some of the most studied and well characterized catalytic systems in alkane ODH.[16] For example, VO_x/SiO_2 achieves 60% propylene selectivity at 10% propane conversions, with CO_x as main

byproducts.[17] Several measures have been explored to improve olefin yield on vanadia catalysts like: tuning of surface acidity, the use of binary or ternary metal oxide systems, or controlled synthesis of the active site. Unfortunately, these synthetic approaches which alter surface acidity, near surface electronic properties, or active site accessibility fail to produce propylene yields necessary for industrial implementation.

In 2016, Grant *et. al.* identified hBN as a highly reactive and selective catalyst for ODH. hBN surpassed performance metrics of VO_x/SiO_2, exhibiting a 79% propylene selectivity and 12% ethylene selectivity at 14% propane conversion, while CO_2 and CO selectivities totaled 8%.[17–21] These boron based catalysts are indeed promising, especially given that the main byproduct is also of value. Since its discovery, several studies have examined chemical and mechanical pretreatments, controlled synthesis of model materials, and reactor design schemes to maximize olefin yield.[10,22,23] Other computational and experimental studies have aimed to understand the fundamental mechanisms at play. The primary challenge in understanding BN catalyzed ODHP is that the operating catalyst surface is formed under ODHP reaction temperatures (>500 ºC) is highly amorphous and dynamic. Extensive kinetic, computational, and spectroscopic studies indicate that the oxyfunctionalization of the BN surface is necessary for ODHP reactivity and that an oxidic boron layer is necessary for reactivity.[24–26] Therefore, generating structure–performance

relationships for this system has required a wide array of analytical and reaction tools to fully characterize the system under a variety of conditions.

1.3 Thesis research goals and recognitions of peer contributions

Gaining molecular insights in the BN catalyzed ODHP of propane has been a highly collaborative and creative journey. I am grateful to Dr. Joe Grant for his initial discovery, as well as Dr. Alyssa Love, Dr. Juan Venegas, Dr. Melissa Cendejas, and Dr. Lesli Mark all of whom I worked closely with in studying this system.

The goals of the work presented are:

- Characterize the growth of the oxyfunctionalized boron layer and its relationship to the reaction progress and process parameters
- Characterize surface acid–base reactivity via isopropanol decomposition reactions
- Characterize surface acid–base reactivity via formic acid decomposition reactions
- Examine the role of O_2 and probe proposed homogeneous reaction pathways.
- Design new boron–based materials to improve olefin yield

Chapter 2 examined the growth of the oxyfunctionalized layer as a function of the reaction progress and develops direct correlation between growing tri–coordinated oxygenated B networks and the increasing reactivity and selectivity of the reaction during the catalyst's activation period. The significance of a set of reaction parameters was then examined to identify process levers conducive to oxyfunctionalization quantified by XPS. Chapter 3 characterizes the oxyfunctionalized

boron layer and probes its chemical behavior through adsorptive and prototypical reactions. Probing the surface transformation of a different but relaxed oxide surface to understand what catalytic properties arise on the post reaction surface. Chapter 4 focused primarily on the kinetic behavior of O_2 under variable conditions. A kinetic model is built to explain empirical results which account for the impact on observed product distributions. Hypothesized mixed surface-gas reaction mechanisms are probed experimentally and computationally. The knowledge generated from these studies are applied to a structured catalyst bed design for boron-catalyzed ODHP. Chapter 5 summarizes this work and discusses outlooks for further studies on boron-based catalysts for the partial oxidation of alkanes. Therein, the progress of ODHP catalysts is also discussed.

1.4 References

1. Energy.Gov. Chemicals Industry Profile | Department of Energy. *Advanced Manufacturing* Available at: https://www.energy.gov/eere/amo/chemicals-industry-profile. (Accessed: 9th April 2022)
2. Tiffany Vass, Peter Levi, Alexandre Gouy & Hana Mandová. Chemicals – Analysis – IEA Tracking Report November 2021. *iea.org* (2021). Available at: https://www.iea.org/reports/chemicals. (Accessed: 10th July 2022)
3. Rightor, E. G. & Tway, C. L. Global energy & emissions reduction potential of chemical process improvements. *Catal. Today* **258**, 226–229 (2015).
4. Marsh, M. & Wery, J. Filling the propylene gap–shaping the future with on–purpose technologies. *UOP, Honeywell* (2019).
5. Coherent Market Insights. Ethylene And Propylene Market Size And Forecast To 2027. 0–160 (2019). Available at: https://www.coherentmarketinsights.com/market-insight/ethylene-and-propylene-market-3007. (Accessed: 9th April 2022)
6. Blue Wave Consulting. Global Propylene Market- Industry Size, Share, Growth, Opportunity and Forecast, 2018–2028, Segmented By Derivatives. (2022). Available at: https://www.blueweaveconsulting.com/report/global-propylene-market. (Accessed: 9th April 2022)
7. Prophecy Market Insights. Global Propylene Market Size by Derivative. *Market Research Report PMI* 0–168 (2022). Available at: https://www.prophecymarketinsights.com/market_insight/Global-Propylene-Market-By-Derivatives-164. (Accessed: 9th April 2022)
8. Zimmermann, H. & Walzl, R. Ethylene. *Ullmann's Encyclopedia of Industrial Chemistry* (2000). doi:doi:10.1002/14356007.a10_045
9. Amghizar, I., Vandewalle, L. A., Van Geem, K. M. & Marin, G. B. New Trends in Olefin Production. *Engineering* **3**, 171–178 (2017).
10. Grant, J. T. *et al.* Boron and Boron-Containing Catalysts for the Oxidative Dehydrogenation of Propane. *ChemCatChem* 1–5 (2017). doi:10.1002/cctc.201701140
11. Coherent Market Insights. Propylene Market Size, Trends And Forecast To 2025. *Market Research Report / Bulk Chemicals* 0–179 (2018). Available at: https://www.coherentmarketinsights.com/market-insight/propylene-market-1997. (Accessed: 9th April 2022)
12. Sattler, J. J. H. B., Ruiz-Martinez, J., Santillan-Jimenez, E. & Weckhuysen, B. M. Catalytic Dehydrogenation of Light Alkanes on Metals and Metal Oxides. *Chem. Rev.* **114**, 10613–10653 (2014).
13. Cavani, F., Ballarini, N. & Cericola, A. Oxidative dehydrogenation of ethane and propane: How far from commercial implementation? *Catal. Today* **127**, 113–131 (2007).
14. National Academies of Sciences and Medicine, E. *The Changing Landscape of Hydrocarbon Feedstocks for Chemical Production: Implications for Catalysis: Proceedings of a Workshop*. (The National Academies Press, 2016). doi:10.17226/23555
15. Tian, J. *et al.* Hexagonal boron nitride catalyst in a fixed-bed reactor for exothermic propane oxidation dehydrogenation. *Chem. Eng. Sci.* **186**, 142–151 (2018).

16. Cavani, F., Ballarini, N. & Cericola, A. Oxidative dehydrogenation of ethane and propane: How far from commercial implementation? *Catal. Today* **127**, 113–131 (2007).
17. Grant, J. T. *et al.* Selective oxidative dehydrogenation of propane to propene using boron nitride catalysts. *Science (80-.).* **354**, 1570–1573 (2016).
18. Venegas, J. M., McDermott, W. P. & Hermans, I. Serendipity in Catalysis Research: Boron-Based Materials for Alkane Oxidative Dehydrogenation. *Acc. Chem. Res.* **51**, 2556–2564 (2018).
19. T., G. J. *et al.* Boron and Boron-Containing Catalysts for the Oxidative Dehydrogenation of Propane. *ChemCatChem* **9**, 3623–3626 (2017).
20. Venegas, J. M. *et al.* Selective Oxidation of n -Butane and Isobutane Catalyzed by Boron Nitride. *ChemCatChem* **9**, 2118–2127 (2017).
21. Grant, J. T. *et al.* Boron and Boron-Containing Catalysts for the Oxidative Dehydrogenation of Propane. *ChemCatChem* **9**, 3623–3626 (2017).
22. Shi, L. *et al.* Progress in selective oxidative dehydrogenation of light alkanes to olefins promoted by boron nitride catalysts. *Chem. Commun.* **54**, 10936–10946 (2018).
23. Honda, Y., Takagaki, A., Kikuchi, R. & Oyama, S. T. Oxidative Dehydrogenation of Ethane Using Ball-milled Hexagonal Boron Nitride. **47**, 1090–1093 (2018).
24. Love, A. M. *et al.* Probing the Transformation of Boron Nitride Catalysts under Oxidative Dehydrogenation Conditions. *J. Am. Chem. Soc.* **141**, 182–190 (2019).
25. Zhang, Z., Jimenez-Izal, E., Hermans, I. & Alexandrova, A. N. Dynamic Phase Diagram of Catalytic Surface of Hexagonal Boron Nitride under Conditions of Oxidative Dehydrogenation of Propane. *J. Phys. Chem. Lett.* **10**, 20–25 (2019).
26. Venegas, J. M. *et al.* Why Boron Nitride is such a Selective Catalyst for the Oxidative Dehydrogenation of Propane. *Angew. Chemie Int. Ed.* **59**, 16527–16535 (2020).

Chapter 2. Characterizing the Growth of the Oxyfunctionalized Layer on BN and Identifying the Effect of Reaction Parameters on Layer Growth

Publication in preparation. Supplemental materials for Chapter 2 located in Appendix B.

Section 2.3 includes X-ray Raman Spectroscopy from an ongoing manuscript:

Cendejas, M. C.; Paredes, O.; **Agbi, T.O.;** Jansen, J.H.; Kurumbail, U.; Dong, S.; Sokaras, D.; Bare S. R.; Hermans, I., Tracking Surface Changes on hBN during the Oxidative Dehydrogenation of Propane Using Operando X-Ray Raman Spectroscopy, (Manuscript in preparation, 2022)

Personal contributions to manuscript: I contributed to characterization data, data analysis, data interpretation and experimental insights with the primary author.

Section 2.3 also includes statistical experiments initially thought of by Dr. Joe T Grant, who provided preliminary data. Personal contributions: I reran experiments run by Dr. Joe T Grant. I designed additional DoE's (appendix) and ran all additional catalytic reactions and XPS analyses. I provided the data interpretation for his and my data, which have since been combined as duplicates and triplicates within the overall study.

2.1. A Brief Introduction to Boron Oxide Catalysts for the Partial Oxidation of Light Alkanes to Alkenes and Oxygenates

The early work of Yasushi *et. al.* demonstrated that composite catalysts composed of boron oxide (B_2O_3) and additional oxides (e.g. MgO, Al_2O_3, P_2O_5) were active and selective for the partial oxidation of ethane to ethylene and acetaldehyde.[1] Kinetic studies by Hatano and coworkers for the selective partial oxidation of methane,

ethane, and propane over on mixed boron phosphorous oxides (B–P–O) further suggested contributions of gas phase reactivity to the overall reaction mechanism.[2] Later, Buyevskaya *et. al.* extended this mechanism to the describe the selective partial oxidation of propane propylene over B_2O_3 / Al_2O_3 – on of the highest performing supported boron oxide ODHP catalysts at the time.[3–5] Although identifying the specific speciation of boron active sites is an ongoing research goal of the field, consistent across these studies was the correlation between tri–coordinated oxygenated boron species and catalytic performance. These BO_x and B–OH motifs were necessary and active reactive oxygen species (ROS) in the reaction mechanism for the partial oxidation of alkanes and have since been observed across various borides independent of the heteroatom, supported boron materials, and boron fixed in zeolitic frameworks recently.[6–8] Although promising, facile hydrolysis and volatilization of B_2O_3, which has a melting point of 450 ºC, make B_2O_3 supported catalysts unstable as they would leach boron and diminish in catalytic performance. Efforts have been made to stabilized BO_x phases on metal oxide supports or within zeolitic frameworks. However, BO_x leaching still occurred and some metal oxide supports readily interacted with reaction intermediates and diminished olefin yeilds.[3,4,7] We observed this in our characterization and study of silica supported BO_x catalysts for ODHP.[7] We also observed that immobilization of BO_3 units within an MWW zeolitic framework exhibited little to no catalytic reactivity for ODHP.[9]

Thus, the observation of BN as a highly stable and active ODHP catalyst that features similar BOx properties brought renewed energy to boron-based catalysts for ODHP. The anti-oxidation properties of BN make it an attractive material for protective coatings and lubricants. BN oxidation conventionally occurs above 900-1000 ºC in air or pure O_2 environments. However, we show that BN readily oxyfunctionalizes between 400-500 ºC under alkane/air mixtures (e.g., typical ODHP conditions).[6,10,11] This oxyfunctionalization features BO_3 like coordination environments where B sites may feature 1 to 2 hydroxyl groups that contribute uniquely to catalytic performance.[12] Herein we aim to characterize the growth of this oxyfunctionalized layer and probe the reactivity of these hydroxyl features to aid structure-performance relationships.

2.2. Characterizing the growth of the oxyfunctionalized layer on BN under ODHP

Commercial BN exhibit relative amounts of O impurity that alter the initial activation period of BN for ODHP. Generally, an activation period on several commercial BN samples has been observed under a variety of conditions. During the activation period, propane and oxygen conversions increase significantly and product selectivity is improved. To understand the significance of this activation period, we tracked the growth of oxyfunctionalized layer and the reaction using propane as the main alkane. Note, TOS is also referred to as reaction progress during this transient period.

We examined this activation period by treating 300 mg BN samples independently under ODHP conditions using a continuous flow reactor. Reactivity and reaction products were monitored via online-gas chromatography (GC) (figure 2.1). Conversions of both O_2 and propane exhibited parallel s-curves as a function of reaction progress, figure 2.1a. The ratio of propane to oxygen conversions was approximately 1.7 and remained consistent observed throughout the activation, which is slightly below the ideal stoichiometric ratio of 2 for the homogeneous reaction. Similarly, the reaction rates for propane and propylene parallel s-curves as CO and CO_2 decreased relatively linearly, figure 2.1b. Reaction products showed an increase in olefin selectivity which remained steady after 3hr, figure 2.1c. An inflection point at 4hr was observed for the rate of propane consumption and preceded the 6hr inflection for propane (and oxygen) conversion (figure 2.1d). This last result indicated that while the reaction rate approached steady state early, conversions of O_2 and propane is further driven by an increase in homogeneous radical reaction pathways and remaining surface restructuring.

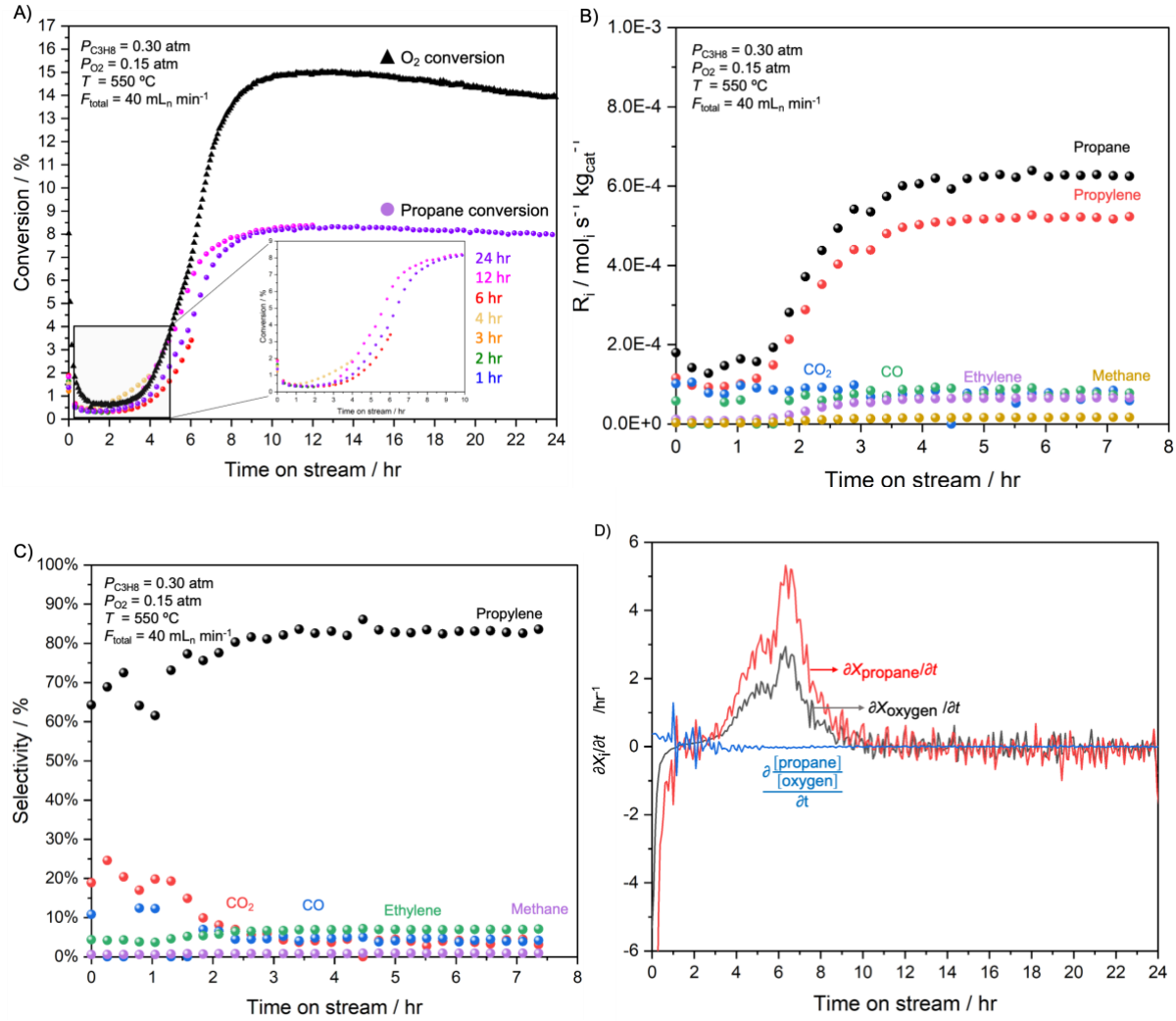

Figure 2.1. a) Oxygen and propane conversions, X, b) product reaction rates, and c) product selectivities as a function of time on stream, TOS, for BN treated under conditions: T = 550 °C, F_{total} = 80 mLn min^{-1}, P_{total} = *0.3 atm* C_3H_8 , *0.15 atm* O_2 , *0.55 atm* N_2. d) Example of derivation of inflection point via instantaneous rates of change for oxygen and propane conversions and ratio of propane to oxygen taken as the first derivative of TOS vs. conversion.

Analysis of the samples via X-ray Photoelectron Spectroscopy (XPS) illustrated an asymptotic relationship between O content and reaction progress (figure 2.2a) where O content increased from 5.7% at 0hr to 11.4% at 6hr (i.e., the inflection point) to 9.6% at steady state. Deconvolution of the O 1s spectra revealed that bridging oxygens belonging to B-O-B connectivity (533 eV) within an oxide network account

for a majority of the increase in O content and exhibited an s-curve as a function of reaction progress that was parallel to reactant conversions. Surface hydroxyls primarily belonging to B-OH groups (534 eV) also increased as a function of reaction progress and exhibited a positive correlation with propane conversion, figure 2.2b. This coincides with increasing olefin selectivity. Furthermore, core-level X-ray Absorption Spectroscopy (XAS) illustrates the growing BO_3 coordination environment (194 eV) in B K-edge as a function of reaction progress, figure 2.2c. These results support observations of the transformation from BN_3 to BO_3, BOH, and B-O-B coordination environments reported on fresh and spent BN.[6] This surface restructuring during the activation period, also showed the diminishing of BNO (532 eV) features. Assignments for BN, BNO / B-O-B, and BO/-OH functionalities as a function of reaction progress were also observed at 190.1, 190.8 and 192 eV respectively in the B 1s region, figure B.2.

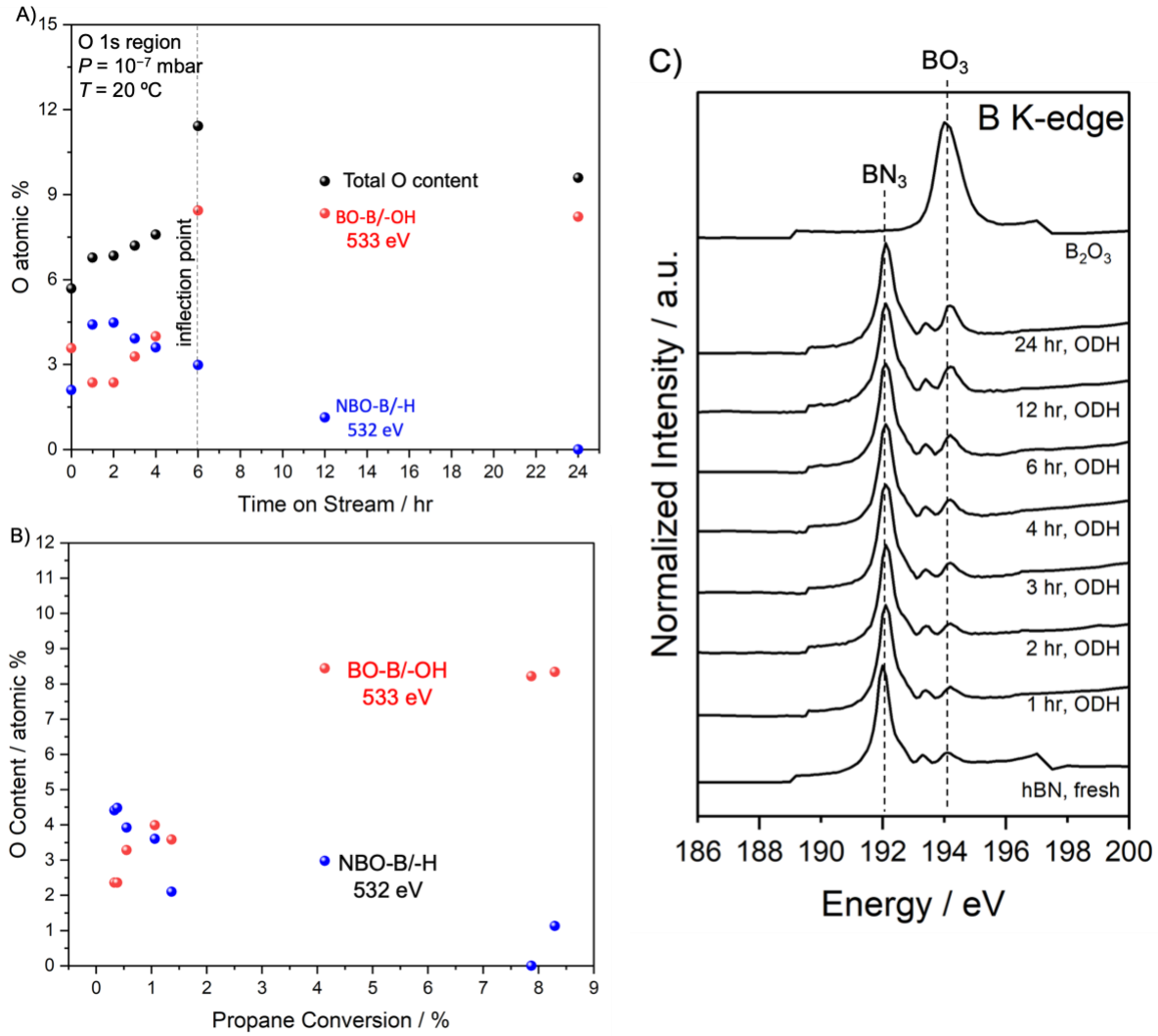

Figure 2.2. XPS quantification of O content (atomic %) for all BN samples treated as a function of a) time on stream and b) propane conversion during the activation period. c) XAS spectra of B K-edge for all BN samples analyzed with BN3 (192 eV) and BO3 (194 eV) coordination environments marked. BN samples independently treated under the following conditions: T = 550 °C, F_{total} = 80 mLn min^{-1}, P_{total} = *0.3 atm* C_3H_8, *0.15 atm* O_2 , *0.55 atm* N_2.

We examined the surface functional groups via Attenuated Total Reflectance FT-IR (ATR-IR), (figure 2.3). Increasing bands at 3448 and 3435 cm^{-1}consistent with hydroxyl stretches within the borate network on non-bridging oxygens, and an increasing band at 3208 cm^{-1} consistent with increasing in-plane B-OH bending

were observed, figure 2.3a.[13] The increasing in hydrogen bonding and hydroxyl nests on the growing oxyfunctionalized surface agrees with our previous spectroscopic observations on fresh and spent BN and silica supported BO_x. The spectrum for pristine BN (i.e., 0 hr TOS) was subtracted from all other spectra to generate difference spectra that were further deconvoluted to extract details from 1300 and 750 cm^{-1} regions, figure 2.3b. Growing peaks at 1508, 1441, 1316, 1253, 1050, 912, 754, and 670 cm^{-1} were observed. Similar to the fundamental B–N–B stretching and out of plane bending modes for bulk BN observed at 1305 and 747 cm^{-1} respectively in figure 2.3a, enhancements at 1316 and 754 cm^{-1} were assigned to growing disordered turbostratic–BN layers in figure 2.3b. 1508 cm^{-1} was assigned to N–O stretching and was expectedly in comparatively low concentrations. 1441, 1253, 670 cm^{-1} correspond to B–O stretching in boroxyl rings and B–O–B asymmetric stretching typical of metaborate units, and bending vibrations in trigonal planar BO_3 units.[13] The growth of BO_4 tetrahedra can be observed by the increasing intensity 1050 and 920 cm^{-1} attributed to stretching vibrations within the tetrahedra. Examining the integrated areas of 1253 and 1050 cm^{-1} as indices for BO_3 and BO_4 growth respectively, figure 2.3c showed that both networks developed within the first hour with approximately a 3:1 ratio of BO_3 to BO_4 coordination. BO_3 concentration surpassed BO_4 and peaked at 6 hr, paralleling the behaviors of oxygen and propane conversions. Interconversion of BO_4 to BO_3 was observed as both networks return to their initial 3:1 ratio at steady–state reactivity.

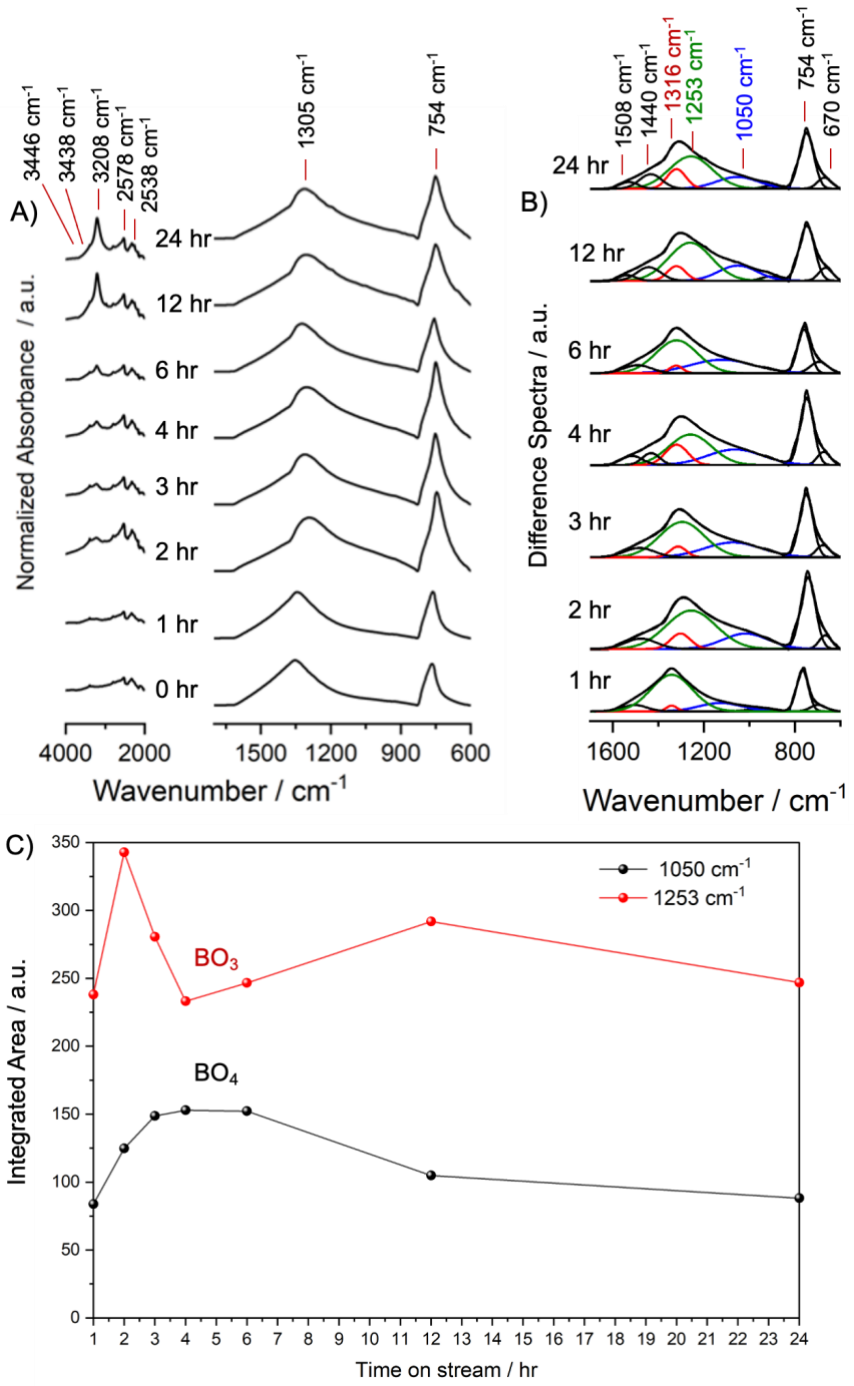

Figure 2.3. (a) *Ex-situ* ATR-FTIR spectra of BN samples at different times on stream. All spectra are normalized to the main BN feature in the fresh sample. (b) Deconvoluted difference spectra (i.e., BN 0hr is subtracted from each spectra). Color variation denotes peaks of interest. (c) Integrated areas of deconvoluted signals at 1253 and 1050 cm^{-1} and their respective (d) instantaneous rates of change.

Ex-situ characterization of the growing oxyfunctionalized layer by XPS, XAS, and ATR-IR illustrate that an increase in tri-coordinated oxygenated boron species featuring B-OH and B-O-B connectivity contribute to the rise BN's catalytic reactivity and selectivity. Under these conditions, reaction progress and BO_3 growth were correlational during the activation period on BN. These results agree with the assertion that increased BO_3 concentrations may accelerate the reaction.[141512] Once the reaction achieved steady-state neither the surface concentrations of BO_3 nor the total surface O content increased appreciably. This may suggest that above a particular concentration, BO_3 can maintain steady state conditions and further incorporation of O_2 into the oxyfunctionalized layer becomes limited.

2.3. Determining the Effect of Reaction Parameters on the Extent of BN Oxyfunctionalization

Buyevskaya and coworkers performed isotopic $^{18}O_2$ pulse experiments via temporal-analysis- of products (TAP) reactor and showed that increased loadings of B_2O_3 on Al_2O_3 diminished $O^{16}O^{18}$ yield between 470 and 570 ºC.[3-5] They proposed that increased B_2O_3 suppressed dissociative O_2 adsorption. They attribute the high olefin selectivity observed to the decrease in O_2 dissociation on the surface. This is a significant observation given the key role surface oxyfunctionalization plays in the proposed Eley-Rideal mechanism in BN catalyzed ODHP. It is necessary to understand which process parameters promote BN oxyfunctionalization under in the partial oxidation of alkanes. We identified 6 parameters likely to promote

oxyfunctionalization: alkane identity, temperature (*T*), total gas flowrate (F_T), alkane feed concentration (P_{alkane}), oxygen feed concentration (P_{O2}), and time on stream (TOS). 50 mg of BN were independently treated under ODHP conditions according to a 2-level full factorial experimental design—exemplified in table 2.1. The atomic % of O on the BN surface as quantified by XPS and used as a measure of oxyfunctionalization. Using Analysis of Variance (ANOVA) of the O content, we determined the significance of main 2-way interaction effects via *p* and *t* values. *p*-values measure the statistical significance of an observed result and lower p-values indicate higher probability of achieving the result (e.g., the null hypothesis may be rejected). *t*-values measure the deviation of the result from the standard variations within the sampled data set (i.e., null hypothesis) and is a related probability that the result achieved may reject the null hypothesis. We used the conventional values of $p < 0.05$ and $+2 > t < -2$ for our confidence levels.

Table 2.1. 2-level full experimental design for methane and isobutane.

Terms	Process Variable / units	Experimental Design	
	Single Terms	Low / −1	High / +1
1	Alkane Identity	methane	isobutane
2	Temperature / ºC	400	600
3	Feed Flowrate / $mL_n\ min^{-1}$	20	80
4	P_{alkane} / atm	0.10	0.40
5	P_{O2} / atm	0.05	0.20
6	Time on Stream / hr	4	12

A 2-level full design was used to compare methane and isobutane—alkanes with significantly different partial oxidation reactivities under similar conditions. Calculated t- and *p*-values show that alkane identity, *T*, and F_{total} were significant main effects,

and alkane identity* T and P_{alkane}* T were significant 2-way interactions, illustrated in figure 2.4. All other main effects and 2-way interactions did not show a significant correlation with the extent of oxyfunctionalization.

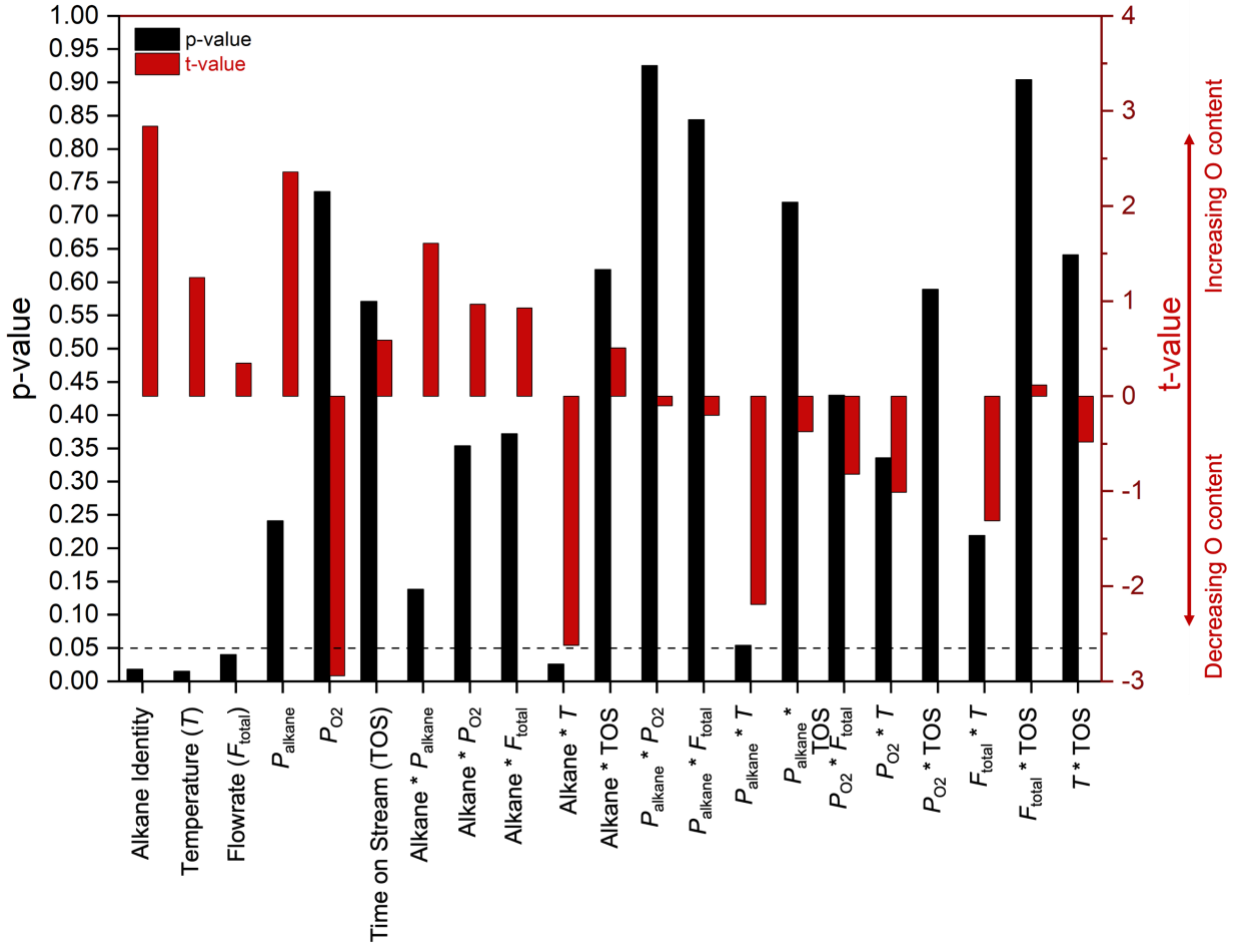

Figure 2.4. Calculated t and p-values for single and 2-way interaction effect on oxyfunctionalization from ANOVA of 2-level full experimental design comparing methane and isobutane as alkanes of interest. 50 mg of BN were independently tested in random experimental order and examined via XPS.

We attributed the high significance of alkane identity (p = 0.018, t = 2.84) to the difference in C-H activation, where $R_{isobutane} > R_{methane}$. The t-value of 2.84 indicated a significant positive effect for oxyfunctionalization. This result is supported by previous XAS performed by our group, which probed surface transformation of BN_3

to BO_3 coordination. This transformation correlated positively as BN was contacted with higher order alkanes—C2–C4 alkanes were examined—under consistent reaction conditions (i.e., P_{alkane} = 0.3 atm, P_{O2} = 0.15 atm, P_{N2} = 0.55 atm, T = 450 ºC, TOS = 4 hrs), figure 2.5. Increasing alkane reactivity at 450 ºC coincided with increasing BO_3 coordination at 194 eV in the B K-edge region. This result further supports the correlation between alkane conversion and BO functionality established in figure 2.2b.

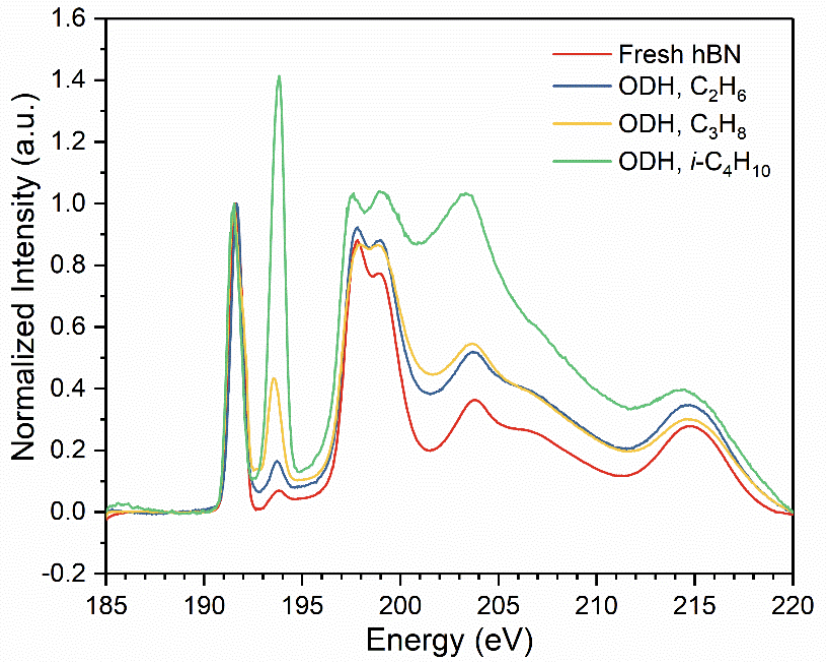

Figure 2.5. *ex-situ* XAS spectra of B k-edge for BN: fresh and treated under the following conditions P_{alkane} = 0.3 atm, P_{O2} = 0.15 atm, P_{N2} = 0.55 atm, T = 450 ºC, TOS = 4 hrs. Alkanes tested were ethane, propane, and isobutane. (ref. 16)

F_{total} (p = 0.04, t = 0.35) exhibited low significance and low magnitude of that effect. Short contact times, which produced lower conversions, produced slightly higher O content. TOS (p = 0.57, t = 0.59) exhibited no significant effect under the conditions tested. The results for both F_{total} and TOS can be attributed to the facile hydrolysis

and volatilization of boron oxides under these conditions. Buyevskaya *et al.* showed that supported boron oxide catalysts were made unstable under reaction conditions due to the volatilization of the oxide, which contributed to some catalyst deactivation. We can therefore propose that high conversions, achieved by long contact times, and long TOS do not necessarily result in higher O content. P_{O2} nor any of its interaction terms exhibited significant effects. Literature shows that steam and/or pure O_2 alone cannot readily oxyfunctionalize BN at these temperatures, which is a first order explanation for the low significance for P_{O2}. In fact, although both the oxidant and alkane are necessary to oxyfunctionalize the surface at these temperatures, $P_{O2} * P_{alkane}$, exhibited the lowest significance of all terms ($p = 0.925$). These results, in combination with the low significance of the P_{alkane} term, illustrate that the extent of oxyfunctionalization is less dependent on the respective levels of reactants themselves. T ($p = 0.015$, $t = 1.25$) exhibited high significance, but the magnitude of the t–value suggests that this term does not contribute significantly to O content on its own. In fact, t–values for $P_{alkane} * T$ ($p = 0.054$, $t = -2.19$) and alkane identity $* T$ ($p = 0.026$, $t = -2.62$) suggest that the effect of T is most relevant in conduction with the alkane.

We streamlined our experimentation to examine only four factors: alkane identity, T, F_{total}, and a P_{alkane} using a 2–level ½ factorial design for pairwise comparisons of methane, ethane, propane, and isobutane. These design schemes are outlined in

Appendix B, tables B.1– B.9. Within the depth penetration of XPS (20 nm) all main effects and 2–way interactions did not show an appreciable effect on the extent of oxyfunctionalization, figure B1. There exists then a complex relationship between these parameters and may require high order interactions to model. One relationship not directly measured in the above study, but worth considering, is the effect that the reaction may have on removing the oxyfunctionalized layer. This could explain a break down in the reaction parameters themselves as they do not directly sample these interactions. XPS showed that steady–state O content of remained at 9.6% despite the ongoing reaction. This may be an effect of a dynamic relationship between the oxyfunctionalized layer and some of the reaction intermediates or products. Recent work from our group, led by Dr. Melissa Cendejas shows early support for this hypothesis. There, *operando* X–ray Raman Spectroscopy (XRS) was used to examine surface changes on BN under a reaction mixture of propane, oxygen, and He at 550 ºC. The effect of H_2O was examined by cyclically cofeeding steam to the dry reaction mixture, figure 6a. While the dry reaction mixture promoted BO_3 functionality (194 eV), co–fed steam reversibly decreased BO_3 functionality and a concomitant decrease in propylene production was observed, figure 3a and 3b. We hypothesize then that steam may promote volatilization of the oxyfunctionalized surface or depress its relative concentration to BN_3.This agrees with the assertion that the extent of oxyfunctionalization is not easily described by process parameters.

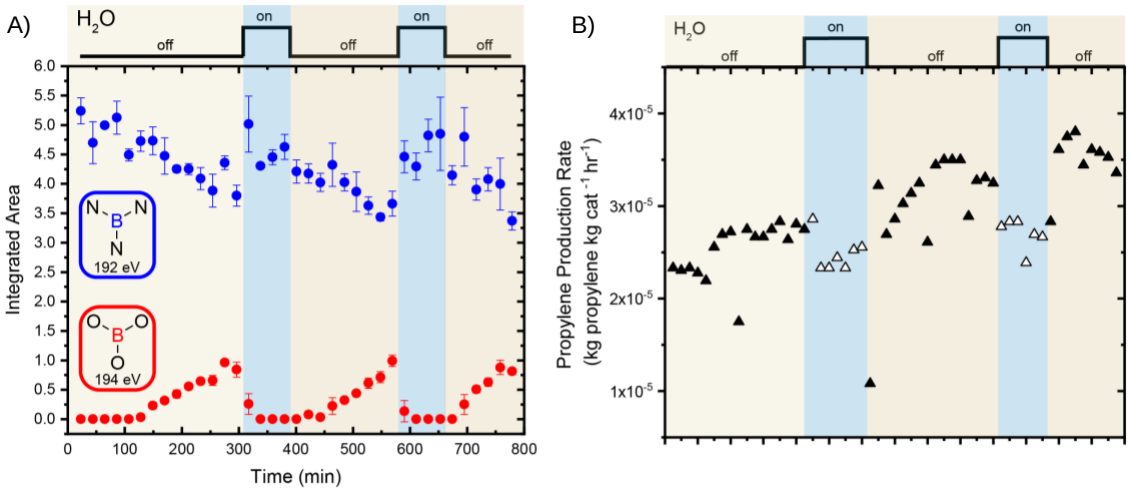

Figure 2.6. a) Quantification of BN_3 and BO_3 chemical environments and b) propylene production rate as functions of TOS and variable cofed steam added to the reaction mixture. Reaction conditions: T = 550 C, 10 ml min^{-1} total flow rate (1.4 $mLmin^{-1}$ C_3H_8, 3.5 $mLmin^{-1}$ 20% O2/N2, 5.1 $mLmin^{-1}$ He). (Manuscript in progress).

2.4. Discussion of characterizing growth and surface structures of oxyfunctionalized BN

A statistical analysis of reaction parameters suggests that alkane and O_2–derived intermediates or reaction products like OOH and H_2O mediate surface functionalization, as seen by P_{alkane} * T and alkane identity * T terms. The reactants did not show a direct effect on the extent of oxyfunctionalization as evidenced by low P_{O2}, P_{alkane}, and P_{O2} * P_{alkane} p– and t– values. *operando* XRS would suggest that reaction conditions with increasing H_2O concentrations from increased alkane/O_2 conversions (or higher T) could simultaneously decrease propylene selectivity and BO_3 coordination environments. This observation agrees well with XPS, XAS, and ATIR–IR characterization during the activation period of BN, wherein growing BO_3 coordination, growing alkane/O_2 conversions, and growing propylene

selectivity all coincide. The asymptotic behavior of the total surface O content as a function of reaction progress may also support the assertions by Buyevskaya *et. al.*, such that high extents of oxyfunctionalization may suppress further O_2 dissociation and result in the steady state value of 9.6% O atomic. More specifically, the increase in thermodynamically stable BO_3 species may contribute to the observed effect. While it is clear from previous O_2 cutoff experiments that the ODHP reaction can not be sustained, this result may indicate that above a given extent of oxyfunctionalization, the key role of O_2 may no longer be dissociative adsorption.

Analysis of the B 1s region showed 95% BN_3 and 5% BO_3 in fresh BN, and 50% BN_3 and 50% BO_3–type in spent BN (24hrs TOS). Our previous Solid-State NMR (SSNMR) studies revealed a 95% BN_3 and 5% BO_3 on fresh BN and 70% BN_3 and 30% BO_3 on BN (24hrs TOS).[6] The higher surface O content suggests that the oxide layer does not grow inwards appreciably. Shieh et. al. proposed a general model for the oxidation kinetics of BN above 800 ºC in O_2.[17] They note that the induction period observed in the conversion of BN to B_2O_3 if the amount of time necessary for the initial B_2O_3 layer to form. They propose that O_2 reacts at the interface of the B_2O_3 and BN and therefore diffusion of O_2 through the oxide layer is a kinetically relevant step in the oxidation of BN. It is not clear that this is the case in the low temperature oxyfunctionalization of BN—which seems to resemble facile oxidation of diboride compounds 400–500 ºC in air or pure O_2. However, slow diffusion of O_2 through the

boron oxide surface rather than reaction with the oxide surface may explain the results obtained by Buyevskaya *et. al.* and suggest that in the limit of an increasing boria like surface, the kinetically relevant roles for O_2 may not involve surface dissociation particularly at higher P_{O2}. In that respect, the removal of BO_3 units by H_2O may allow for increased dissociative adsorption of O_2 and—according to Buyevskaya *et. al.*—a decrease in propylene selectivity, which we observe.

2.5 References

1. Murakami, Y., Otsuka, K., Wada, Y. & Moikawa, A. Partial Oxidation of Ethane over Boron Oxide Added Catalysts. *Chem. Lett.* 545–548 (1989).
2. Otsuka, K., Uragami, Y., Komatsu, T. & Hatano, M. The partial oxidation of light alkanes (CH4, C2H6, C3H8) over B–P mixed oxides. *Stud. Surf. Sci. Catal.* **61**, 15–23 (1991).
3. Buyevskaya, O. V., Müller, D., Pitsch, I. & Baerns, M. Selective Oxidative Conversion of Propane to Olefins and Oxygenates on Boria–Containing Catalysts. *Nat. Gas Convers. V* **119**, 671–676 (1998).
4. Buyevskaya, O. V., Kubik, M. & Baerns, M. Factors Determining the Selectivity in the Oxidative Dehydrogenation of Propane over Boria–Alumina Catalysts. in *Heterogeneous Hydrocarbon Oxidation* 155–169 (1996).
5. Steinfeldt, N., Buyevskaya, O. V, Wolf, D. & Baerns, M. Comparative Studies of the Oxidative Dehydrogenation of Propane in Micro–Channels Reactor Module and Fixed–Bed Reactor. in *Natural Gas Conversion VI* (eds. Iglesia, E., Spivey, J. J. & Fleisch, T. H. B. T.–S. in S. S. and C.) **136**, 185–190 (Elsevier, 2001).
6. Love, A. M. *et al.* Probing the Transformation of Boron Nitride Catalysts under Oxidative Dehydrogenation Conditions. *J. Am. Chem. Soc.* **141**, 182–190 (2019).
7. Love, A. M. *et al.* Synthesis and Characterization of Silica–Supported Boron Oxide Catalysts for the Oxidative Dehydrogenation of Propane. *J. Phys. Chem. C* **123**, 27000–27011 (2019).
8. Mark, L. O. *et al.* Highly Selective Carbon–Supported Boron for Oxidative Dehydrogenation of Propane. *ChemCatChem* **13**, 3611–3618 (2021).
9. Altvater, N. *et al.* B-MWW Zeolite: The Case Against Single-Site Catalysis. *Angew. Chem. Int. Ed.* **132**, 1–6 (2020).
10. Zhang, Z., Jimenez–Izal, E., Hermans, I. & Alexandrova, A. N. Dynamic Phase Diagram of Catalytic Surface of Hexagonal Boron Nitride under Conditions of Oxidative Dehydrogenation of Propane. *J. Phys. Chem. Lett.* **10**, 20–25 (2019).
11. Venegas, J. M. *et al.* Why Boron Nitride is such a Selective Catalyst for the Oxidative Dehydrogenation of Propane. *Angew. Chemie Int. Ed.* **59**, 16527–16535 (2020).
12. Liu, Z. *et al.* Understanding the Unique Antioxidation Property of Boron–Based Catalysts during Oxidative Dehydrogenation of Alkanes. *J. Phys. Chem. Lett.* **12**, 8770–8776 (2021).
13. Gautam, C., Yadav, A. K. & Singh, A. K. A Review on Infrared Spectroscopy of Borate Glasses with Effects of Different Additives. *ISRN Ceram.* **2012**, 428497 (2012).
14. Lu, W.–D. *et al.* Ordered macroporous boron phosphate crystals as metal–free catalysts for the oxidative dehydrogenation of propane. *Chinese J. Catal.* **41**, 1837–1845 (2020).
15. Lu, W. D. *et al.* Supported Boron Oxide Catalysts for Selective and Lowerature Oxidative Dehydrogenation of Propane. *ACS Catal.* **9**, 8263–8270 (2019).
16. Venegas, J. M. Mechanistic Insights on the Oxidative Dehydrogenation of Light Alkanes Catalyzed by Boron–based Catalysts.
17. Shieh, M. D. & Lee, C. A more general structural model which includes the induction time for gas–solid reactions–II. *Chem. Eng. Sci.* **48**, 1851–1857 (1993).

Chapter 3. Prototypical Decomposition Reactions to Probe acid–base activity of oxyfunctionalized BN

Publication in preparation. Supplemental materials for Chapter 3 located in Appendix C.

3.1. Characterizing acido–basic reactivity of oxyfunctionalized BN via isopropanol decomposition

Boron oxides lack redox capabilities; thus, catalytic performance has often been characterized via surface acidity / basicity. Our current understanding of boron–based catalytic activity suggests that single active sites do not fully characterize the heterogeneous catalytic behavior.[1–4] Requirements for activity include surface mobility of BO within the oxyfunctionalized layer. Early attempts at site quantification have ultimately supported these recent understanding of the system. Colorio *et. al.* employed temperature programmed desorption and calometric techniques using NH_3, pyridine, and SO_2 probe molecules to examine B_2O_3 / Al_2O_3 catalysts and found no definitive correlation between acidity and the selective conversion of ethane to ethylene.[5–7] This is contrast to the number of studies on vanadia catalysts which correlate acidity to catalytic performance, despite disagreeing accounts.[8–11] Corma *et. al.* proposed that the acidity of the lattice O in V–Mg–O catalysts could describe catalytic selectivity, whereby increased nucleophilicity improved propylene selectivity.[12] Simply put, traditional adsorptive studies via NH_3, CO_2, and pyridine chemical probes have been attempted, but a good deal of ambiguity about boron–based catalytic performance remains.

Boron oxide is known to exhibit Lewis acidicity.[13,14] The formation of boric acid from the reaction of boron oxide and water is a well-known pathway that imparts weakly acidic properties to these boron-based catalysts.[5–7] The development of B-OH within the borate network and resulting -OH nests during the activation period illustrate that surface B-OH groups generated are not completely re-oxidized or dehydrated under reaction conditions. In fact, B-OH species have been show to participate in the reaction network through interactions with O_2 and interaction with neighboring B-OH sites.[15] Our goal therefore is to understand the role of acidity imparted by the oxyfunctionalized surface comprised of hydroxyl and bridging oxygen groups that may generally be described by $B(OH)_3O_{3-x}$ (where x = 0–3) and B-O-B.[1] Herein, we use the oxidation of isopropanol (IPA) to probe surface acidity of the oxyfunctionalized layer. Surface catalyzed IPA decomposition yields propylene via acid catalyzed dehydration or acetone via (redox) dehydrogenation, scheme 3.1.[16] This technique is widely used to measure acidity and redox properties of metal oxides and can enable discrimination between surface reaction pathways.[16–22]

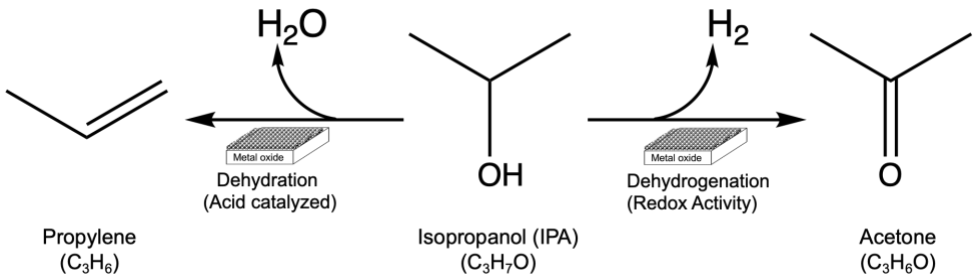

Scheme 3.1. Decomposition of isopropyl alcohol (IPA) on a metal oxide surface to propylene and H_2O via dehydration or acetone and H_2 via dehydrogenation.

This is also particularly useful in examining catalysts for the partial oxidation of alkanes since both pathways typically share surface alkoxide intermediates. Isopropoxides have been proposed as likely ODHP intermediates and may be relevant to in the formation of the olefin and observed oxygenates (e.g., acrolein, isopropanol, formaldehyde, etc.). Resini *et al.* presented evidence for ionic bonding of isopropoxy groups on highly acidic V_2O_5 / Al_2O_3 with perpendicular CO bonding to the surface, and covalent bonding and bent groups on V_2O_5 / SiO_2 via combined *in-situ* IR, UV-Vis, and Raman.[23] These isopropoxides are short lived under the high temperatures necessary for propane ODH and the reduced temperatures of IPA oxidation increases surface coverage of isopropoxy groups to enable spectroscopic observation of their decomposition pathways. Computational approaches by Lu et. al. suggest that oxyphilic B sites, particularly present in BO_3 coordination environments, may scavenge alkoxy radicals and prevent over-oxidation pathways in the ODH of ethane to ethylene.[24] From this perspective, observation of C-O scission pathways of surface alkoxides can also offer insights into the ODHP mechanism.

3.2 Catalytic IPA decomposition over oxyfunctionalized BN in flow-through reactor

IPA oxidation reaction were examined via flow-through reactor in the temperature range 200-350 ºC. A saturated feed of 5% O_2 / 4.7% IPA / bal. N_2 was contacted with 100 mg of catalyst in a quartz plug flow reactor and reaction products were

analyzed via on-line GC. Water was not quantified under these conditions. IPA conversion on spent BN decreased from 34% with 100% propylene selectivity to 7.7% conversion with 92.6% propylene and 7.4% acetone selectivity within 2 hrs, figure 3.1a. ODHP generated oxyfunctionalization exhibited a clear increase in acidic character, which initially exhibited nearly three times the rate of IPA consumption and IPA conversion compared to fresh BN. This acidity was immediately titrated as IPA dehydration proceeded, suggesting that the presence of O_2 did not quickly regenerate highly active sites. The main role of co-fed O_2 in the decomposition reactions of IPA has been proposed to be the prevention of reduction of the metal oxide.[16] Therefore, the transformation of the oxyfunctionalized surface is not merely due to reduction of surface species. Steady-state IPA conversion on spent BN was also lower than that of fresh BN. Although both fresh and spent BN likely share a similar concentration of sites that catalyze dehydration at steady-state, one explanation for the reduced activity on the spent material may be the proximity of those titrated sites. We expect that agglomeration of B-O species in the oxyfunctionalized layer provides adjacent sites for activation of IPA (e.g., bridging B-O-B sites), and that the decrease in activity may suggest that the proximity of the titrated sites may further inhibit activation of the alcohol.[2] As the overall reaction rate decreased on spent BN, there was a simultaneous increase in dehydrogenation and decrease in dehydration activity, figure 3.1b. The proportional relationship between $r_{propylene}$ / $r_{acetone}$ has been established as a useful index to relate dehydration and

dehydrogenation activity across catalysts.[18,25] The $r_{propylene}$ / $r_{acetone}$ value for spent BN (figure 3.1c) illustrate the drastic increase in dehydration reactivity on the oxyfunctionalized surface compared to fresh BN and to a 4 wt% V_2O_5/SiO_2. 4 wt% V_2O_5/SiO_2 was similarly examined, as the reactivity and selectivity of vanadia catalysts in ODHP have been attributed to their acidity.[8,9] The comparatively high $r_{propylene}$ / $r_{acetone}$ value for 4 wt% V_2O_5/SiO_2 surpasses steady state values for fresh and spent BN, but is nearly tripled by the initial oxyfunctionalized surface. This may suggest the intense acidification of the BN surface during ODHP conditions and may be one reason for the superiority of BN to vanadia catalysts under ODHP conditions.

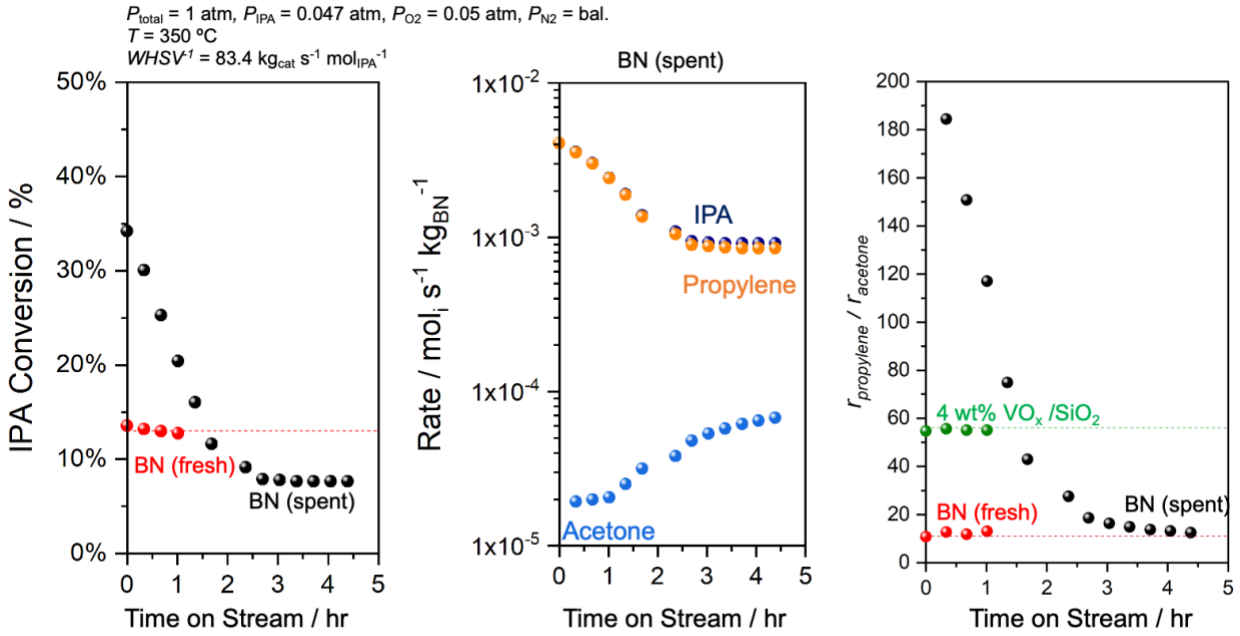

Figure 3.1. a) IPA conversion, b) reaction rates for IPA, acetone, and propylene, and c) the rate ratio of propylene to acetone as functions of time on stream for BN (fresh), BN (spent), and 4 wt% V_2O_5 / SiO_2 ("VO_x/SiO_2). Experiment done with saturated feed of 5% O_2 / 4.7% IPA / bal. N_2.

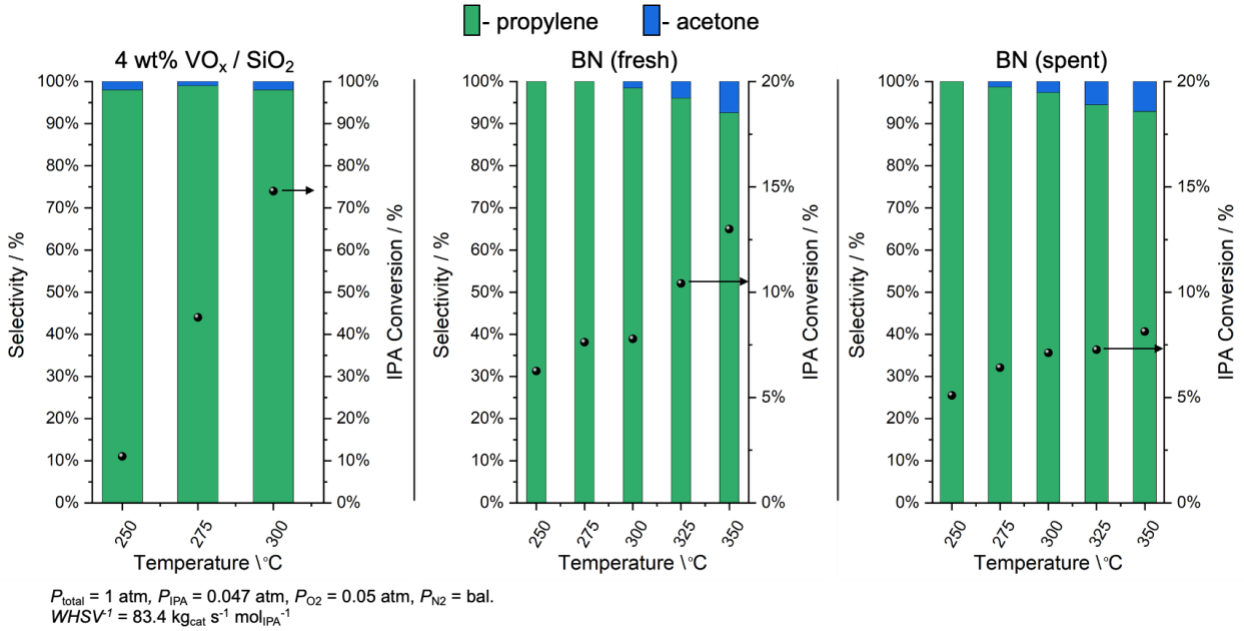

Figure 3.2. IPA conversion and selectivity to acetone and propylene as a function of temperature for 4 wt% V_2O_5 / SiO_2 ("VO_x/SiO_2) , fresh BN, and spent BN. Experiment done with saturated feed of 5% O_2 / 4.7% IPA / bal. N_2.

4 wt% V_2O_5 /SiO_2 showed significantly higher conversion and selectivity than fresh and spent BN at steady-state, reaching 20% IPA conversion at 250 ºC and 90% IPA conversion by 300 ºC (figure 3.2). 99% propylene selectivity was observed within this temperature range. This result agreed with high IPA dehydration activity reported for supported vanadia catalysts.[16,20,26] IPA conversion on fresh BN increased from 5 to 11% between 250 and 350 ºC. Propylene was the sole product observed for fresh BN below 300 ºC, and minor amounts of acetone (~4%) formed at and above 300 ºC. Spent BN increased in IPA conversion from 4.6 to 9% between 250 and 350 ºC. Although propylene was the main product at all temperatures examined, acetone was observed at 275 ºC. These results show that the titrated oxyfunctionalized surface lowered the temperature necessary for IPA dehydrogenation to acetone.

Steady-state product selectivities for fresh and spent BN samples were compared at isoconversion, table 3.1. Spent BN exhibited lower IPA consumption rate and higher selectivity to acetone than fresh BN. Reactions on the oxyfunctionalized surface result in lower concentration of active centers capable of carrying on the reaction. This may be attributed to the saturation of the surface with B-OH groups which may significantly reduce reactivity of to the alcohol. A computation study by Lu *et. al.* would suggest that adsorption / reaction of the alcohol or alkoxy radical (if present) as breaking the B-OH bond would be rate limiting.[24]

Table 3.1. Isoconversion comparison for fresh and spent BN at 300 ºC, at 1atm, with a feed composition of 5% O_2 / 4.7% IPA / bal. N_2. Less than 1% IPA conversion was observed on quartz chips (blank test) at 300 ºC, figure C.1.

	$-r_{IPA}$ /$mol_{IPA}\ s^{-1}\ kg_{BN}^{-1}$	X_{IPA} /%	$S_{propylene}$ /%	$S_{acetone}$ /%
BN (fresh)	9.6 E -4	4.8	98.3	1.7
BN (spent)	8.0 E -4	4.9	96.8	3.2

Hussein and Gates examined isopropanol adsorption and decomposition on Y_2O_3, which similar to B_2O_3 is a nonreducible oxide with a 3^+ oxidation state for Y, and proposed that metal oxides could bind alcohol molecules via coordination to Lewis acid sites and/or H bonding to molecule to the surface.[19] We adapted their scheme to describe isopropoxide formation over a BO_x surface given known hydroxyl and boroxyl functionalities in scheme 3.2. We expect the initial IPA reaction rate observed on the oxyfunctionalized surface to occur primary according to pathway 2 in scheme

3.2. The dissociative adsorption of IPA via the opening of boroxyl rings is expected to be highly reactive, as bridging O are known to be highly reactive oxygen species. In this scheme, the bridging O^{2-} species readily functions as a Lewis base which can easily perform H–abstractions and the resulting isopropoxide bonds with the adjacent (e^- deficient) B site. We propose that as path 2 proceeds, the accumulation of B–OH and reduced amounts of B–O–B limits surface reaction of isopropanol primarily to pathway 1, which only occurs on hydroxylated surfaces. This coincides with the reduced surface reactivity for IPA decomposition. The decreased rate of IPA decomposition suggests that the reaction between B–OH and IPA is rate limiting, pathway 1. Therefore, in the limit of high BOH coverage formation of surface alkoxides on the BO_x surface may also be limited.

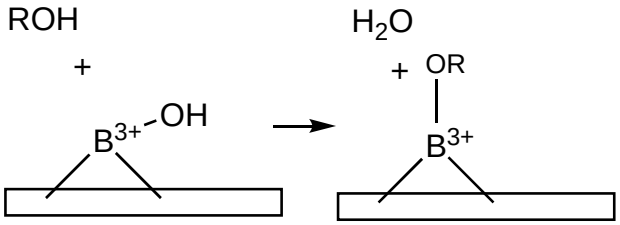

(1) only occurs on hydroxylated surfaces

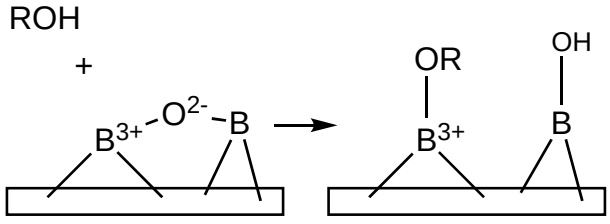

(2) dominant on dehydroxylated surfaces

Scheme 3.2. Proposed reactions between isopropanol on a (1) hydroxylated and (2) dehydroxylated BO_x surface to form isopropoxides.

Analysis of the liquid products from the IPA reactions via ^{1}H NMR(figure C2) also revealed the presence of formaldehyde (C_1) and acetaldehyde (C_2)oxygenates. This suggested that there may be surface C_3 alkoxides that are strongly bound to the surface that decompose via C–C scission. We examined the fate of these surface alkoxides as well as their formation via IPA decomposition on hydroxylated and dehydroxylated BO_x surface via *in–situ* Diffuse Reflectance Infrared FTIR Spectroscopy (DRIFTs).

3.3 Examining Temperature Programmed Decomposition of IPA on Oxyfunctionalized BN via *In–Situ* Drifts–MS

After flow–through IPA oxidation, the spent BN sample was examined via DRIFTs (figure 3.3) under 20% O_2 / Ar at 20 ºC. Major peaks at 3405 and 3218 cm^{-1} were attributed to ν(O–H). of adsorbed water and B–OH nests, respectively.[2] This agrees with the accumulation of B–OH species from the IPA reactions on spent BN. This also indicated that dehydration of adjacent BOH groups and/or the removal of BO–H via O_2 in the reaction feed were slow under the tested reaction conditions. Spent BN was subsequently dehydrated under oxidative conditions (20% O_2 / Ar) at 600 ºC for 3 hrs and cooled to 20 ºC in the *in–situ* DRIFTs cell to parallel dehydration conditions under ODHP temperatures. Surface dehydroxylation was observed by the relaxation in the 3600–3100 cm^{-1} region attributed to ν(O–H). Loss features at 3694, 3670 and 1236 cm^{-1} confirmed reductions in isolated B–OH stretching, adsorbed

water, and in plane B–OH stretching, respectively. We expect the primary surface dehydroxylation pathway under these conditions to proceed via condensation of adjacent >B–OH sites to generate B–O–B linkages.[27] This was supported by the increased intensity at 925 cm^{-1} and 1280–1015 cm^{-1} (broad) regions assigned to B–O out–of–plane bending and general BO functionalities respectively (e.g. 1238 cm^{-1} in–plane B–OH stretching and 1047 cm^{-1}symmetric stretching of B–O).

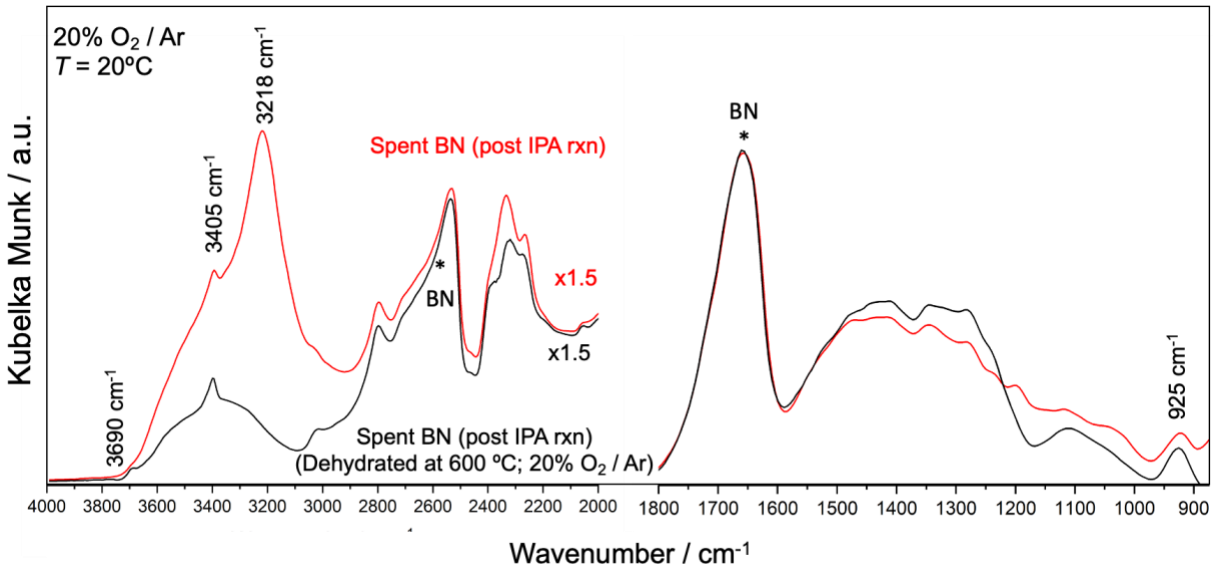

Figure 3.3. DRIFTs spectra of as–is and *in–situ* dehydrated oxyfunctionalized BN. Dehydration was carried out 600 ºC for 3 hrs under 20% O_2 / Ar. All spectra was recorded at 25 ºC and referenced to a blank mirror to observe all BN functionalities.

Adsorption of IPA was carried out by contacting the dehydrated spent BN with a saturated stream of 35.72 torr of IPA in O_2 / Argon. The cell was subsequently evacuated and refilled with pure Ar, figure 3.4. 2975, 2937, 2890 cm^{-1} correspond to ν_{as-CH3}, ν_{s-CH3}, and ν_{CH} vibration modes respectively for methyl groups and the αC–H bond of surface isopropoxy groups based on literature assignments for adsorbed alcoholates on boron surfaces.[28,29] Peaks observed at 3347, 3239, 1015,

and 953 cm^{-1} were assigned to the presence of some adsorbed alcoholates as B–O–R, in-plane B–OH bending, symmetric stretching of B–O, and out-of-plane B–O stretching, respectively. This observation agreed with the dissociative adsorption of IPA on dehydroxylated metal oxides to produce a surface isopropoxide and hydroxide.[16,19] Notably, isolated B–OH groups were consumed as confirmed by the loss feature at 3690 cm^{-1}. This can be attributed to an irreversible adsorption readily observed in the methoxylation of B–OH groups in methanol adsorption studies, illustrated path 1 of scheme 3.2.[28,30] Bands at1165 and 1130 cm^{-1} were assigned to ν_{C-O} and ν_{C-C} stretching modes indicative of terminal and bridged isopropoxides respectively.[19,31–34] Bridged isopropoxides were the dominant isopropoxide bonding orientation based on relative intensity to terminal bonded species.

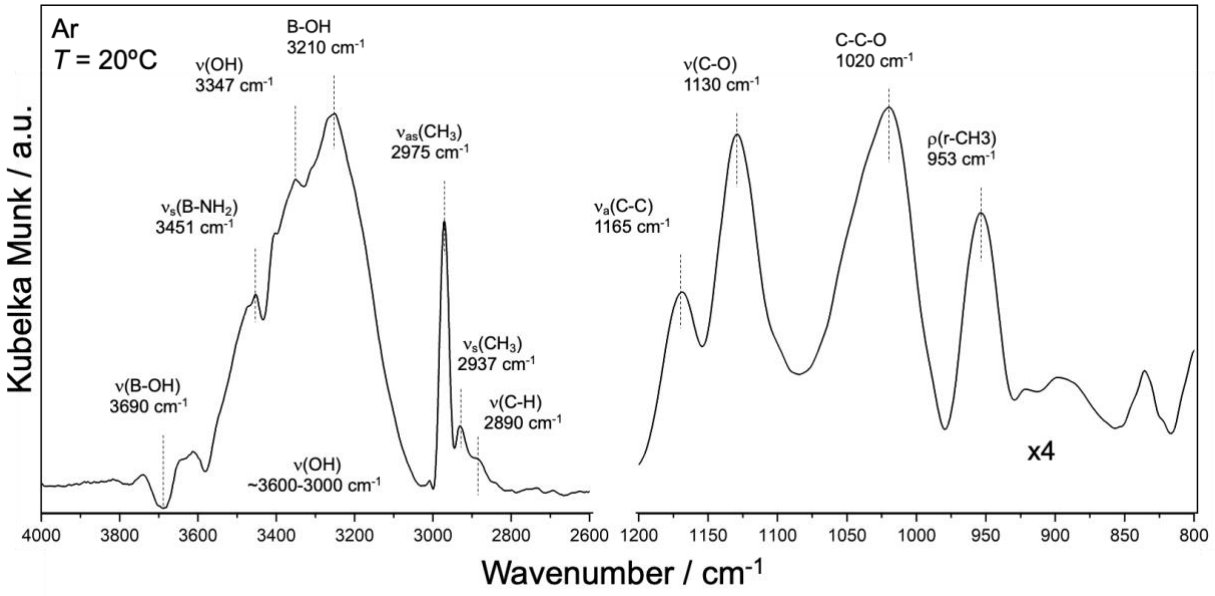

Figure 3.4. DRIFTs spectrum of IPA adsorbed on dehydrated spent BN at 20 ºC via saturated stream of 35.72 torr of IPA in O_2 / Argon. Cell was evacuated prior to analysis. Spectrum was recorded at 25 ºC and referenced dehydrated BN to observe adsorption functionalities.

Temperature program desorption (TPD) of the adsorbed IPA was then carried out by heating the sample to 400 ºC at 5ºC min^{-1} under oxidative conditions, figure 3.5. Three main temperature regions of reactivity were observed in DRIFTs spectra (figure 3.5a): 25 to 47 ºC, 47 to 150 ºC, 180 to 280 ºC. The first region featured signal major signal increases at 1685 and 806 cm^{-1} corresponding to $\nu_{C=O}$ and sp2 alkene C–H bending. H_2O at 1628 cm^{-1} were also observed. This initial range appears to correlate with the initial product TPD curves, figure 3.5b. Between 47 to 150 ºC, major signal increases in the H– interacting –OH groups in the 3600–3200 cm^{-1} were observed and contributed to the continued production of H_2O. Within this region activity was specifically observed for adsorbed water and B–OH groups at 3415 and 3257 cm^{-1}. Isolated B–OH signal was significantly diminished at 3690 cm^{-1} in this temperature range. Activity from isopropoxy groups was marked by intense signal increases at 2974, 1165, 1130, 1018, and 952 cm^{-1} attributed CH_3, bridged isopropoxide, terminal isopropoxide, interactions between the isopropoxy group and B–O surface, and methyl rocking modes respectively. Notably, 1020 cm^{-1} has also been proposed for B–C vibrational modes.[35] The signal for terminal isopropoxides rapidly diminished compared to the bridged isopropoxides. This agreed with Hussein and Gates finding that the bridged isopropoxides were more thermally stable than the terminal isoproxides.[19] In this temperature range propylene, acetone, and H_2O were all observed. A significant amount of desorbed IPA was observed consistent

with molecular adsorption of the alcohol to the surface. Propylene and water reach their respective maxima at 70 ºC. CO_2 and acetone display two maxima, one at 70 ºC and the other at 138 ºC. Terminal isopropoxide initially contributed to the production of propylene and water, while the bridged and molecular alcohol contribute to acetone and CO_2 via slower decomposition. This was in agreement with previous studies that propose absorbed IPA and/or terminal isopropoxides contribute readily to the dehydration product, while bridged isopropoxides contribute to the dehydrogenation product.[19,34] Above 180 ºC, another dehydration event is observed involving adsorbed H_2O and B–OH in the 3600–3200 cm^{-1} region, accompanied by the desorption of H_2O at 1628 cm^{-1} and isolated B–OH consumption. Notably, the signal at 1165 is diminished and 1130 cm^{-1} is the only signal observed in this temperature range. Similarly, the signal interactions between the isopropoxy group and B–O surface at 1018 cm^{-1} was no longer observed. The negative signal of 1685 cm^{-1} suggests significant elimination of acetone at this temperature range. Major signal increases at 931, 784, and 653 cm^{-1} were attributed to sp2 CH bending related to propylene. Dissociated IPA occurred via B–O–B to produce isopropoxy groups with neighboring hydroxyl group. Dissociated IPA occurred via B–OH via H_2O elimination. Assignments for isopropoxy groups on TiO_2 suggest that 1130 cm^{-1} indicated the strongly bonded dissociated IPA, while 1293 and 1252 cm^{-1} indicated strongly and weakly bound non-dissociated IPA.[31] This is in line with the increased thermal stability of bridged isopropoxides observed. Coordination of molecular IPA

to the surface was observed via weak signal at 1247 cm^{-1} in figure 5a. This has also been proposed to indicate coordination between IPA and Lewis acid sites. Carboxylate intermediates (1675, 1368, 1245 cm^{-1}) between 60 and 160 ºC were observed.[36] CO_2 adsorption studies by Kock et. al. on Y_2O_3, which similarly hydroxylates easily, show the high concentrations of mono- and bi- dentate bicarbonate species.[36]

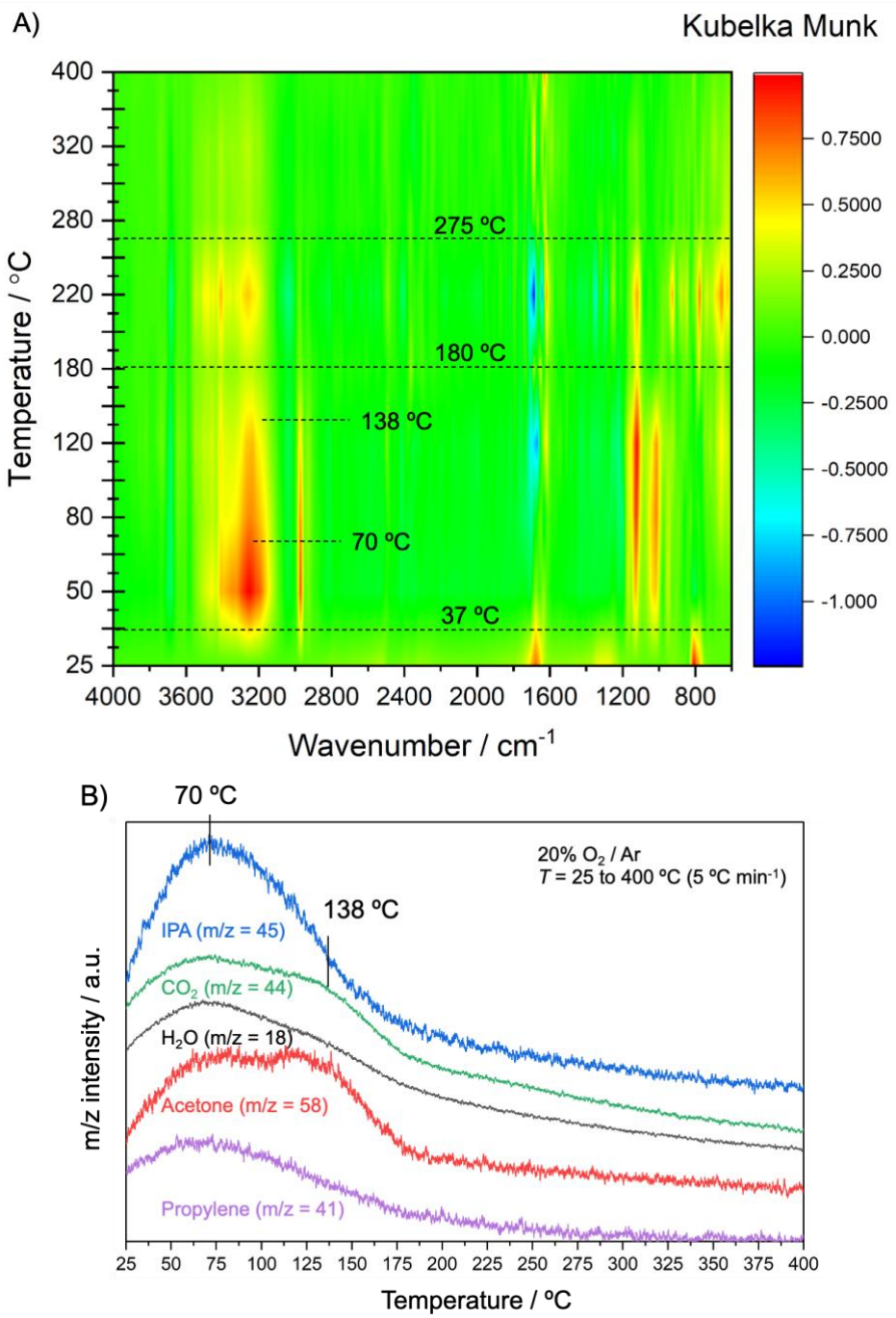

Figure 3.5. a) Contour plot of DRIFTs spectra and b) MS signals for temperature programmed desorption of IPA adsorbed on dehydrated spent BN. TPD was examined from 25 to 400 ºC at 5ºC min^{-1} under oxidative conditions.

Catalytic decomposition of IPA was carried out at 350 ºC using *in–situ* DRIFTs on another oxyfunctionalized spent BN samples (figure 3.6) and then paused to examine

surface reactions. Notably, introduction of IPA increased both isolated B–OH (3690 cm^{-1}) and B–O functionality (3358 cm^{-1}). After IPA is flushed, these B–O species persists and the B–OH signal increased due to continued surface reactions of isopropoxy groups observed via signals at 1165, 1129 and 1082 cm^{-1}. Activity related to formation of CO_2 (2357 and 2347 cm^{-1}) and water (1652 cm^{-1}) persisted alongside continued activity in the hydroxyl region 3600–3200 cm^{-1}. At approximately 90 mins, signal for surface adsorbed water at 3427 cm^{-1} diminished. These results evidence the accumulation of B–OH nests from IPA reactions and their thermal stability under oxidative conditions at 350 ºC. Acetone formation can also be observed by the persistence of C=O (1701 cm^{-1}) and (1280 cm^{-1}) signals. Dehydrogenation of the isopropoxide occurs with highly hydroxylated BO_x and coincided with the persistence of strongly bound bridged isopropoxides.

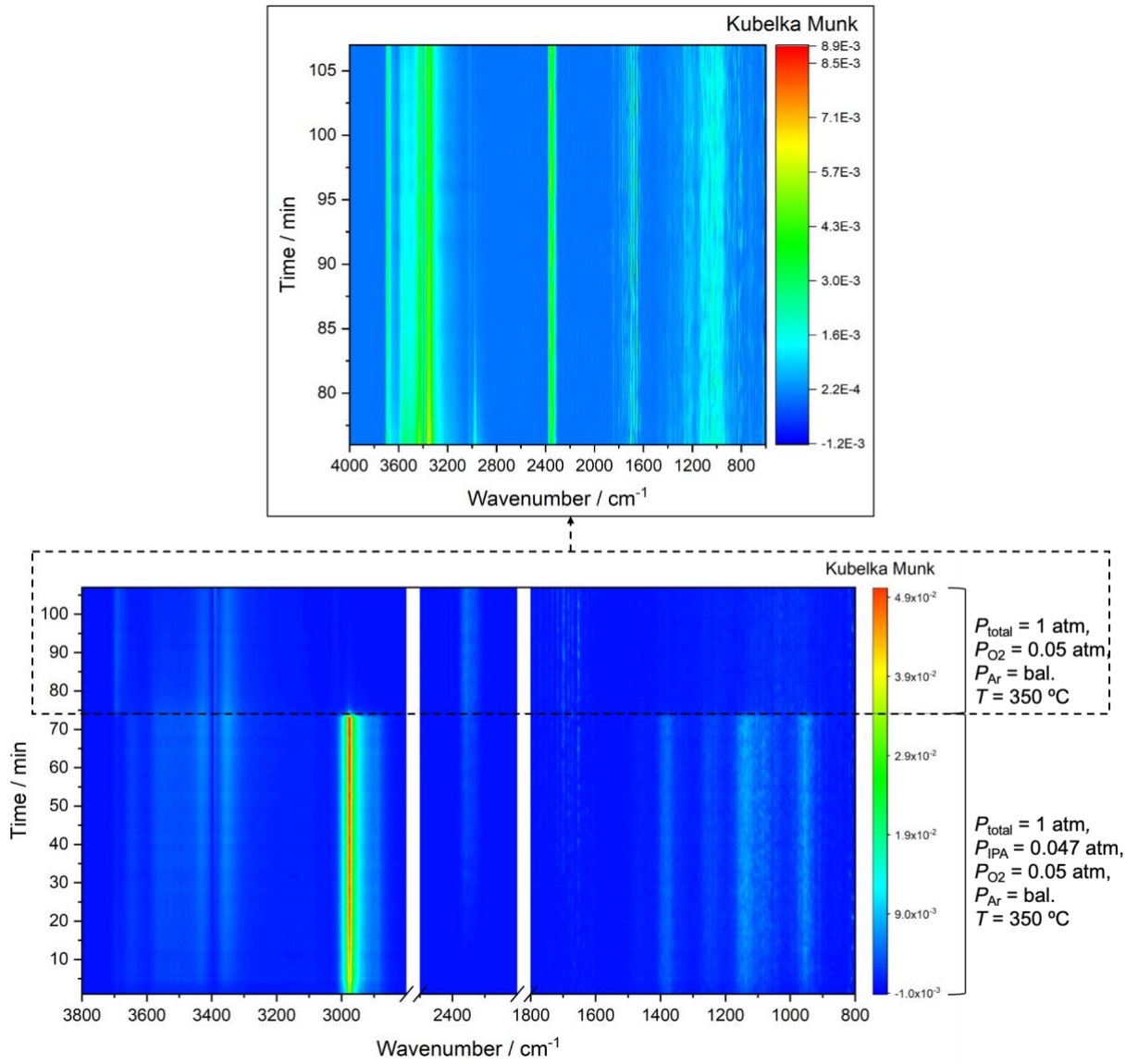

Figure 3.6. Contour plot DRIFTs spectra for *in-situ* continuous flow IPA decomposition on spent BN at 350 ºC under with saturated feed of 5% O_2 / 4.7% IPA / bal. Ar. and under oxidative conditions 5% O_2 / bal. Ar (inset plot). Gaseous isopropanol can be observed primarily in 3000–2800 cm^{-1} region via C–H stretching. Oxyfunctionalized BN sample was held at 350 ºC for 1hr prior to introduction of IPA following the protocol for IPA decomposition via flow through reactor.

3.4 Discussion of IPA interactions with oxyfunctionalized BN

Decomposition of IPA on oxyfunctionalized BN proceeds primarily through dehydration of the IPA. Increasing B–O–B connectivity formed in the BO_x via ODHP

driven agglomeration, creates Lewis acidic B^{3+} centers and Lewis basic O^{2-} centers. The acid–base pair allow for facile dissociative adsorption of IPA via facile O–H scission on reactive adsorbed O. Typically, alcohols undergo O–H scission and then ß–H elimination, which is typically observed as the rate limiting step.[37] Herein, ß–H elimination by the adjacent hydroxyl groups was in fact the rate limiting step under dehydroxylated conditions. However, increased hydroxylation may make the initial adsorption of IPA on B–OH a slow step. B–OH groups are weakly acidic (pKa ~ 9.2), but more acidic than isopropanol (pKa ~16.5). In this case, BOH may behave as a Brønsted acid and donate a proton to the alcohol and the system will pass through an alkyloxonium intermediate, rather than perform O–H scission. There are numerous reaction steps available to the ion from there (scheme C.4), however, the most likely scenario is still the formation of an isopropoxide via pathway 1 in scheme 3.2. Additionally, the competitive reactions of water with BOH may further inhibit the adsorption of IPA. From this we can observe the difference in strongly bound O in B–O–B (Lewis basic / Brønsted basic) and BOH (Brønsted acidic). Adsorbed O has been shown to greatly improve the reactivity of noble metals to alcohols, where it may act as a Brønsted base and initiate the alcohol activation via O–H scission.[38–41] This behavior was observed by B–O–B units which readily performed O–H cleavage. It has also been shown that more weakly bound O species could more readily contribute to dehydrogenation on O/Ag(110) vs. O/Cu(110).[40] Similarly, a difference in reactivity of BOB and BOH in dehydration and dehydrogenation was observed.

Surface reactions proceeds through terminal and bridge bonded isopropoxide intermediates, as well as minor amounts of adsorbed molecular alcohol. Terminal isopropoxides were readily decomposed at much lower temperatures than bridge bonded groups and contributed primarily to the early formation of propylene and some acetone. This suggests that C–O scission is preferred over B–O scission for these terminal isopropoxides. This agrees with previous assertions for the decomposition of terminal isopropoxide groups contributing to the dehydration product. The more thermally stable bridge bonded isopropoxides decomposed to acetone via subsequent C–H scission. In this case, the regeneration of O^{2-} species occurred through the C–H scission of the ß–H by adjacent hydroxyl groups and the subsequent formation of B–O–B and $H_{2(g)}$. Acetone is then readily desorbed via a favorable B–O scission resulting in the thermodynamically stable BO_3 site. The different strengths of adsorption illustrate how increased hydrogen bonding via accumulated BOH can contribute readily to dehydrogenation products albeit through a slower reaction pathway. Proximity of the hydroxyl groups (isolated B–OH or H–interacting B–OH) would then play an important role in the formation of the dehydration or dehydrogenation product. A summary of these proposed reaction pathways can be observed in scheme 3.3.

The formation of strongly bound isopropoxide groups, represented by B–OR, has implications for the catalyst reactivity as well. These strongly bound and thermally stable surface alkoxides may react to form carboxylate species, which can readily decompose via C–C scission (pathways 5 and 6, scheme 3.3).[42,43] This is supported by FTIR observations of the carboxylate formation, and NMR of the reaction liquid products showing the presence of C_1 and C_2 oxygenates. B–OR sites may also contribute to a decrease in surface reactivity as they appear to be highly thermally stable and may hinder (sterically or through site occupation) the adsorption of IPA to the surface. Lu *et. al.* proposed via DFT calculation that formation and surface reactions of boron alkoxides favor the olefin product and avoid homogeneous combustion of the alkoxy radical.[24] Herein, we observe that these surface reactions can also contribute to strongly bound alkoxides that can undergo C–O scission or subsequent C–H scission. We also observe the combustion of alkoxides that are too strongly bound to the surface.

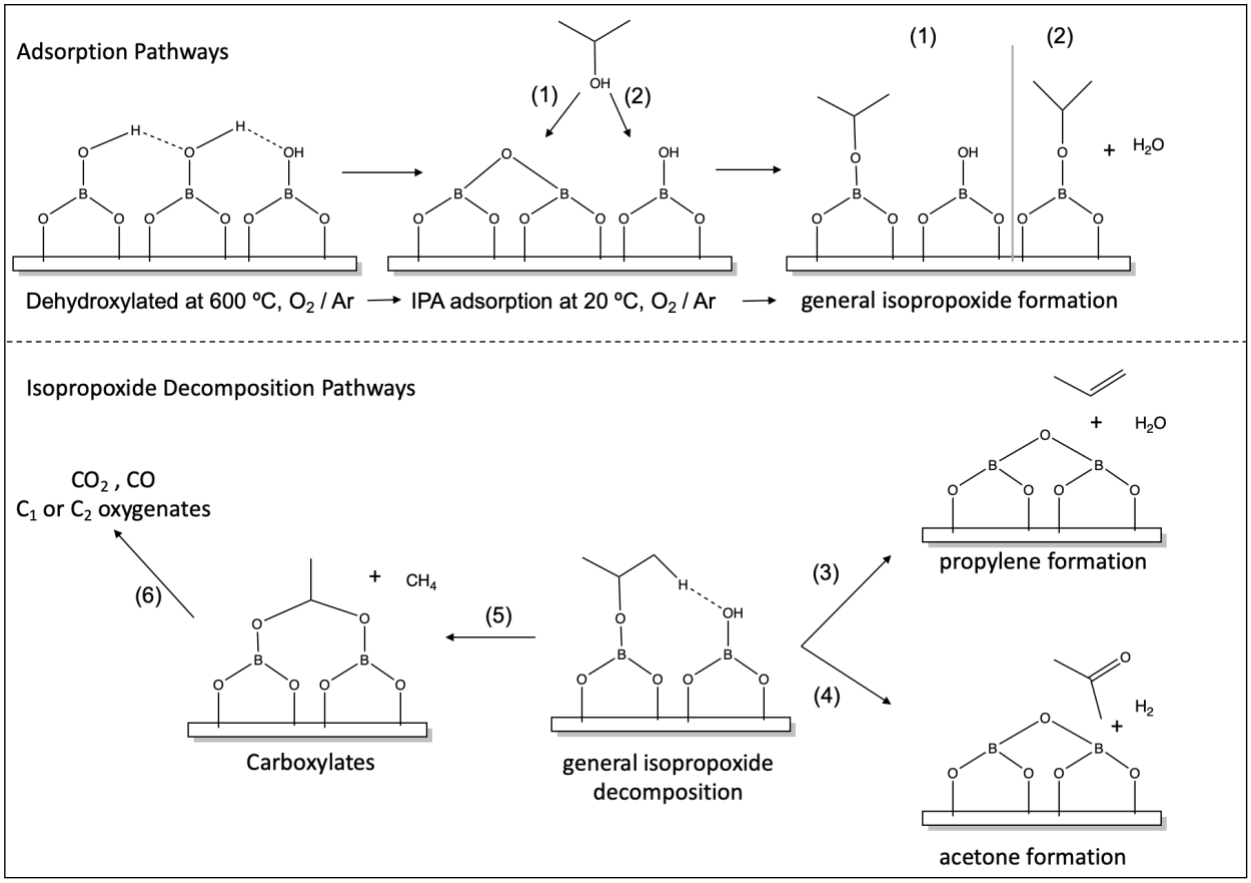

Scheme 3.3. Proposed pathways for the adsorption of IPA on BO_x surface represented primarily by B–O–B and B–OH groups and the subsequent decomposition pathways to propylene, acetone, and C_1 and C_2 oxygenates.

3.5 Probing weakly acidic oxyfunctionalized BN via decomposition of formic acid

We observe a simultaneous decrease in IPA reactivity on oxyfunctionalized BN and increase in weakly acidic surface saturated with BOH (Brønsted acid). The weak surface acidity of boron oxide supported catalysts have been previously reported, although no clear correlations to reactivity have been identified. Bautista *et. al.* studied the acidity of B_2O_3 catalysts supported on $AlPO_4$ and Al_2O_3 and proposed that both systems had a mix of Brønsted and Lewis acidity at all boria loadings, and

Brønsted acidity increased with increasing boria content.[44] Colorio *et. al.* showed an increase in weaker acid sites via ammonia microcalorimetry when boria was added in excess of a monolayer and that subsequent agglomeration of boron oxides exhibited the acidity of bulk boron oxide.[5–7,45] Correlations for surface reaction pathways for acid–catalyzed IPA decomposition can be ambiguous for materials with low surface acidity. To overcome this, we examined the decomposition of formic acid over oxyfunctionalized BN to further probe surface acidity. Formic acid (FA) decomposition has been widely studied as a basic probe catalytic activity on metal oxides and has been shown to be a particularly useful prototypical reaction for low acidic (and highly basic) catalysts where the IPA index loses correlation.[25] FA decomposition similarly proceeds via a dehydration pathway to CO and H_2O, and a dehydrogenation pathway to CO_2 and H_2, scheme 3.4. Dehydrogenation activity of FA to CO_2 has also been shown to correlate strongly with basicity of metal oxide catalysts and are consistent with basic chemical probe chemisorption studies.

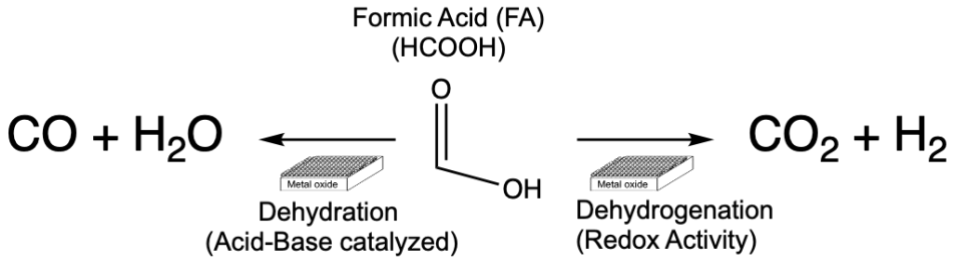

Scheme 3.4. Decomposition of formic acid (FA) on a metal oxide surface to CO and H_2O via dehydration or CO_2 and H_2 via dehydrogenation.

It is commonly proposed that decomposition of IPA on metal oxides occurs via acid sites.[18,25,46] For nonreducible oxides IPA dehydrogenation has been proposed to occur via adjacent acid and base sites. In the case of FA, which donates a proton to the metal oxide to produce formate intermediates and surface hydroxyl groups, it is commonly proposed that dehydrogenation occurs over basic sites. Using FA, a strong reducing agent, we increased the BOH concentration and probe the surface reactivity at saturation coverages of B–OH on oxyfunctionalized BN.

3.6 Catalytic FA decomposition in flow-through reactor

Herein, we further investigated the acid–base capabilities of the oxyfunctionalized surface via formic acid (FA) decomposition via continuous flow reactivity. A saturated feed of 4.7% FA/ bal. N_2 was contacted with 100 mg of catalyst in a quartz plug flow reactor and reaction products were analyzed via on-line GC. H_2 and water were not quantified under these conditions. FA reaction rates for both fresh and spent BN, at 300 ºC, exhibited transient periods of ~1hr, figure 3.7a. This is notably shorter than the transient period observed in IPA oxidation. During this period, FA reaction rate decreased from 3.28 x 10^{-3} to 2.9 x 10^{-3} mol_{HCOOH} s^{-1} kg_{cat}^{-1} on fresh BN, suggesting the titration of certain active species. One explanation of this would be the generation of B–OH_2 species on isolated B–OH sites, which may further react with FA to generate BH or B–OR species that may be inactive. FA reaction rate initially decreased, then increased on spent BN from 2.5 x 10^{-3} to 2.9 x 10^{-3} mol_{HCOOH}

s^{-1} kg_{cat}^{-1}. This is in line with the initial decrease in activity during the accumulation of B–OH and steady-state reactivity at saturation coverage of BOH previously proposed for IPA oxidation. Our hypothesis from IPA oxidations was that the accumulation of BOH groups decomposed IPA via hydroxyl nests. These hydroxyl nests primarily performed dehydration of IPA with some increase in dehydrogenation activity. Therefore, we would expect the specific increase in BOH using a strong acid like FA to achieve the similar result and contribute to the dehydration reactivity. The rate of CO to CO_2 formation, r_{CO} / r_{CO2}, was used to compare dehydration to dehydrogenation reactivity for fresh and spent BN, figure 3.7b. r_{CO} / r_{CO2} remained near constant at ~ 1.25 for fresh BN and grew from ~2.25 to 4.5 for spent BN during the 1hr transient period. Within the transient period the oxyfunctionalized surface is expected to reach BOH saturation, and indeed this resulted increased the relative dehydration reactivity observed.

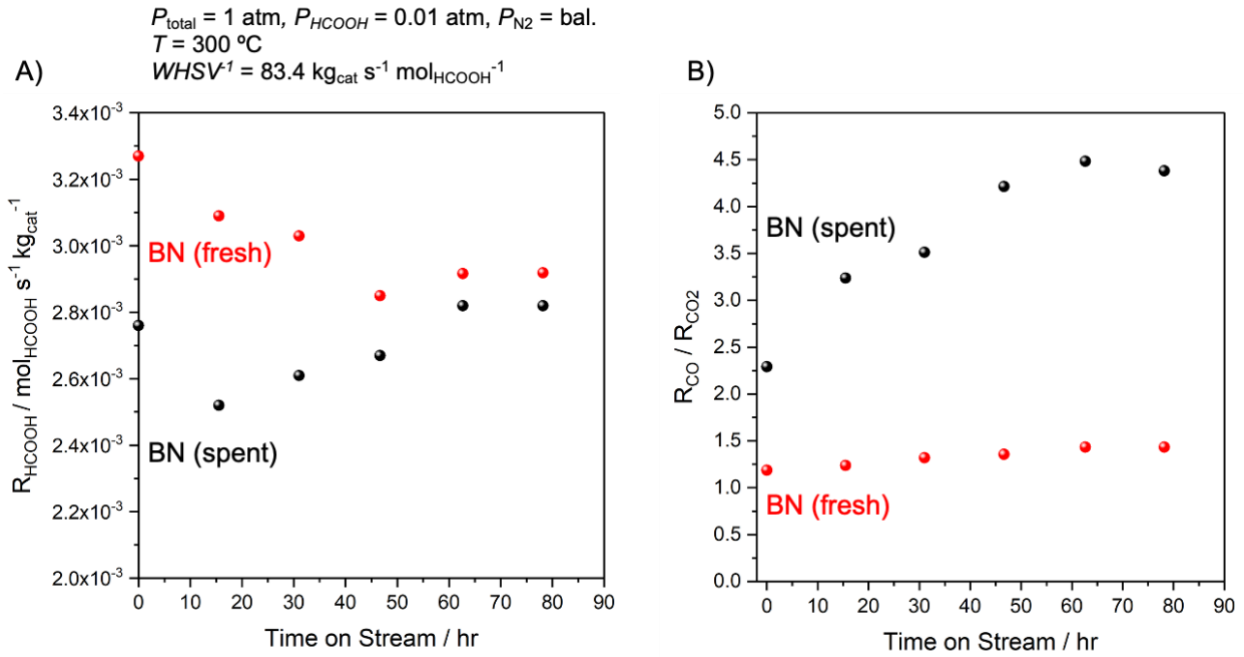

Figure 3.7. a) FA reaction rate and b) rate ratio of CO to CO_2 for fresh and spent BN as a function of time on stream at 300 °C.

The rate of FA decomposition for both fresh and spent BN converges on 2.9 x 10^{-3} mol_{HCOOH} s^{-1} kg_{cat}^{-1}. Active species on both surface exhibit similar reactivity, but the relative concentration of species and likely their proximity to one another exhibit vastly different product distributions.. This is illustrated by the product selectivities observed at isoconversion, table 3.2. Approximately 20% FA conversion yields 58.2% and 81% selectivity to CO on fresh and spent BN respectively.

Table 3.2 Isoconversion comparison of fresh and spent BN measured at 300 °C, 5% FA / N_2.

Sample	X_{HCOOH} / %	S_{CO2} / %	S_{CO} / %
BN (fresh)	19.92	41.8	58.2
BN (spent)	19.69	19	81

We expect FA to protonate B–O–B and B–OH to >BOH and >B–OH_2 groups respectively. From these results, we see that the proximity and/or concentration of these BOH groups drastically impacts the product selectivity. An increase in the hydroxyl nests, appears to favor C–O scission of the surface formate or molecular formic acid. To further probe surface reactions in the presence of BOH groups, we examined formate decomposition using DRIFTs–TPD–MS. Additionally, we aimed to understand whether H–COOH, HCOO–H, and/or HCO–OH were dissociated by the surface. Compared to the proposed C–H, O–H, and C–OH bond breaking steps, C=O (740 kJ mol^{-1}) is extremely energy intensive and was not considered.[47–49]

3.7 DRIFTs study of FA surface reactions on oxyfunctionalized BN

Adsorption of FA was carried out by contacting dehydrated spent BN with a saturated stream of 35.72 torr of FA in Argon in an *in–situ* DRIFTs cell. The cell was subsequently evacuated, figure 3.8. As expected, significant increase in isolated B–OH and H–bonded B–OH groups were observed at 3690 and 3213 cm^{-1} respectively. 3447, 2745, and 842 cm^{-1} correspond to non–structural interlayer water (H–O–H symmetric and asymmetric vibrations), –OH vibrations, and vibrations for surface hydroxyls respectively.[50] These peaks reflect the generation of interlayer H_2O and B–OH_2 species. 2950 cm^{-1} correspond to δCH stretching for H bonded molecular formic acid.[51] Peaks at 2484 and 2434 cm^{-1} were assigned to $CO_{2\ (g)}$. Asymmetric stretching of adsorbed CO_2 was observed at 2365 cm^{-1}. 1710 and 1165 cm^{-1} were

assigned to the asymmetric and symmetric CO_2 vibrations for carboxylate species.[52] The dull shoulder at 1657 cm^{-1} and an associated signal at 1398 cm^{-1} were assigned respectively to asymmetric and symmetric stretching of bicarbonate species at very low concentrations.[36] 1606 and 1258 cm^{-1} were assigned symmetric and asymmetric O–C–O vibrations. $\Delta = \nu_s(OCO) - \nu_{as}(OCO)$ can be used to differentiate between bidentate bridged (Δ~250–190 cm^{-1}) or monodentate formate species (Δ > 300 cm^{-1}). The calculated value of 348 cm^{-1} suggests the formation of monodentate species. This agrees with the computational work of Nurazar *et. al.*, where DFT calculations and simulated IR spectra show formic acid dissociation on carbon doped BN nano–cages preferentially forms monodentate formate bound to B sites.[53] These monodentate species were the dominant surface species. Faint shoulders at 2945, 2885, and 1655cm^{-1} can also be assigned to asymmetrical formate species coordinated to Lewis acid sites.[51]

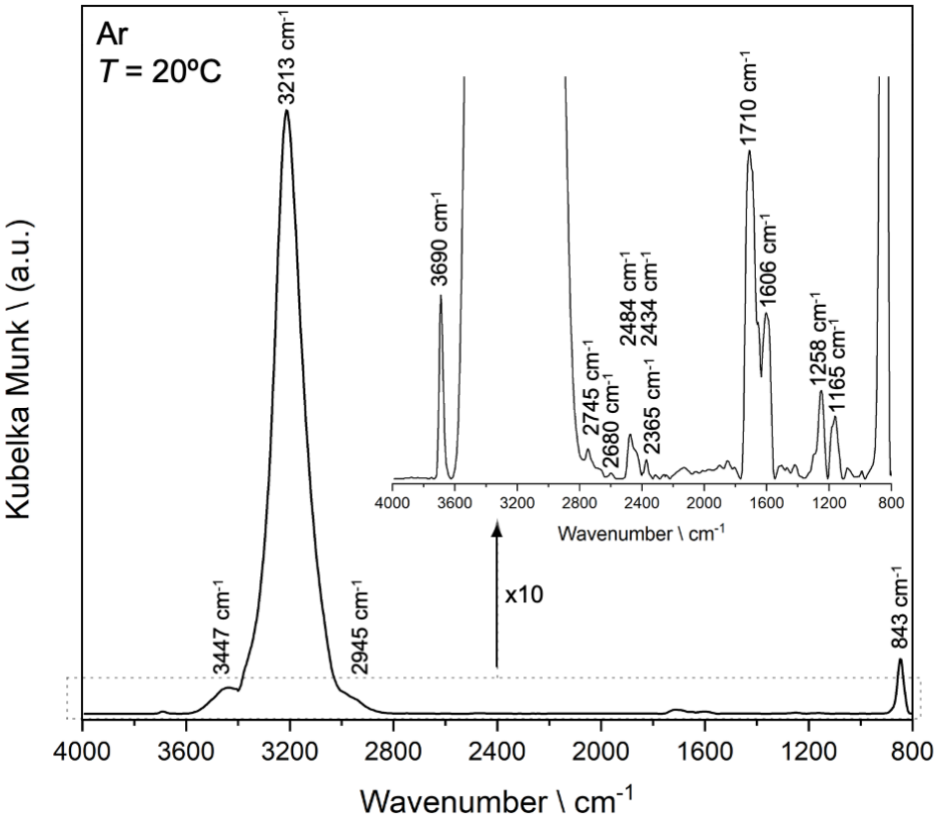

Figure 3.8. DRIFTs spectrum of FA adsorbed on dehydrated spent BN at 20 ºC via saturated stream of 35.72 torr of FA in Argon. Cell was evacuated prior to analysis. Spectrum was recorded at 25 ºC and referenced to dehydrated BN to observe adsorption functionalities.

The dissociation of formic acid to BOH and monodentate formate is reminiscent of the terminal isopropoxide as the main adsorption mode for IPA adsorbed on the oxyfunctionalized surface. These observations agree with the oxyphilicity of the tri-oxygenated B sites which prefer the formation of B–O–C bonds rather than B–C. Notably, the 1020 cm^{-1}, which may be assigned to B–C or C–OH stretching was also absent. We may expect that surface reactions may proceed through B–O bond breaking rather than C–O bonds, as C–O bonds are stronger than B–O bonds (1076 and 806 kJ mol^{-1} respectively).[54] Catalytic FA reactions suggest that C–O scission

readily occurs and contributes to high rates of CO formation. This may be partially due to a favorable BO–OCH scission of surface formates.

TPD–MS was then carried out under Ar from 20 to 400 ºC at 5 ºC min^{-1}, figure 3.9. The desorption of water was observed upon heating as the OH region 3400–3200 cm^{-1} increased in intensity and relaxed between 20 and 70 ºC. Similarly, surface hydroxyl groups at 842 cm^{-1} are active in this temperature range. Dehydration of B–OH was the main contributors to this as 3273 cm^{-1} exhibited the highest intensity during in the temperature range. In–plane B–OH (3341 cm^{-1}) and isolated B–OH sites (3690 cm^{-1}) similarly contributed and were diminished by 70 ºC. These peaks contribute to H_2O as the first major observed in the TPD curve, figure 3.9b, with a maximum peak at 70 ºC. Minor amounts of CO_2 were also produced in this temperature range and begins slightly after the production H_2O began. Increasing signals for $CO_{2(g)}$ (2493 and 2445 cm^{-1}) and $CO_{2(ads)}$ (2385 and 1070 $cm^{-}1$) contribute to this observation.[36] These signals coincide with the significant increase in the formate signal at 1614 cm^{-1}. We expect formate decomposition to be the main contributor to the CO_2, as no desorbed molecular formic acid was observed. Both formate and CO_2 signals appear around 60 ºC and persist up to 400 ºC. An inverse relationship in the signals can be observed as formate decreases slightly in intensity and CO_2 signal increases—this is best observed at 100 ºC in the DRIFTs contour map. This agreed with formate as a reactive intermediate on other metal

surfaces and the rate limiting step being the decomposition of formate.[53] Bands at 3443 and 3339 cm^{-1} reappear when the formate signal is most intense. This suggests that surface H_2O and hydroxyl species are formed participate in the decomposition of formate. After 70 ºC H_2O decreased steadily up to 400 ºC, with a shoulder at 110 ºC which coincides with the diminishing 3443 and 3339 cm^{-1} bands. CO_2 quickly became the main product observed with maxima at 145 ºC, 161 ºC, and 250 ºC, suggesting that there is a variety adsorbed formate species with different desorption energies. Notably, after 160 ºC the signal at 1686 cm^{-1} is significantly diminished suggesting the disappearance of C=O. Similarly, above this temperature 3400 cm^{-1} band reappears suggesting the accumulation of adsorbed H_2O and other hydroxyls between 3900–3600 cm^{-1}. H_2 and CO products were formed in minor amounts between 120 and 220 ºC, with maxima at 161 ºC.

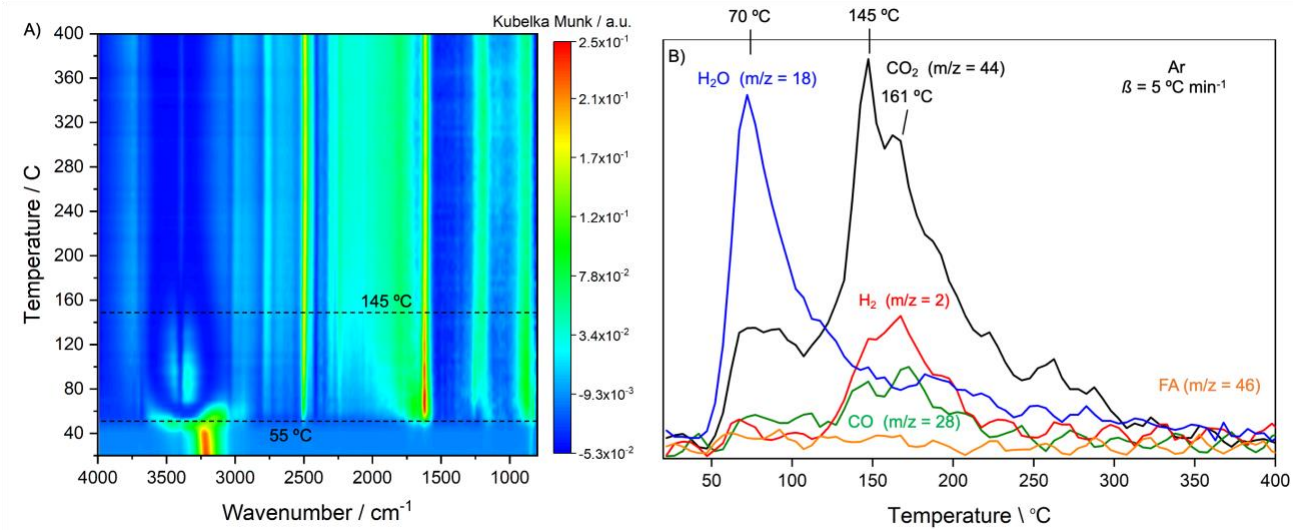

Figure 3.9. a) Contour plot of DRIFTs spectra and b) MS signals for temperature programmed desorption of FA adsorbed on dehydrated spent BN. TPD was examined from 20 to 400 ºC at 5ºC min^{-1} under non-oxidative conditions.

Dissociative adsorption of formic acid did not occur via C–OH scission in appreciable amounts as CO_2 was the main product observed. However, C–OH scission cannot be ruled out entirely as CO was observed in minor amounts. The persistent signals in the C–H region 3000–2800 cm^{-1} during the TPD were combination modes of C–H and C–O stretching (primarily at 2984 cm^{-1}).[55] This also suggested that the C–H scission of formic acid may not have occurred appreciably in the adsorption. Notably, minor amount of monodentate carbonate intermediates (1675, 1368, 1245 cm^{-1}) were also observed between 60 and 160 ºC.[36] Therefore, dissociation of HCOO–H was more likely than H–COOH and HCO–OH in the adsorption of FA and the ß–H–abstraction occurred subsequently via surface reactions. This is consistent with the reaction of surface bound alkoxides in the IPA study.

3.8 Discussion of FA interactions with oxyfunctionalized BN

Dehydration and subsequent dehydrogenation are the two distinct reaction pathways observed in the TPD curves. All major signals associated with the B–OH and adsorbed water are drastically diminished early in the temperature ramp. We propose that these dehydration steps include the ß–H cleavage of adsorbed formate. Strong H–bonding of within the BOH nests would suggest that the adjacent hydroxyl groups and ß–H have strong interactions. Dehydration of the BOH and an adjacent formate ultimately generate CO_2. CO_2 may initially be stabilized as a carboxylate briefly on B–O groups, or immediately desorb into the gas phase alongside water. This would

account for the early smaller CO_2 peaks. Thermally stable formate (at 1614 cm^{-1}) slowly decomposed to CO_2 suggesting that they are strongly bound, particularly after the dehydration steps. Coelution of CO_2 and H_2 suggests dehydrogenation pathways are present. One such pathway may be the formation H–abstraction from formate via B–O–B linkages which are expected to have formed after the initial dehydration. The reappearance of the band at 3440 cm^{-1} could then be attributed to the formation of bridging hydroxyl groups or water.[56] Fully describing the complex reaction network for the decomposition of formate requires further experimentation. However, a simplified model for the pathways observed and a viable path to the generation of the main products CO_2 and H_2 is described by scheme 3.5.

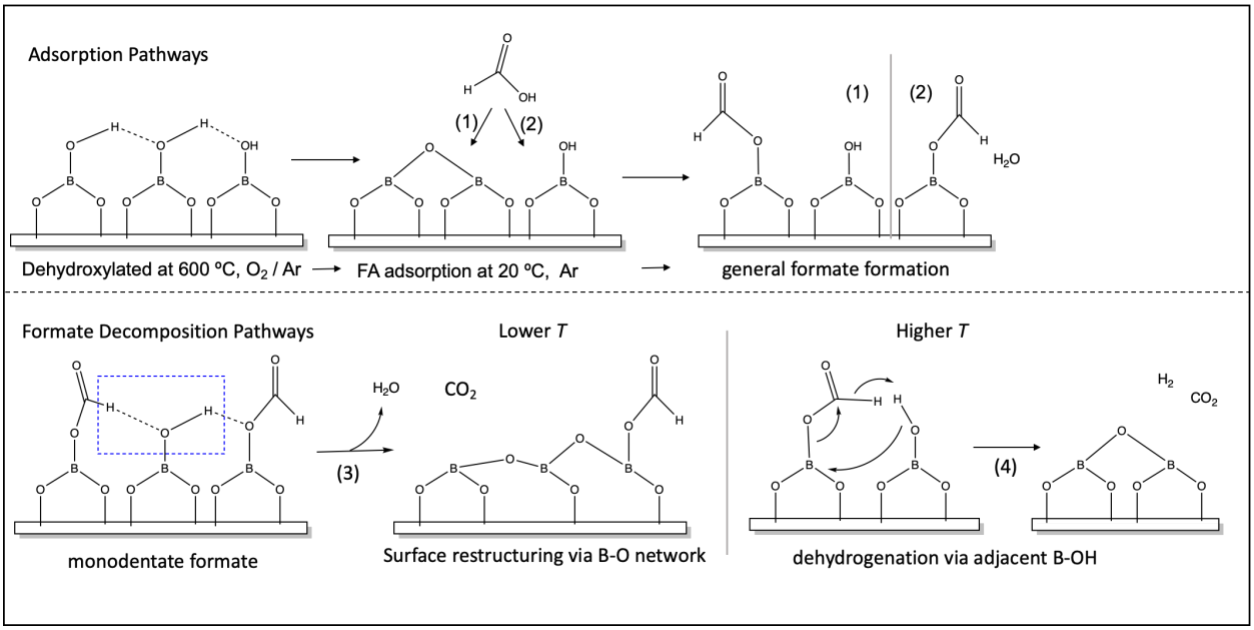

Scheme 3.5. Proposed pathways for the adsorption of FA on BO_x surface represented primarily by B–O–B and B–OH groups and the subsequent decomposition pathways to main products H_2O, CO_2 and H_2

These results show that the surface reactions over BO_x proceed via dehydrogenation, particularly at higher temperatures. Strongly bound formate, similar to strongly bound isopropoxides, undergo dehydrogenation steps at higher temperatures. In the case of FA decomposition, the major observation of CO_2 is also in line with CO desorption energy being relatively higher than CO_2.[57] Contrastingly, the flow through reactions for both FA and IPA decomposition indicate that the BO_x layer proceeds via dehydration reactions primarily. For both reactions, the O–H bond is initially broken in the adsorption of the molecule to the surface and generally C–O scission is a favored pathway. This agrees with the relative bond strengths of B–O and C–O bonds and the ability for the borate network to restructure to accommodate addition electrons from O bonds. In the case of FA decompositions, TPD experiments do not account for the stable surface complexes formed between formic acid and formate, which also been proposed.[56] This could suggest that CO formation on spent BN may be associated with homogeneous reactions and/or interactions between adsorbed intermediates and formic acid. Both studies indicate that terminally bonded alkoxides are readily formed on the oxyfunctionalized surface and are the primary reactive intermediates. The preference for C–O cleavage is in line with Lu *et. al.* proposal that the oxyphilicity of thermodynamically stable BO_3 can readily react with alkoxy radicals and produce olefins from the surface alkoxide intermediate. These studies offer insight into the role of surface alkoxides in the overall product selectivity in BN catalyzed ODHP.

3.9 References

1. Love, A. M. *et al.* Probing the Transformation of Boron Nitride Catalysts under Oxidative Dehydrogenation Conditions. *J. Am. Chem. Soc.* **141**, 182–190 (2019).
2. Love, A. M. *et al.* Synthesis and Characterization of Silica-Supported Boron Oxide Catalysts for the Oxidative Dehydrogenation of Propane. *J. Phys. Chem. C* **123**, 27000–27011 (2019).
3. Grant, J. T. *et al.* Boron and Boron-Containing Catalysts for the Oxidative Dehydrogenation of Propane. *ChemCatChem* **9**, 3623–3626 (2017).
4. Venegas, J. M. *et al.* Selective Oxidation of n -Butane and Isobutane Catalyzed by Boron Nitride. *ChemCatChem* **9**, 2118–2127 (2017).
5. Colorio, G. C., Bonnetot, B., Vedrine, J. C. & Auroux, A. Characteristics of Alumina Boria Catalysts Used in Ethane Partial Oxidation. *Stud. Surf. Sci. Catal.* **82**, 143–149 (1994).
6. Colorio, G. C., Auroux, A. & Bonnetot, B. Calorimetric Study of the Acidity of Alumina-Boria Catalysts by Gaseous Ammonia Adsorption. *J. Therm. Anal.* **38**, 2565–2573 (1992).
7. Colorio, G., Védrine, J. C., Auroux, A. & Bonnetot, B. Partial Oxidation of Ethane Over Alumina-Boria Catalysts. *Appl. Catal., A* **137**, 55–68 (1996).
8. Blasco, T., Nieto, J. M. L., Dejoz, A. & Vazquez, M. I. Influence of the Acid-Base Character of Supported Vanadium Catalysts on Their Catalytic Properties for the Oxidative Dehydrogenation of n-Butane. *J. Catal.* **157**, 271–282 (1995).
9. López Nieto, J. M. *et al.* Selective Oxidation of n-Butane and Butenes over Vanadium-Containing Catalysts. *J. Catal.* **189**, 147–157 (2000).
10. Fu, Y. *et al.* Characterization and reactivity of SnO2-doped V2O5/ɣ-Al2O3 catalysts in dehydrogenation of isobutane to isobutene. *J. Mol. Catal. A Chem.* **221**, 163–168 (2004).
11. Moggi, P., Morselli, S., Lucarelli, C., Sarzi-Amadè, M. & Devillers, M. Vanadium and niobium mixed-oxide catalysts obtained via sol-gel: preparation and catalytic behaviour in oxidative dehydrogenation of propane. in *Oxide Based Materials* (eds. Gamba, A., Colella, C. & Coluccia, S. B. T.-S. in S. S. and C.) **155**, 427–439 (Elsevier, 2005).
12. Corma, A., Nieto, J. M. L. & Paredes, N. Influence of the Preparation Methods of V-Mg-O Catalysts on Their Catalytic Properties for the Oxidative Dehydrogenation of Propane. *J. Catal.* **144**, 425–438 (1993).
13. Zhao, L.-Y., Chen, J.-Y., Li, W.-C. & Lu, A.-H. B2O3: A heterogeneous metal-free Lewis acid catalyst for carbon dioxide fixation into cyclic carbonates. *J. CO2 Util.* **29**, 172–178 (2019).
14. Sivaev, I. B. & Bregadze, V. I. Lewis acidity of boron compounds. *Coord. Chem. Rev.* **270–271**, 75–88 (2014).
15. Shi, L., Wang, D. & Lu, A.-H. A viewpoint on catalytic origin of boron nitride in oxidative dehydrogenation of light alkanes. *Chinese J. Catal.* **39**, 908–913 (2018).
16. Kulkarni, D. & Wachs, I. E. Isopropanol oxidation by pure metal oxide catalysts: number of active surface sites and turnover frequencies. *Appl. Catal. A Gen.* **237**, 121–137 (2002).
17. Rekoske, J. E. & Barteau, M. A. Kinetics and selectivity of 2-propanol conversion on

oxidized anatase TiO2. *J. Catal.* **165**, 57–72 (1997).
18. Ai, M. The Oxidation Activity and Acid–base Properties of Mixed Oxide Catalysts Containing Titania. I. The TiO2–MoO3 and TiO2–V2O5 Systems. *Bull. Chem. Soc. Jpn.* **49**, 1328–1334 (1976).
19. Hussein, G. A. M. & Gates, B. C. Surface and Catalytic Properties of Yttrium Oxide: Evidence from Infrared Spectroscopy. *J. Catal.* **176**, 395–404 (1998).
20. Sun, Q., Fang, D., Wang, S., Shen, J. & Auroux, A. Structural, acidic and redox properties of V2O5/NbP catalysts. *Appl. Catal. A Gen.* **327**, 218–225 (2007).
21. Luis, G. Isopropanol adsorption–oxidation over V2O5—A mass spectrometry study. *J. Mol. Catal. A Chem.* **247**, 31–35 (2006).
22. Zhu, J. H., Dong, J. & Xu, Q. Decomposition of isopropanol: A sensitive probe reaction to reveal the influence of zeolite on the catalytic function of supported Pt. *React. Kinet. Catal. Lett.* **63**, 67–73 (1998).
23. Resini, C., Montanari, T., Busca, G., Jehng, J.–M. & Wachs, I. E. Comparison of alcohol and alkane oxidative dehydrogenation reactions over supported vanadium oxide catalysts: in situ infrared, Raman and UV–vis spectroscopic studies of surface alkoxide intermediates and of their surface chemistry. *Catal. Today* **99**, 105–114 (2005).
24. Liu, Z. *et al.* Understanding the Unique Antioxidation Property of Boron–Based Catalysts during Oxidative Dehydrogenation of Alkanes. *J. Phys. Chem. Lett.* **12**, 8770–8776 (2021).
25. Ai, M. Activities for the decomposition of formic acid and the acid–base properties of metal oxide catalysts. *J. Catal.* **50**, 291–300 (1977).
26. Meira, D. M., Cortez, G. G., Monteiro, W. R. & Rodrigues, J. A. J. Vanadium oxides supported on hydrotalcite–type precursors: the effect of acid–base properties on the oxidation of isopropanol . *Brazilian Journal of Chemical Engineering* **23**, 351–358 (2006).
27. Saha, S. *et al.* Syntheses, characterization and reactivity of Lewis acid–base adducts based on B–N dative bonds. *J. Organomet. Chem.* **745–746**, 329–334 (2013).
28. Takezawa, N. & Kobayashi, H. On the CH stretching bands of surface alcoholates formed on metal oxides—A reply to Morrow, Thomson and Wetmore. *J. Catal.* **28**, 335–336 (1973).
29. Baraton, M. I., Merle–Mejean, T., Quintard, P. & Lorenzelli, V. Surface characterization by FT–IR spectroscopy of an aerogel precursor to cordierite. *J. Phys. Chem.* **94**, 5930–5934 (1990).
30. Baraton, M. I., Merle, T., Quintard, P. & Lorenzelli, V. Surface activity of a boron nitride powder: a vibrational study. *Langmuir* **9**, 1486–1491 (1993).
31. Barakat, C., Gravejat, P., Guaitella, O., Thevenet, F. & Rousseau, A. Oxidation of isopropanol and acetone adsorbed on TiO2 under plasma generated ozone flow: Gas phase and adsorbed species monitoring. *Appl. Catal. B Environ.* **147**, 302–313 (2014).
32. Rossi, P. F., Busca, G., Lorenzelli, V., Saur, O. & Lavalley, J. C. Microcalorimetric and FT–IR spectroscopic study of the adsorption of isopropyl alcohol and hexafluoroisopropyl alcohol on titanium dioxide. *Langmuir* **3**, 52–58 (1987).
33. Bensitel, M., Moraver, V., Lamotte, J., Saur, O. & Lavalley, J.–C. Infrared study of

alcohols adsorption on zirconium oxide: reactivity of alkoxy species towards CO2. *Spectrochim. Acta Part A Mol. Spectrosc.* **43**, 1487–1491 (1987).

34. Hussein, G. A. M., Sheppard, N., Zaki, M. I. & Fahim, R. B. Infrared spectroscopic studies of the reactions of alcohols over group IVB metal oxide catalysts. Part 1.—Propan-2-ol over TiO2, ZrO2 and HfO2. *J. Chem. Soc. Faraday Trans. 1 Phys. Chem. Condens. Phases* **85**, 1723–1741 (1989).
35. Romanos, J. *et al.* Infrared study of boron–carbon chemical bonds in boron-doped activated carbon. *Carbon N. Y.* **54**, 208–214 (2013).
36. Köck, E. M., Kogler, M., Bielz, T., Klötzer, B. & Penner, S. In Situ FT-IR Spectroscopic Study of CO2 and CO Adsorption on Y2O3, ZrO2, and Yttria-Stabilized ZrO2. *J. Phys. Chem. C. Nanomater. Interfaces* **117**, 17666 (2013).
37. Montemore, M. M., van Spronsen, M. A., Madix, R. J. & Friend, C. M. O2 Activation by Metal Surfaces: Implications for Bonding and Reactivity on Heterogeneous Catalysts. *Chem. Rev.* **118**, 2816–2862 (2018).
38. Ayre, C. R. & Madix, R. J. The adsorption and reaction of 1,2-propanediol on Ag(110) under oxygen lean conditions. *Surf. Sci.* **303**, 279–296 (1994).
39. Barnes, C., Pudney, P., Guo, Q. & Bowker, M. Molecular-beam studies of methanol partial oxidation on Cu(110). *J. Chem. Soc. Faraday Trans.* **86**, 2693–2699 (1990).
40. Wachs, I. E. & Madix, R. J. The selective oxidation of CH3OH to H2CO on a copper(110) catalyst. *J. Catal.* **53**, 208–227 (1978).
41. Liu, X., Madix, R. J. & Friend, C. M. Unraveling molecular transformations on surfaces: a critical comparison of oxidation reactions on coinage metals. *Chem. Soc. Rev.* **37**, 2243–2261 (2008).
42. Hussein, G. A. M. Formation, characterization, and catalytic activity of gadolinium oxide. Infrared spectroscopic studies. *J. Phys. Chem.* **98**, 9657–9664 (1994).
43. Zaki, M. I. & Sheppard, N. An infrared spectroscopic study of the adsorption and mechanism of surface reactions of 2-propanol on ceria. *J. Catal.* **80**, 114–122 (1983).
44. Bautista, F. M. *et al.* Acidity and catalytic activity of AlPO4–B2O3 and Al2O3–B2O3 (5–30wt% B2O3) systems prepared by impregnation. *Appl. Catal. A Gen.* **170**, 159–168 (1998).
45. Cucinieri-Colorio, G., Bonnetot, B., Védrine, J. C. & Auroux, A. New developments in selective oxidation II. In Cortés Corberán V, Vic Bellón S (eds). *Elsevier Sci. Publ.* 143 (1994).
46. Columbia, M. R. & Thiel, P. A. The interaction of formic acid with transition metal surfaces, studied in ultrahigh vacuum. *J. Electroanal. Chem.* **369**, 1–14 (1994).
47. Ruscic, B. Active Thermochemical Tables: Sequential Bond Dissociation Enthalpies of Methane, Ethane, and Methanol and the Related Thermochemistry. *J. Phys. Chem. A* **119**, 7810–7837 (2015).
48. Gribov, L. A., Novakov, I. A., Pavlyuchko, A. I., Kulago, I. O. & Orlinson, B. S. “Spectroscopic” Calculations of CH Bond Dissociation Energies for Ethane, Propane, Butane, Isobutane, Pentane, Hexane, and Neopentane Using Fundamental Vibration Frequencies. *J. Struct. Chem. 2003 446* **44**, 961–969 (2003).
49. Takanabe, K. & Iglesia, E. Mechanistic Aspects and Reaction Pathways for Oxidative Coupling of Methane on Mn/Na 2 WO 4 /SiO 2 Catalysts. *J. Phys. Chem. C* **113**,

10131–10145 (2009).
50. Krukowski, E. G. *et al.* FT-IR study of CO2 interaction with Na+ exchanged montmorillonite. *Appl. Clay Sci.* **114**, 61–68 (2015).
51. Popova, G. Y., Andrushkevich, T. V, Chesalov, Y. A. & Stoyanov, E. S. In situ FTIR Study of the Adsorption of Formaldehyde, Formic Acid, and Methyl Formiate at the Surface of TiO2 (Anatase). *Kinet. Catal.* **41**, 805–811 (2000).
52. Collins, S. E., Baltanás, M. A. & Bonivardi, A. L. Infrared spectroscopic study of the carbon dioxide adsorption on the surface of Ga2O3 polymorphs. *J. Phys. Chem. B* **110**, 5498–5507 (2006).
53. Esrafili, M. D. & Nurazar, R. Metal-Free Decomposition of Formic Acid on Pristine and Carbon-Doped Boron Nitride Fullerene: A DFT Study. *J. Clust. Sci.* **26**, 595–608 (2015).
54. Cottrell, T. L. *The strengths of chemical bonds*. (Butterworths Scientific Publications, 1958).
55. Ito, K. & Bernstein, H. J. THE VIBRATIONAL SPECTRA OF THE FORMATE, ACETATE, AND OXALATE IONS. *Can. J. Chem.* **34**, 170–178 (1956).
56. Kabay, N. & Bryjak, M. Chapter 9 - Boron Removal From Seawater Using Reverse Osmosis Integrated Processes. in (eds. Kabay, N., Bryjak, M. & Hilal, N. B. T.-B. S. P.) 219–235 (Elsevier, 2015). doi:https://doi.org/10.1016/B978-0-444-63454-2.00009-5
57. Agrawal, K., Roldan, A., Kishore, N. & Logsdail, A. J. Dehydrogenation and dehydration of formic acid over orthorhombic molybdenum carbide. *Catal. Today* **384–386**, 197–208 (2022).
58. Yu, J. & Savage, P. E. Decomposition of Formic Acid under Hydrothermal Conditions. *Ind. Eng. Chem. Res.* **37**, 2–10 (1998).

Chapter 4. Probing Homogeneous Reactions in Oxidative Dehydrogenation of Propane over Oxyfunctionalized BN

Publication in preparation.

Section 4.2 was adapted in part from the following publication:

Venegas, J. M.; Zhang, Z.; **Agbi, T. O.;** McDermott, W. P.; Alexandrova, A.; Hermans, I. Why Boron Nitride Is Such a Selective Catalyst for the Oxidative Dehydrogenation of Propane. *Angew. Chemie Int. Ed.* **2020**, *59* (38), 16527–16535.

Personal contributions to publication: Experimental data collection for the kinetic control of O_2 on reaction products (figure 4.2). Refining microkinetic model reaction steps. Data interpretation.

4.1. Mechanisms for partial oxidation of alkanes on boron-based catalysts

B_2O_3 is often classified as a non-reducible catalyst. Non-reducible metal oxides like MgO and CaO have been shown to be highly effective catalyst for the oxidative coupling of methane (OCM) and selective in the partial oxidation of alkanes.[1] Amongst this class of catalysts, many exhibit radical homogeneous reactions that contribute to the overall reactivity and product selectivity.[2–6] Our previous reaction studies have evidenced, in the absence of mass or heat transfer limitations, have evidenced this radical mediated hetero-homogeneous mechanism for the partial oxidation of light alkanes over oxyfunctionalized BN.[7–12] This observation agrees with proposed mixed mechanisms for B_2O_3 / Al_2O_3 catalysts in the oxidation of ethane to acetaldehyde and ethylene, and the oxidation of propane to propylene.[13–20] The early works of Murakami *et. al.*, Colorio *et. al.*, and Buyevskaya *et. al.* suggested that the

B_2O_3 could generate alkyl radicals which desorb from the catalyst surface and further react to products, scheme 4.1.

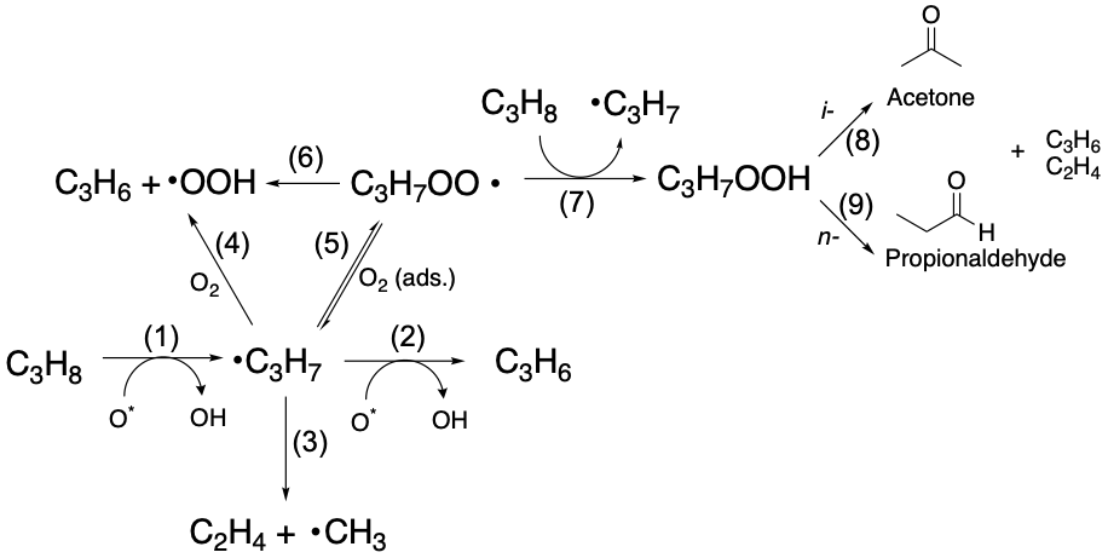

Scheme 4.1. Adapted reaction mechanism for the partial oxidation of propane over supported boron oxide catalysts as proposed by Hatano *et. al.* (1991) and later Buyevskaya *et. al.* (1996). Reaction pathways are numbered in parenthesis.

H–abstraction from propane via activated surface oxygen species (O*) was proposed as an initial step in this mechanism. The early assumption of B_2O_3 catalysts was that they followed the initial step for propane activation proposed for several vanadia catalysts like Corm *et. al.* proposed mechanism for V–Mg–O catalysts.[21] The redox active VO_x catalysts proceed via Mars–van Krevelen (MvK) mechanism. In this mechanism, the alkane undergoes sequential H–abstractions on the catalyst surface and reduced surface is rapidly reoxidized via dissociatively adsorbed O_2. The result is a first order dependence of the propane reaction rate on P_{alkane} and a zero order dependence on P_{O2}. [22–24] However, on boron oxides the subsequent desorption of the propyl radical was considered one of many differentiating factors between boron

oxide catalysts and vanadia catalysts. The propyl radical undergoes decomposition via C–C scission to ethylene and a methyl radical or subsequent H–abstraction via surface or gas phase reaction pathways to propylene. As such, boron oxide catalysts proceed via a different mechanism than VO_x. Murakami and Buyevskaya observed non–linear (i.e., supralinear) relationship between the reaction rate and P_{alkane} and Langmuir type adsorption of model for O_2.[13] These studies laid fairly strong ground work for us to investigate the reactivity of BN. Importantly, our extensive high field SSNMR, XAS, XPS, DRIFTs, and Raman studies have shown that that oxyfunctionalized layer differs from B_2O_3 and $B(OH)_3$ standards although they share similar borate networks.[25–27] In other words, we endeavored to specifically examine and confirm the reaction dynamics of oxyfunctionalized BN. To date, our studies on BN support these findings as we observe a second order rate dependence on P_{alkane} and a 0.25 order rate dependence on P_{O2}.[12,28–30] These observations suggested that oxyfunctionalized BN proceeded via an Eley–Rideal (ER) mechanism which describes reactions between chemisorbed and gas phase reactants.[31,32] Under this mechanism, the desorption of the propyl radical and homogeneous propagation reactions have been understood to be integral to propylene. Herein, we probed the reaction pathways of the propyl radical as a function of O_2 in BN catalyzed ODHP.

4.2. Examining the role of O_2 in homogeneous reaction pathways

Reactions of the propyl radical are primary determinants in the observed product selectivity. Following scheme 4.1, the propyl radical may undergo unimolecular

thermal cracking wherein the C–C bond is broken to produce ethylene and a methyl radical—the unselective pathway. The propyl radical may also undergo further H–abstraction via molecular O_2 (gas phase) or activated surface oxygen species (O^*) (surface reaction) to form propylene, and either HOO• or surface OH respectively. It is also possible, as shown in scheme 4.1, that reactions between the propyl radical and O_2 may form alkylperoxides (QOOH) which may further react to produce a variety of oxygenates. Experimental observations of O_2 reactions with *n*– and *i*– propyl radicals and ethyl radicals via photolysis of C_3H_7–I, by Estupinan *et. al.*, show H–abstraction from both propyl radicals to form propylene and HO_2 was favored over the QOOH formation above 477 ºC.[33] We can conclude from this study that increasing T and P_{O2} favor propylene formation from the pool of propyl radicals generated according to scheme 4.1.

Under fuel rich conditions we expect pathways 1 and 7 in scheme 4.1 to be examined, where propane may be activated via homogeneous propagation steps. Note that pathway 7 may also occur between propane and HOO•. Under fuel lean conditions we limit the activation of propane primarily to the surface O* species in pathway 1. We examined the rate of propylene and ethylene formation as a function of P_{O2} under fuel rich (25% propane) and fuel lean (15% propane) conditions, figure 4.1a and 4.1b respectively. The dependence of propylene formation on P_{O2} was

positive under both conditions, supporting a positive correlation. The dependence of ethylene formation on P_{O2} was negative under both conditions, supporting a negative correlation. This result suggests that pathways 3 and 4 are indeed present on oxyfunctionalized BN and a simplified scheme can be represented by figure 4.1c.

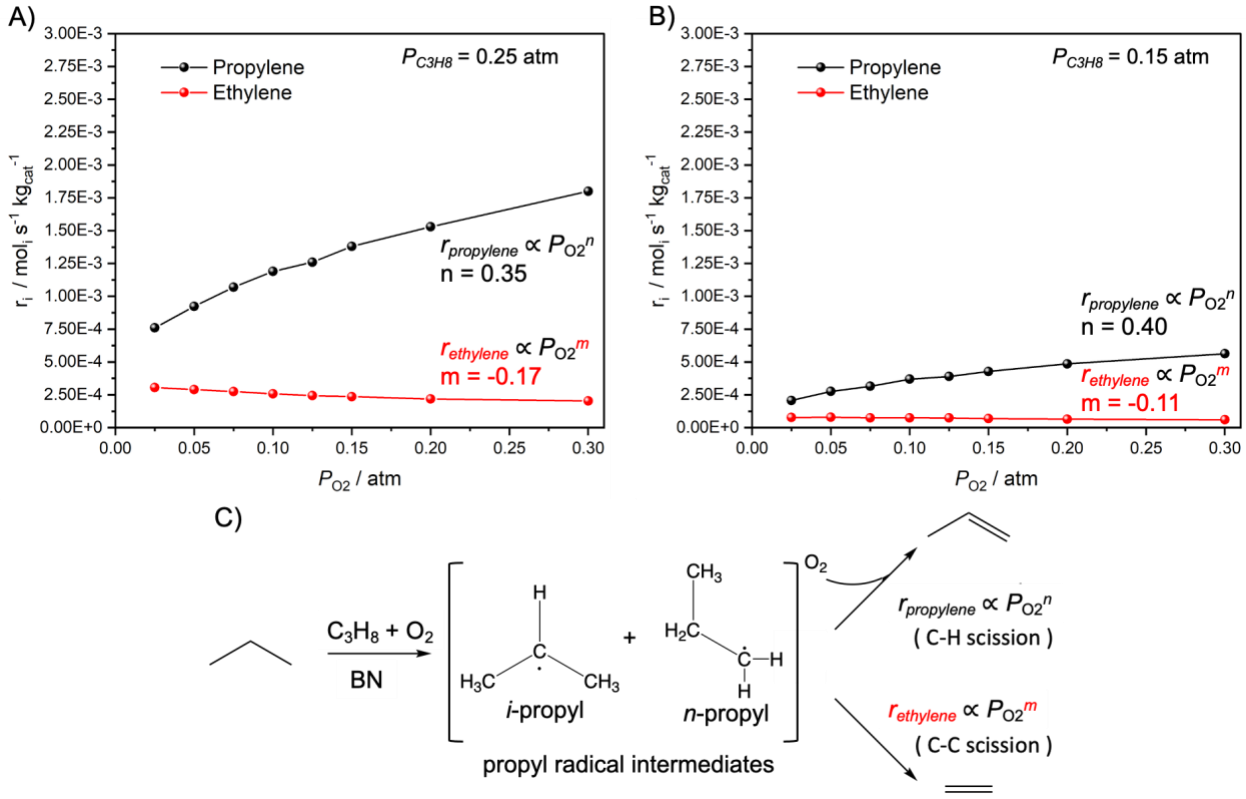

Figure 4.1. Rate of propylene and ethylene formation as a function of P_{O2} with a) P_{C3H8} = 0.25 atm and b) P_{C3H8} = 0.15 atm over 83mg BN at 525 ºC. O_2 reaction orders for the product formation were determined via power laws for each set of conditions. c) Simplified reaction scheme for propyl radical intermediate pathways.

Using this simplified model, we further examined a set of homogeneous reactions for C–H and C–C scissions involving *n*– and *i*–propyl radicals, listed in table 4.1. Kinetic constants for the tabulated reactions, as well as the initial H–abstraction from propane from HOO•, were readily available via the NIST kinetic database. Based on

ß-scission rules, homogeneous C-C scission of *n*-propyl radicals are more probable than with *i*-propyl.[34] We can expect *n*-propyl radicals to preferentially decompose to the unselective products. The relative concentration of *i*-/*n*-C_3H_7 is thus dependent on how the initial H-abstraction of propane occurs. Relatively strong H-abstractors, like >BO•, may be agnostic to primary or secondary H and produce statistical distributions of *i*-/*n*- propyl intermediates, while weaker H-abstracters like HOO• may primarily abstract secondary H.[35] We can then use *i*-/*n*-C_3H_7 as a descriptor for product distribution by compiling the reactions in table 4.1 and examining the relative rates of propylene to ethylene formation (r_{C3H6} / r_{C2H4}) as an index for the rate of C-H to C-C scissions. By examining r_{C3H6} / r_{C2H4} as a function of P_{O2} and *i*-/*n*-C_3H_7, we can probe pathways 2,3,4 in scheme 4.1.

Table 4.1. Simplified homogeneous reaction steps for propane activation and propyl radical decomposition to propylene and ethylene products. Kinetic data and rates were taken from NIST data base.

Step	Reaction	Description
r_1	$C_3H_8 + HO_2\cdot \rightarrow n\text{-}C_3H_7\cdot + H_2O_2$	H-abstraction → *n*-C_3H_7
r_2	$C_3H_8 + HO_2\cdot \rightarrow i\text{-}C_3H_7\cdot + H_2O_2$	H-abstraction → *i*-C_3H_7
r_3	$n\text{-}C_3H_7\cdot + O_2 \rightarrow C_3H_6 + HO_2\cdot$	H-abstraction → C_3H_6
r_4	$i\text{-}C_3H_7\cdot + O_2 \rightarrow C_3H_6 + HO_2\cdot$	H-abstraction → C_3H_6
r_5	$n\text{-}C_3H_7\cdot \rightarrow C_3H_6 + H\cdot$	H-abstraction → C_3H_6
r_6	$i\text{-}C_3H_7\cdot \rightarrow C_3H_6 + H\cdot$	H-abstraction → C_3H_6
r_7	$n\text{-}C_3H_7\cdot \rightarrow C_2H_4 + CH_3\cdot$	C-C scission → C_2H_4
r_8	$i\text{-}C_3H_7\cdot \rightarrow C_2H_4 + CH_3\cdot$	C-C scission → C_2H_4

r_{C3H6} / r_{C2H4} can be represented as a function of P_{O2} and *i*–/*n*–C_3H_7 via eq. 4.1:

$$\frac{R_{C3H6}}{R_{C2H4}} = \frac{[O_2]^n(k_2 + \left(\frac{[iC_3H_7] * k_1}{[nC_3H_7]}\right)) + k_4 + \left(\frac{[iC_3H_7] * k_3}{[nC_3H_7]}\right)}{k_6 + \left(\frac{[iC_3H_7] * k_5}{[nC_3H_7]}\right)} \quad (4.1)$$

Detailed derivation of eq. 4.1 and the kinetic parameters—numbered to match their reactions in table 4.1—can be found in ref. 12. Eq. 4.1 was then computed using three cases for H abstraction of propane (reactions 1 and 2) and which resulted in *i*/*n*–C_3H_7 = 1.5 (homogeneous H–abstraction by HOO•), 0.74 (heterogeneous H–abstraction by >BO•), and 1.06 (computed mixed surface gas abstraction). These cases can be considered upper, middle, and lower bounds for the mix of surface or gas H–abstractions. r_{C3H6} / r_{C2H4} was then experimentally determined under fuel lean and fuel rich conditions. r_{C3H6} / r_{C2H4} was also experimentally determined with and without co–fed steam (10% H_2O), which offered insight into the possible role of H_2O, a major reaction product, pathways 2,3, and 4. The overlap for the experimental results across each set of conditions confirm that the kinetic role of O_2 in the propane reaction rate (not shown) and the product formation pathways were consistent, figure 4.2. Good agreement between the mixed surface–gas H–abstraction pathways and the experimental data tested support the mixed mechanism proposed. As well, upper bound (homogeneous) and lower bound (heterogeneous) activation pathways suggest that while BOx are necessary initiators for the reaction, promotion of gas

phase reactivity may improve propylene formation significantly. Note that these experiments were part of our recent publication using computational and experimental tools to describe fundamental elements of the boron reaction mechanism.[12] While relevant to this thesis, only portions of this study are discussed here for conciseness (see *personal contributions*).

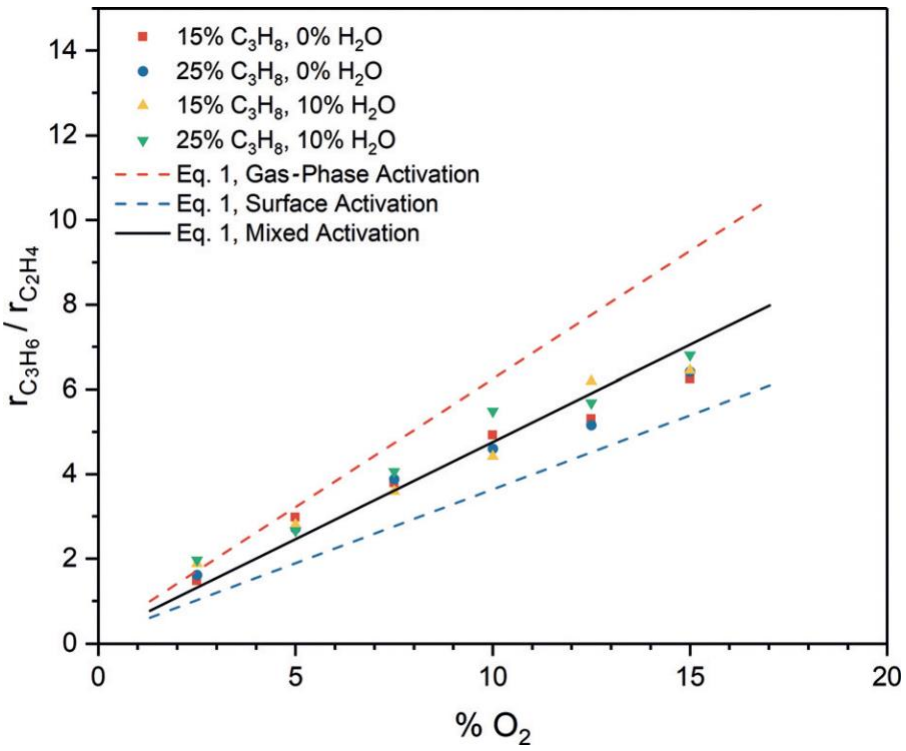

Figure 4.2. Experimental ratio of propylene to ethylene formation rates as a function of P_{O2} examined at 525 ºC over BN. Reaction rates were measure under fuel rich (25% propane) and fuel lean (15% propane) conditions with and without the cofeeding of 10% H_2O (balancing gas was N_2). In all cases, propane conversion was maintained below 5%. Eq. 4.1 is plotted using three different cases where the H–abstractor was either HOO• (red), >BO• (blue), or 42% >BO• and 58% HOO• (black). The values for *i*/*n*–C_3H_7 changed depending on the H–abstractor such that *i*/*n*–C_3H_7 = 1.5 (red), 0.74 (blue), and 1.06 (black). (ref. 12)

4.3 Promotion of Gas Phase Reactivity

These data show that r_{C3H6} / r_{C2H4} may be modeled according to the strength of the H abstractor in the initial H abstraction of propane in this simplified model. From this standpoint, reactor configurations conducive to homogeneous H–abstractions may promote propylene selectivity. One such configuration is the use of a structured bed, which can double the bed void volume of a traditional packed bed design (i.e. 0.4), and exhibits several benefits for highly exothermic industrial applications[36–41] Huff *et. al.* examined ethane ODH over Pt / α–Al_2O_3 foam and reported up to 70% ethylene selectivity at 80% conversion.[42,43] Leibmann *et. al.* examined isobutane ODH over Pt/α–Al_2O_3 foam and achieved 70% olefin selectivity at 70% conversion, which they attributed to a heterogeneous–homogeneous mechanism under fuel rich conditions.[44] Beretta *et. al.* examined propane ODH over Pt/α–Al_2O_3 foam.[45] They observed primarily combustion products in a blank annular reactor, but >55% olefin selectivity in the presence of the catalyst. They further examined propane ODH over Pt/α–Al_2O_3 supported on a metallic porous monolith with >80% void fraction achieved an enhanced total olefin yield of 50%.[45,46] They attribute the enhancement to auto–thermal homogeneous reactions and proposed that the catalyst behaved as an igniter and homogeneous gas phase reactions were responsible for the resulting olefin yield in propane ODH. Liu *et. al.* is, to our knowledge, the first to examine propane ODH via BN wash–coated straight channeled cordierite honeycomb monolith.[47] They achieve 82% selectivity to propane at 16.8% propane conversion,

with high rate of propane consumption at various temperatures. From these considerations, the inclusion of oxyfunctionalized BN throughout a structured catalyst design is an attractive design to probe relevant homogeneous phase reactions and achieve increased propylene yield.[7]

4.3.1 Reaction studies and characterization of 3D printed oxyfunctionalized BN–Kaolinite structured catalysts for the oxidative dehydrogenation of propane to propylene

We collaborated with Dr. Fateme Rezaei and her PhD student Khaled Baamran of Missouri University of Science and Technology to create 3D printed BN kaolinite monoliths. They have developed expertise in 3D printing catalysts for a variety of applications and patented a printing process for 3D printed zeolites monoliths for CO_2 capture.[48] This catalyst design approach provides a roadmap for a high throughput synthesis of stable and modular (i.e. ability to change surface area to void fraction ratios) structured catalysts. Herein, we examine the stability, reactivity, and selectivity of 3D printed structured catalysts consisting of oxyfunctionalized BN and kaolinite in staggered channel design to promote gas mixing. We expect the promotion of gas phase radical oxidation pathways to selectively promote rate the rate of propane conversion and enjoy higher r_{C3H6} / r_{C2H4} values.

In a typical synthesis, BN was oxyfunctionalized under ODHP conditions (T= 525 ºC, P_{tot} = 0.3 atm C_3H_8, 0.15 atm O_2, 0.55 atm N_2) for 12hrs. Desired amounts of oxyfunctionalized BN, kaolinite, and methylcellulose (MC) were mixed with DI water and well mixed to a slurry over 48hr. The slurry is then stirred vigorously and heated gently until a paste is formed. Rheological tests of the paste (not shown) were done to determine a synthetic protocol that produced "ink" suitable for 3D printing. Monoliths were 3D printed to specific dimensions for a quartz tube reactor (figure 4.3) using this ink via syringe and dried at room temperature. Samples tested were labeled in the following manner: 50wt%BN-Kaolinite was labeled "50BNK." Traditional packed bed configurations were conventionally labeled as the catalyst used.

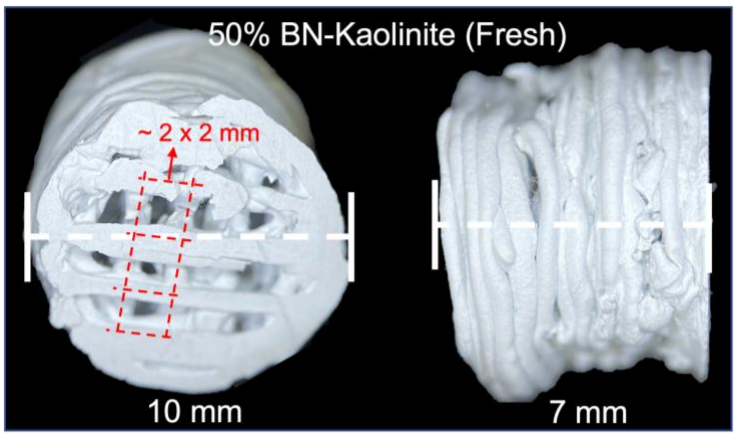

Figure 4.3. Image of 3D printed oxyfunctionalized BN kaolinite monolith with relevant dimensions.

ODHP reactivity of structured BNK catalysts were examined at 525 ºC and compared to packed bed configurations of kaolinite, BN, and a 50-50 mixed bed of BN and kaolinite, figure 4.4. Under these conditions, 50BNK sample exhibited 90.5%

propylene selectivity compared to 83.5% exhibited by BN. Although kaolinite showed limited reactivity (~1% conversion), it exhibited 91.8% propylene selectivity. The addition of the kaolinite to the mixed bed therefore contributed higher olefin selectivity, achieving and 88.5% propylene selectivity. Kaolinite 3D monolith, 0BNK, exhibited higher reactivity than a packed bed of kaolinite but much lower propylene selectivity (45.5%) and produced the most CO_x observed (48.5%). The difference in product selectivities between kaolinite and 0BNK illustrate that homogeneous partial oxidation of propane cannot solely achieve higher propylene selectivity, and that >BO• radical initiators are required to improve olefin yield. This was further supported by the increase in olefin selectivities between 5 and 50 wt% BN in 5BNK and 50BNK monoliths.

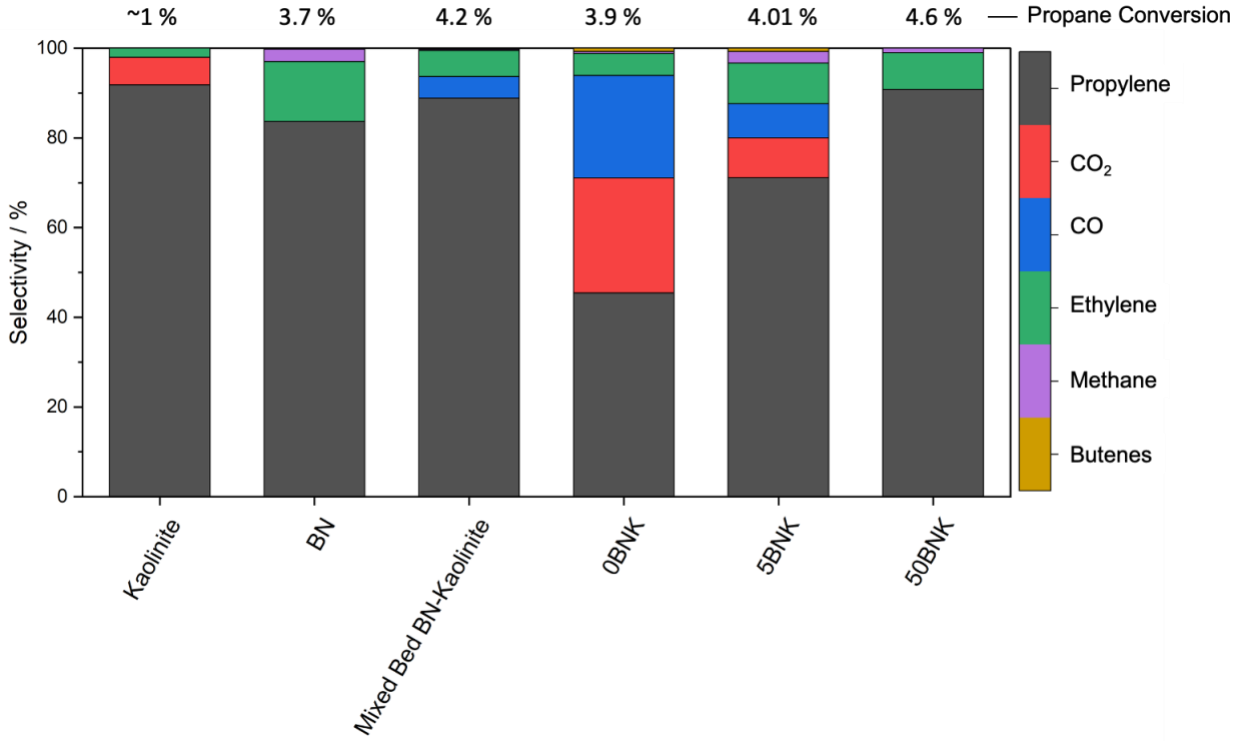

Figure 4.4. Isoconversion comparison of kaolinite, BN, packed bed of mixed BN and kaolinite pellets, and structured BNK catalysts. T= 525 ºC, P_{tot} = 0.3 atm C_3H_8, 0.15 atm O_2, 0.55 atm N_2.

We attribute the increase in propylene selectivity in 50BNK to an increase in homogeneous reactivity and therefore increased H-abstraction of propyl radicals to propylene, as discussed. If this were the case, we would expect to see an increase in the experimental r_{C3H6} / r_{C2H4} value as a function of P_{O2}. This was observed in figure 4.5. 50BNK exhibited r_{C3H6} / r_{C2H4}values compared to the mixed bed, indicating that the change in reactor configuration contributed to the promotion of C-H scission over C-C cracking. However, the enhancement in 50BNK compared to BN cannot solely be attributed to an increase in homogeneous reactivity. The mixed bed exhibited higher r_{C3H6} / r_{C2H4} values than BN indicating that interactions between

kaolinite and reactive intermediates may also favor C–H scission. Enhancements in the catalytic performance of 50BNK can be assumed to be related to the promotion of homogeneous reactions and favorable interactions with kaolinite.

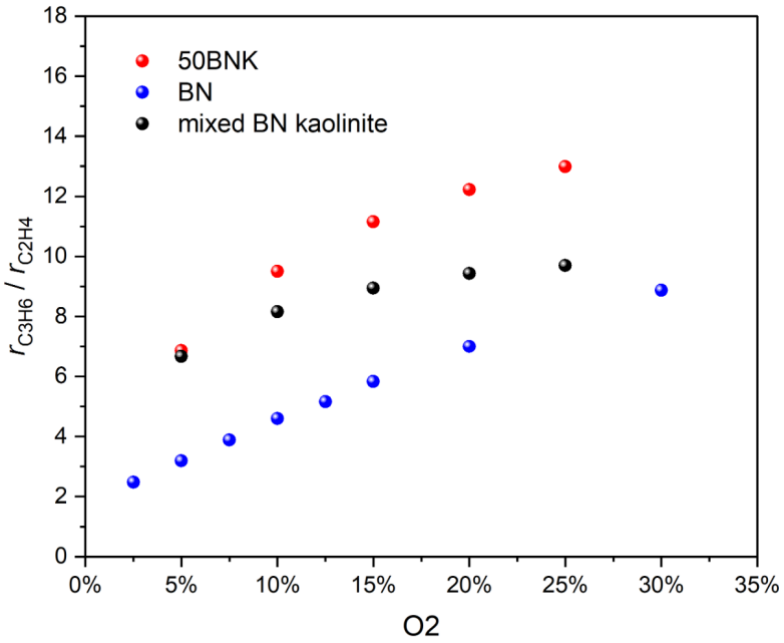

Figure 4.5. r_{C3H6} / r_{C2H4} ratios as a function of P_{O2} for 50BNK, BN, and mixed BN kaolinite packed bed at P_{C3H8} = 0.3 atm, with N_2 as the balancing gas. T = 525 ºC

The rate of propane consumption was examined as a function of P_{O2} and P_{C3H8} respectively, figure 4.6. 50BNK, assumed to promote to the homogeneous reactivity, showed consistent reaction orders of 2.2 and 0.25 for propane and O_2 respectively. This result further supports that these reaction orders observed on BN are indeed representative of homogeneous reaction pathways. The O_2 reaction order of 0.25 observed on the mixed bed agreed with BN. However, the propane exhibited a reaction order of 1.45. Further analysis is necessary to determine if kaolinite is

quenching radical intermediates from BN and limiting propane activation to surface H–abstractions.

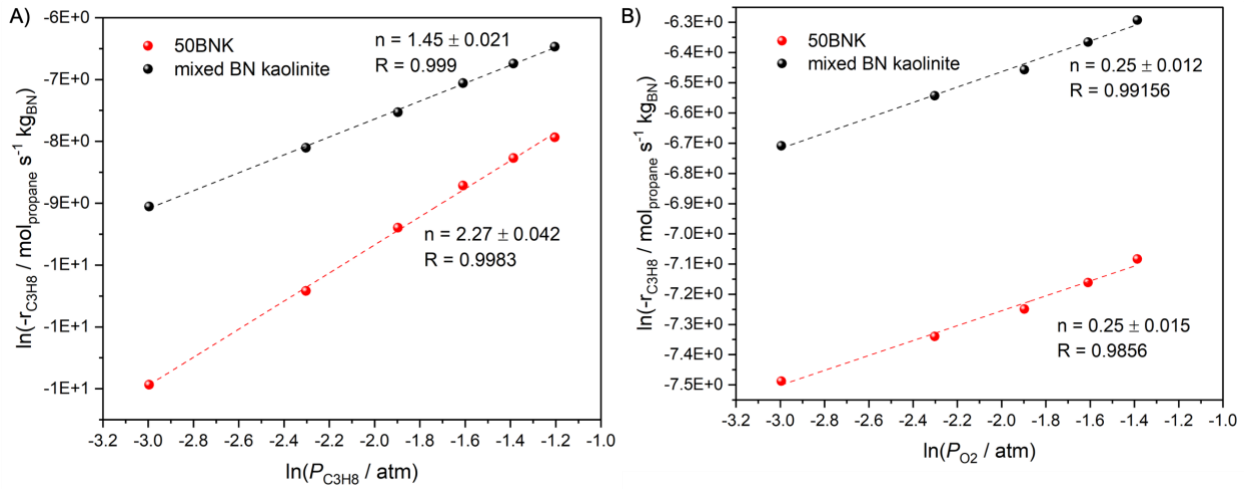

Figure 4.6. Dependence of the propane consumption rate on a) alkane partial pressure at P_{O2} = 0. 15 atm and b) O_2 partial pressure at P_{C3H8} = 0.30 atm. T = 525 ºC, P_{tot} = 1 atm with N_2 as the balance gas.

The 3D monoliths showed the hypothesized increase in r_{C3H6} / r_{C2H4} values as a function of O_2 and agreement to the kinetics observed on BN. Figure 4.7a, showed that higher wt% of BN within the monolith (i.e., 50BNK) exhibited conversion–selectivity trends comparable to BN. The poor performance of 5BNK indicated a threshold of BN required ignite and maintain selective reaction pathways, particularly in the presence of the kaolinite. Propane reaction rates were examined as a function of propane conversion to determine how the reaction products impacted propane activation, figure 4.7b. The rate of propane consumption increased slightly as a function of conversion for 50BNK. 5BNK exhibited a decreased reaction rate at low conversions and increased slightly at higher conversions. Surprisingly, the rate of propane consumption decreased with increasing conversion for the BN in a

traditional packed bed. Deshlara *et. al.* showed that the rate of propane activation increased with propane conversion in the presence of 0.005 kPa of NO, because the NO_x mediated C–H activation pathway produced OH radical intermediates favorable for further homogeneous propane activation.[3549] They show that the opposite was true for a V_2O_5 catalyst where adsorption of H_2O on lattice oxygens inhibit C–H activation.[50] While there some ambiguity on the overall chain branching and termination steps in BN catalyzed ODH, our recent IPA and FA studies suggest that an increase in B–OH groups may cause the reduction of activity observed in figure 4.7b.

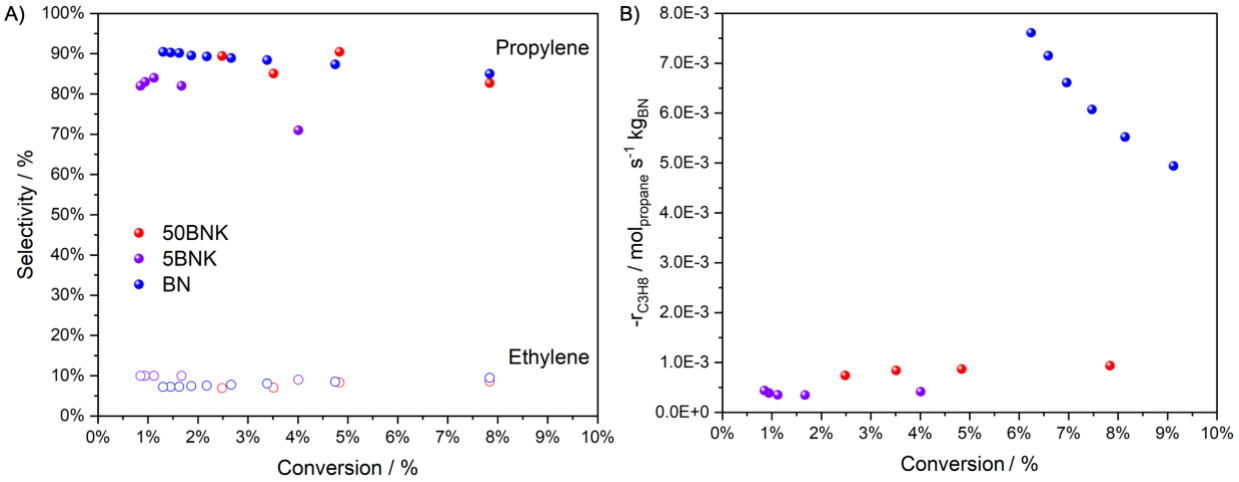

Figure 4.7. a) product selectivities and b) propane consumption rate as a function of propane conversion for 50BNK, 5BNK, and BN. T= 525 ºC, P_{tot} = 0.3 atm C_3H_8, 0.15 atm O_2, 0.55 atm N_2. Experiments in b were performed under differential conditions < 10% propane conversion.

50BNK showed a reduction in apparent activation energies, E_{app}, of products and reactants between 490–525 ºC compared to BN tested under similar conditions, figure 4.8. The reduction of E_{app} for ethylene was relatively low (16 kJ mol^{-1})

compared to propane (23 kJ mol^{-1}) and propylene (29 kJ mol^{-1}). This observation indicates that the main effect of 50BNK is the facile production of propylene, which is reflected by the favorable product selectivities observed. This supports increased C–H activation by a homogeneous radical pool and the production of stable *i*–propyl radicals in the gas phase.

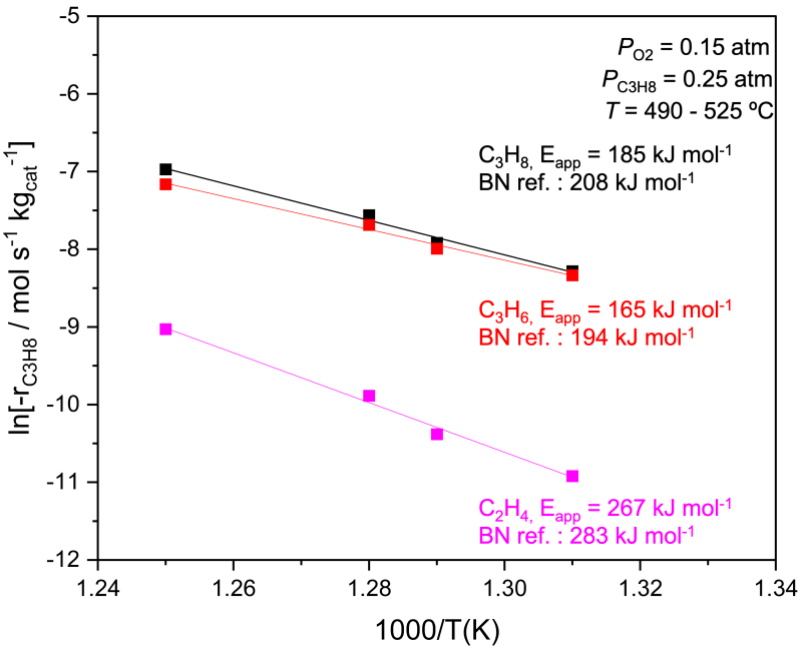

Figure 4.8. Arrhenius plot for the reaction rates as a function of 1/*T* during ODHP over 50BNK. *T*=500–550 °C, P_{tot} = 0.3 atm C_3H_8, 0.15 atm O_2, 0.55 atm N_2. Total flow rate was adjusted between 40–100 mL_n min^{-1} at each temperature to maintain a propane conversion below 5%.

We examined the stability of 50BNK for more than 2 weeks, figure 4.9. The selected timeframe surpasses our previous 100hr BN stability test and Lu et. al. 15hr stability test for BN wash coated monoliths. We demonstrate that 15.87% propane conversion with propylene and ethylene selectivities of 78.4% and 11.6% respectively can be steadily maintained for 2 weeks on 50BNK. Additionally, we show that 50BNK

can also exhibit a higher performance at 32% propane conversion with propylene and ethylene selectivities of 63.6% and 15.7% respectively, by increasing the contact time, for an additional 42 hours. At this condition we achieve ~20% propylene yield and ~25% total olefin yield.

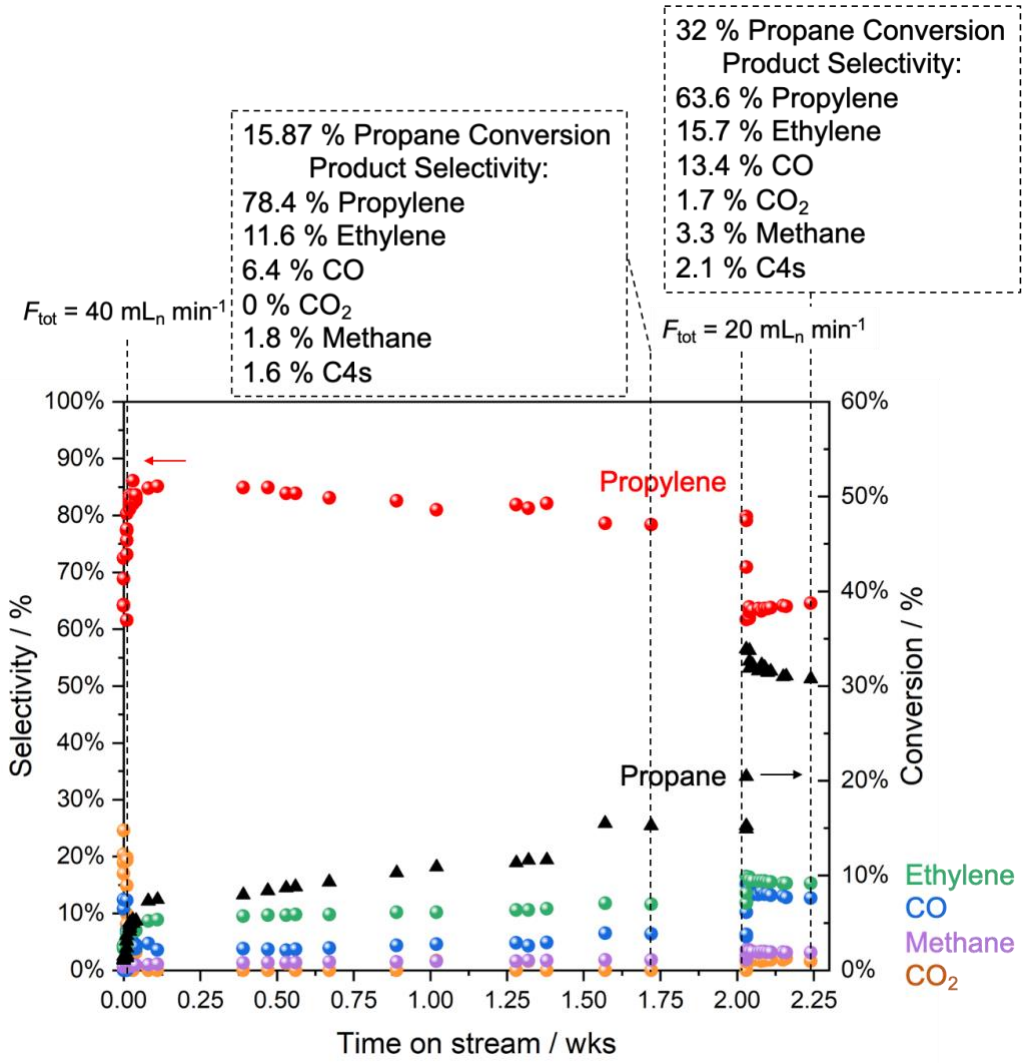

Figure 4.9. 50BNK stability of product selectivities and propane consumption as a function of time on stream. T= 525 ºC, P_{tot} = 0.3 atm C_3H_8, 0.15 atm O_2, 0.55 atm N_2.

4.3.2. Characterization of 3D printed oxyfunctionalized BN-Kaolinite structured and the role of kaolinite.

Indeed, 3D printed BN kaolinite (BNK) monoliths show promise for the development of cost effective and stable structured beds with competitive performance in the partial oxidation of propane. Kaolinite, $Al_2Si_2O_5(OH)_4$, is a cheap mineral clay binder commonly used in the preparation of zeolitic catalysts for oil and gas conversions.[51] It is a naturally occurring hydrous alumna silicate where repeated layers of silicon tetrahedral sheets on aluminum octahedral sheets form a dioctohedral 1:1 phyllosilicate structure.[52] These sheets feature reactive hydroxyl groups and can easily intercalate compounds that: form strong hydrogen bonds or strong dipole interactions with the silicate layer.[53] Thus, binder–matrix effects of kaolinite on the catalytic performance of zeolites have been widely researched. The acidic properties have been observed to play a catalytic role in the FCC and other refinery processes.[54] Misk *et. al.* showed that using kaolinite as a binder with zeolite 5A decreased the rate of coke formation from propylene and found that polyaromatic coke resided primarily within the binder.[55] Understanding the dehydroxylation of kaolinite has therefore been an important step in determining its reactivity. Between 400–650 ºC, kaolinite is known to dehydroxylate via reaction of adjacent OH groups and the elimination of structural water, eq. 4.2:[56]

$$Al_2Si_2O_5(OH)_4 \rightarrow Al_2O_3{\bullet}2SiO_2 + 2H_2O \qquad (4.2)$$

Near 550 ºC, the sheet structure is destroyed and semi-amorphous metakaolinite is formed.[5257] From these considerations, the interaction of acidic sites from kaolinite with reactive intermediated from BN should be further examined to understand the role of kaolinite as a binder in the 3D printed BNK monoliths.

Prior to reactivity testing, all samples were dried *in-situ* in the quartz reactor at 525 ºC under oxidative conditions 30% O_2 / N_2 for 4 hrs to promote surface dehydroxylation. XPS analysis of the fresh and spent BNK samples are shown in figure 4.10a. The formation of metakaolinite in the spent 50BNK can be observed in comparison to kaolinite in the fresh 50BNK (undehydrated). Conversion of Si-OH / Al-O-Si-OH at 105.6 eV and SiO_x at 104.01 eV were dehydrated primarily to an SiO_2 surface (103. 2 eV), similar to the quartz SiO_2 (103.0) reference in the Si 2s spectra. Similarly, higher oxidation AlOOH (76.33 eV) were transformed primarily to Al-OH (75.48 eV) species in the Al 2p spectra. Minor amounts of Al_2O_3 (74.1 eV) may indeed be present but were not observed on either sample via XPS under these conditions. The O1s spectra shifted to lower binding energies for spent 50BNK due to the dehydroxylation of higher binding energy Si-OH, Al-OH, and likely B-OH sites. The main O 1s peak in the spent material agrees with the 532.5 eV signal of O species in SiO_2. The spent material exhibited oxyfunctionalization of BN (191 eV) with the appearance of BO_3 units and $B_yO_xH_z$ at 194 and 192.97 eV respectively in the B 1s spectra. Fresh 50BNK exhibited C-O, O=C-O, and carbonate like / bound O=C-

O at 289.6, 288.1, and 286.7 eV respectively in the C 1s spectra. These carbaceous species are created via the pretreatment of BN powders in alkane / O_2 mixtures prior to mixture with kaolinite. However, the post reaction surface featured high amounts of C–C (284.8 eV) and minor amounts of O=C–O (286.77 eV). This is indicative of surface reactions of alkyl intermediates on metakaolinite. Similarly, deposition of organic material on the quartz sand at the end of the reactor tube was observed, figure 4.10b. XPS of the C 1s region of these quartz chips (spent) exhibited signals for C–C, C–O–C, and O=C–O at 284.8 eV, 286.6 eV, and 288.6 eV respectively. The physical distance between the catalyst bed and the organic build up at the base of the reactor tube suggests that the compounds were long lived and immediately condensed in a cool location. We assume this is indicative of the formation of oxygenates. Notably, high volumes of condenser fluid were similarly observed throughout the reaction. This would suggest that an increase in homogeneous reactions also increased the pathways 5,7,8, and 9 in scheme 4.1. Further analysis of the organic material via NMR, Raman, TGA–MS, and FTIR is necessary to test this hypothesis.

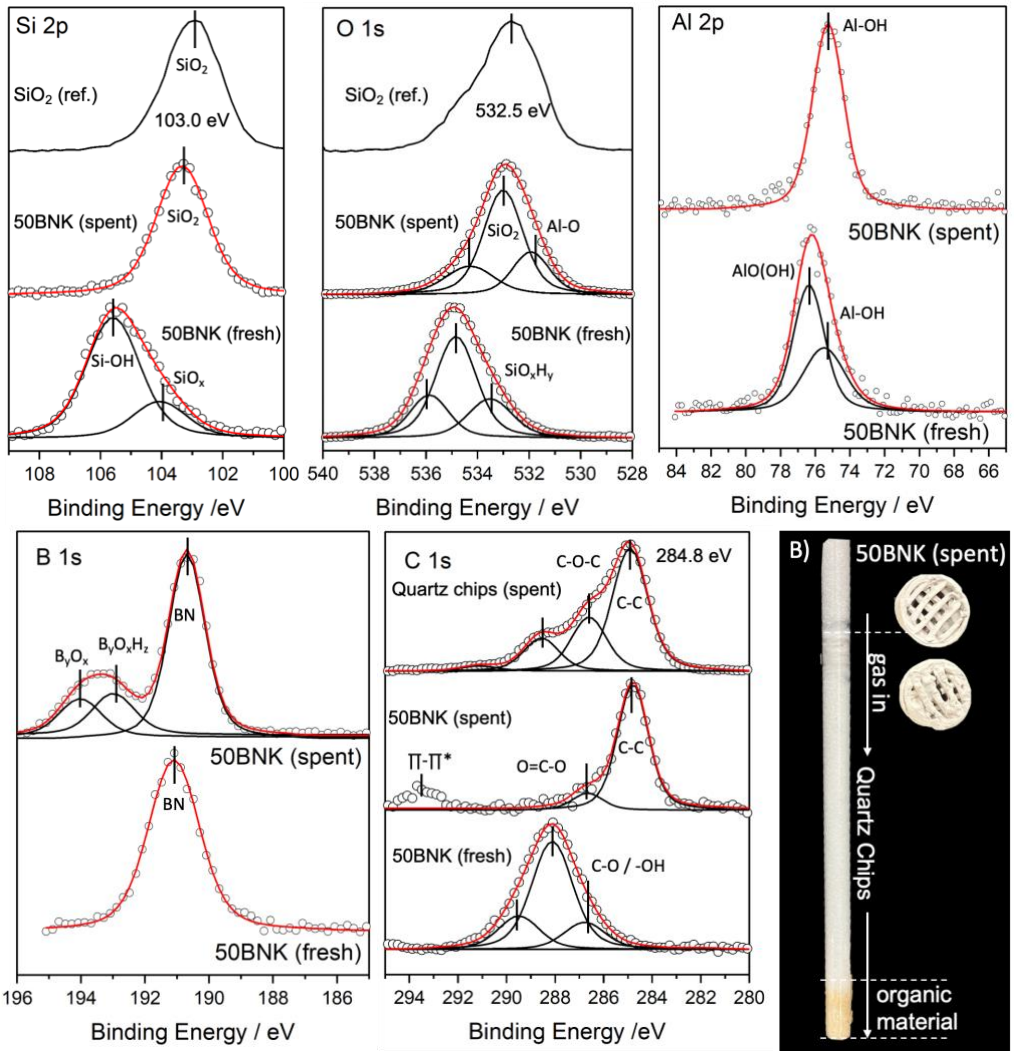

Figure 4.10. a) XPS of fresh and spent 50BNK and spent quartz sand. C1s, O1s, B1s, Si2p, and Al2p regions were analyzed, and various species are identified. b) Image of the spent 50BNK with slight yellowish tone and organic material on spent quartz sand at the base of the quartz reactor tube.

ATR-IR of fresh and spent kaolinite powders were compared to fresh and spent BNK samples, figure 4.11, to determine surface functional groups. Expectedly, fresh kaolinite and fresh 50BNK both exhibit 3690, 3618, 939, 910 cm^{-1} were attributed to the -OH stretching on the inner surface of kaolinite, -OH stretching of inner hydroxyl groups in kaolinite, Al-OH stretching, and -OH stretching of inner surface Al-OH deformations, respectively.[52,53,56-60] 1113, 1036, and 1003 cm^{-1} were

assigned to S–O stretches respectively. Hydroxyl interacting B–OH groups were observed at 3215 cm^{-1}, B–O functionality and fundamental BN modes were present in the broad feature from 1600–1300 cm^{-1}. Notably, all bands at 3690, 3618, 939, 910 cm^{-1} are no longer observed in spent kaolinite or 50BNK indicative of the formation of metakaolinite. Similarly, distinctive Si–O stretches at 1113, 1036, and 1003 cm^{-1} were replaced by a broad amorphous band between 1200–950 cm^{-1}. A slight increase in BOH functionality at 3215 cm^{-1} can be observed in spent 50BNK.

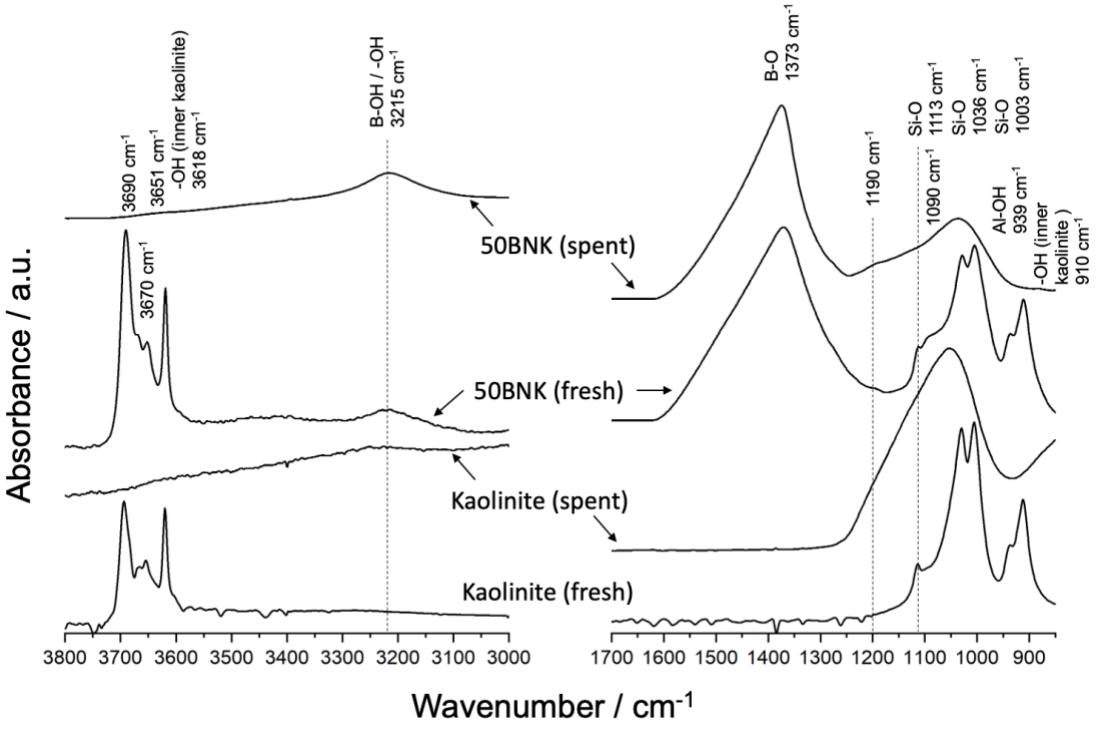

Figure 4.11. ATR–IR of fresh and spent kaolinite powders and fresh and spent 50BNK monoliths. All spectra were recorded at room temperature under atmospheric conditions.

4.4. Discussion on the homogeneous reaction pathways catalyzed by oxyfunctionalized BN

Reaction and kinetic studies were used to compare homogeneous reaction pathways proposed for B_2O_3 / Al_2O_3 with BN catalyzed ODHP. These boron-based materials share similar reaction mechanisms under the conditions tested. However, BN is more stable and more selective than the B_2O_3 / Al_2O_3 catalysts, which report high selectivities to CO_x. Homogeneous reaction pathways were further probed via 3D printed BN Kaolinite monoliths. These monoliths showed comparable kinetics, reactivity, and selectivity to BN. They also exhibited higher r_{C3H6} / r_{C2H4} values, lower apparent activation energies, and more favorable interactions of the products on the reaction rate compared to BN. These results were promising, however contributions by kaolinite and/or metakaolinite to the rate of propane consumption must be further understood. The mixed BN and kaolinite packed bed showed a 1.45 order rate dependence on P_{C3H8} compared to the typical 2.2 order observed, which suggests a decrease in homogeneous propane activation due to the presence of kaolinite.

The possible role of oxygenates must be further investigated to determine whether they contribute combustion products. Although the high temperatures may favor pathway 4 rather than 5, as discussed earlier, confirmation of this for boron oxide reaction mechanism is still necessary. To-date, we have observed oxygenate by-products of propionaldehyde, acetone, and formaldehyde via NMR of the condenser

fluid. There have also been proposals of the formation of propylene oxide from high conversion over BN—although we have not directly observed this.[61] Experimental observation of 50BNK showed a significant increase in organic liquid products, which may suggest that gas phase reactivity contributes to their formation. Walling *et. al.* show that primary and tertiary alkoxy radicals reacted with various substrates at comparable rates, but the rate of ß-scission of branched alkoxy radicals were significant faster than primary alkoxy radicals.[62,63] The results of figure 4.1 would confirm that secondary peroxy radicals formed likely decompose via pathway 5 or 6 relatively quickly and contribute to propylene formation. However, primary peroxy or alkoxy radicals may decompose to combustion products or formaldehyde or propionaldehyde.

The deleterious effect of propane conversion on propane reaction rate over BN is particularly interesting. Based on the radical oxidation pathways suggested for BN, the products (like H_2O) and reactive intermediates should contribute to higher rates. However, this result suggests that propylene, water, and/or radical intermediates inhibit propane activation. We have previously established the rate enhancement of propane when H_2O is cofed to the reaction mixture. One possible explanation for this is that propylene is known to be a radical scavenger and has been employed as such in several studies. Blake and Hinshelwood showed used propylene as a free radical scavenger to investigate free radical chain mechanisms in homogeneous formic acid

decomposition. They found that the addition of propylene had no effect on the rate of formic acid decomposition.[64] Their study and similar research have been used to probe the likelihood of OH or H chain carriers in the decomposition of formic acid.[65] Freeman *et. al.* use propylene as a radical scavenger for H atoms in the radiolysis of ethanol vapor to probe the free radical chain mechanism to pyrolysis products.[66] One highly examined propagation step in these studies is the facile reaction of propylene and H radicals to form propyl radicals: $H + C_3H_6 \rightarrow C_3H_7$. If in fact propylene production scavenges H radicals to form propyl radicals, then the effect observed in figure 4.7b may indicate that H atoms function as important radical chain carriers within BN catalyzed ODH. Early evidence of this may be present. In our ongoing collaboration with UCLA, we aim to generate computational spectra of surface structures observed experimentally via NMR and XPS. Thus far, the addition of protons to preliminary models of the BN surface show better alignment with *in-situ* XPS experiments.

4.5 References

1. Cavani, F. & Trifirò, F. Selective oxidation of light alkanes: interaction between the catalyst and the gas phase on different classes of catalytic materials. *Catal. Today* **51**, 561–580 (1999).
2. Leveles, L., Fuchs, S., Seshan, K., Lercher, J. A. & Lefferts, L. Oxidative conversion of light alkanes to olefins over alkali promoted oxide catalysts. *Appl. Catal. A Gen.* **227**, 287–297 (2002).
3. Leveles, L., Seshan, K., Lercher, J. A. & Lefferts, L. Oxidative conversion of propane over lithium–promoted magnesia catalyst: I. Kinetics and mechanism. *J. Catal.* **218**, 296–306 (2003).
4. Voskresenskaya, E. N., Anshits, A. G. & Roguleva, V. Oxidant activation over structural defects of oxide catalysts in oxidative methane coupling. *Catal. Rev.* **37**, 101–143 (1995).
5. Amenomiya, Y., Birss, V. I., Goledzinowski, M., Galuszka, J. & Sanger, A. R. Conversion of Methane by Oxidative Coupling. *Catal. Rev.* **32**, 163–227 (1990).
6. Swaan, H. M., Toebes, A., Seshan, K., van Ommen, J. G. & Ross, J. R. H. The kinetic and mechanistic aspects of the oxidative dehydrogenation of ethane over Li/Na/MgO catalysts. *Catal. Today* **13**, 201–208 (1992).
7. Venegas, J. M. & Hermans, I. The Influence of Reactor Parameters on the Boron Nitride–Catalyzed Oxidative Dehydrogenation of Propane. *Org. Process Res. Dev.* **22**, 1644–1652 (2018).
8. Venegas, J. M. *et al.* Selective Oxidation of n –Butane and Isobutane Catalyzed by Boron Nitride. *ChemCatChem* **9**, 2118–2127 (2017).
9. Grant, J. T., Venegas, J. M., McDermott, W. P. & Hermans, I. Aerobic Oxidations of Light Alkanes over Solid Metal Oxide Catalysts. *Chem. Rev.* **118**, 2769–2815 (2018).
10. Venegas, J. M. *et al.* Selective Oxidation of n–Butane and Isobutane Catalyzed by Boron Nitride. *ChemCatChem* **9**, 2118–2127 (2017).
11. McDermott, W. P., Venegas, J. & Hermans, I. Selective Oxidative Cracking of n–Butane to Light Olefins over Hexagonal Boron Nitride with Limited Formation of COx. *ChemSusChem* (2019). doi:10.1002/cssc.201901663
12. Venegas, J. M. *et al.* Why Boron Nitride is such a Selective Catalyst for the Oxidative Dehydrogenation of Propane. *Angew. Chemie Int. Ed.* **59**, 16527–16535 (2020).
13. Murakami, Y., Otsuka, K., Wada, Y. & Moikawa, A. Partial Oxidation of Ethane over Boron Oxide Added Catalysts. *Chem. Lett.* 545–548 (1989).
14. Otsuka, K., Uragami, Y., Komatsu, T. & Hatano, M. The partial oxidation of light alkanes (CH4, C2H6, C3H8) over B–P mixed oxides. *Stud. Surf. Sci. Catal.* **61**, 15–23 (1991).
15. Steinfeldt, N., Buyevskaya, O. V, Wolf, D. & Baerns, M. Comparative Studies of the Oxidative Dehydrogenation of Propane in Micro–Channels Reactor Module and Fixed–Bed Reactor. in *Natural Gas Conversion VI* (eds. Iglesia, E., Spivey, J. J. & Fleisch, T. H. B. T.–S. in S. S. and C.) **136**, 185–190 (Elsevier, 2001).
16. Buyevskaya, O. V., Müller, D., Pitsch, I. & Baerns, M. Selective Oxidative Conversion of Propane to Olefins and Oxygenates on Boria–Containing Catalysts. *Nat. Gas Convers. V* **119**, 671–676 (1998).
17. Buyevskaya, O. V., Kubik, M. & Baerns, M. Factors Determining the Selectivity in the

Oxidative Dehydrogenation of Propane over Boria–Alumina Catalysts. in *Heterogeneous Hydrocarbon Oxidation* 155–169 (1996).

18. Colorio, G., Védrine, J. C., Auroux, A. & Bonnetot, B. Partial Oxidation of Ethane Over Alumina–Boria Catalysts. *Appl. Catal., A* **137**, 55–68 (1996).
19. Colorio, G. C., Bonnetot, B., Vedrine, J. C. & Auroux, A. Characteristics of Alumina Boria Catalysts Used in Ethane Partial Oxidation. *Stud. Surf. Sci. Catal.* **82**, 143–149 (1994).
20. Cucinieri–Colorio, G., Bonnetot, B., Védrine, J. C. & Auroux, A. New developments in selective oxidation II. In Cortés Corberán V, Vic Bellón S (eds). *Elsevier Sci. Publ.* 143 (1994).
21. Chaar, M. A., Patel, D. & Kung, H. H. Selective oxidative dehydrogenation of propane over VMgO catalysts. *J. Catal.* **109**, 463–467 (1988).
22. Jiang, X. *et al.* Oxidative dehydrogenation of propane to propylene with soft oxidants via heterogeneous catalysis. *ACS Catal.* **11**, 2182–2234 (2021).
23. Chen, K., Khodakov, A., Yang, J., Bell, A. T. & Iglesia, E. Isotopic tracer and kinetic studies of oxidative dehydrogenation pathways on vanadium oxide catalysts. *J. Catal.* **186**, 325–333 (1999).
24. Carrero, C. A., Schloegl, # R, Wachs, I. E. & Schomaecker, R. Critical Literature Review of the Kinetics for the Oxidative Dehydrogenation of Propane over Well–Defined Supported Vanadium Oxide Catalysts. (2014). doi:10.1021/cs5003417
25. Love, A. M. *et al.* Probing the Transformation of Boron Nitride Catalysts under Oxidative Dehydrogenation Conditions. *J. Am. Chem. Soc.* **141**, 182–190 (2019).
26. Love, A. M. *et al.* Synthesis and Characterization of Silica–Supported Boron Oxide Catalysts for the Oxidative Dehydrogenation of Propane. *J. Phys. Chem. C* **123**, 27000–27011 (2019).
27. Mark, L. O. *et al.* Highly Selective Carbon–Supported Boron for Oxidative Dehydrogenation of Propane. *ChemCatChem* **13**, 3611–3618 (2021).
28. T., G. J. *et al.* Boron and Boron-Containing Catalysts for the Oxidative Dehydrogenation of Propane. *ChemCatChem* **9**, 3623–3626 (2017).
29. Grant, J. T. *et al.* Boron and Boron–Containing Catalysts for the Oxidative Dehydrogenation of Propane. *ChemCatChem* **9**, 3623–3626 (2017).
30. Grant, J. T. *et al.* Boron and Boron–Containing Catalysts for the Oxidative Dehydrogenation of Propane. *ChemCatChem* 1–5 (2017). doi:10.1002/cctc.201701140
31. Ashfold, M. N. R. & Rettner, C. T. *Dynamics of gas–surface interactions*. **3**, (Royal Society of Chemistry, 1991).
32. Weinberg, W. H. Eley–Rideal Surface Chemistry: Direct Reactivity of Gas Phase Atomic Hydrogen with Adsorbed Species. *Acc. Chem. Res.* **29**, 479–487 (1996).
33. Estupiñán, E. G., Klippenstein, S. J. & Taatjes, C. A. Measurements and modeling of HO 2 formation in the reactions of n–C 3H 7 and i–C 3H 7 radicals with O 2. *J. Phys. Chem. B* **109**, 8374–8387 (2005).
34. Glassman, I. & Yetter, R. A. Explosive and General Oxidative Characteristics of Fuels. in *Combustion* 75–145 (Elsevier, 2008). doi:10.1016/B978–0–12–088573–2.00003–8
35. Yu, P., Liu, Y., Deshlahra, P. & Wong, H. W. Detailed Kinetic Modeling of NO x–

Mediated Oxidative Dehydrogenation of Propane. *Ind. Eng. Chem. Res.* **60**, 13553–13561 (2021).
36. Twigg, M. V. & Richardson, J. T. Theory and Applications of Ceramic Foam Catalysts. *Chem. Eng. Res. Des.* **80**, 183–189 (2002).
37. Twigg, M. V & Richardson, J. T. Fundamentals and Applications of Structured Ceramic Foam Catalysts. *Ind. Eng. Chem. Res.* **46**, 4166–4177 (2007).
38. Richardson, J. T., Peng, Y. & Remue, D. Properties of ceramic foam catalyst supports: pressure drop. *Appl. Catal. A Gen.* **204**, 19–32 (2000).
39. Twigg, M. V & Richardson, J. T. Structured ceramic foams as catalyst supports for highly exothermic processes. in *Scientific Bases for the Preparation of Heterogeneous Catalysts* (eds. Gaigneaux, E. M. et al.) **162**, 135–142 (Elsevier, 2006).
40. Hickman, D. A., Haupfear, E. A. & Schmidt, L. D. Synthesis gas formation by direct oxidation of methane over Rh monoliths. *Catal. Letters* **17**, 223–237 (1993).
41. Horn, R., Williams, K. A., Degenstein, N. J. & Schmidt, L. D. Syngas by catalytic partial oxidation of methane on rhodium: Mechanistic conclusions from spatially resolved measurements and numerical simulations. *J. Catal.* **242**, 92–102 (2006).
42. Huff, M. & Schmidt, L. D. Ethylene formation by oxidative dehydrogenation of ethane over monoliths at very short contact times. *J. Phys. Chem.* **97**, 11815–11822 (1993).
43. Huff, M. & Schmidt, L. D. Production of Olefins by Oxidative Dehydrogenation of Propane and Butane over Monoliths at Short Contact Times. *J. Catal.* **149**, 127–141 (1994).
44. Liebmann, L. S. & Schmidt, L. D. Oxidative dehydrogenation of isobutane at short contact times1This research was supported by NSF CTS-9629902 and by CR & L, Pasadena, TX.1. *Appl. Catal. A Gen.* **179**, 93–106 (1999).
45. Beretta, A., Piovesan, L. & Forzatti, P. An Investigation on the Role of a Pt/Al2O3 Catalyst in the Oxidative Dehydrogenation of Propane in Annular Reactor. *J. Catal.* **184**, 455–468 (1999).
46. Beretta, A., Forzatti, P. & Ranzi, E. Production of Olefins via Oxidative Dehydrogenation of Propane in Autothermal Conditions. *J. Catal.* **184**, 469–478 (1999).
47. Wang, Y., Li, W. C., Zhou, Y. X., Lu, R. & Lu, A. H. Boron nitride wash-coated cordierite monolithic catalyst showing high selectivity and productivity for oxidative dehydrogenation of propane. *Catal. Today* 0–1 (2018). doi:10.1016/j.cattod.2018.12.028
48. 3D printed zeolite monoliths for CO2 removal - The Curators of the University of Missouri. Available at: https://www.freepatentsonline.com/11298675.html. (Accessed: 17th August 2022)
49. Annamalai, L., Liu, Y. & Deshlahra, P. Selective C–H Bond Activation via NO x–Mediated Generation of Strong H–Abstractors. (2019). doi:10.1021/acscatal.9b03862
50. Deshlahra, P., Carr, R. T., Chai, S.-H. & Iglesia, E. Mechanistic Details and Reactivity Descriptors in Oxidation and Acid Catalysis of Methanol. *ACS Catal.* **5**, 666–682 (2015).
51. Vogt, E. T. C., Whiting, G. T., Dutta Chowdhury, A. & Weckhuysen, B. M. Zeolites and Zeotypes for Oil and Gas Conversion. *Adv. Catal.* **58**, 143–314 (2015).

52. Cheng, H., Liu, Q., Yang, J., Ma, S. & Frost, R. L. The thermal behavior of kaolinite intercalation complexes–A review. *Thermochim. Acta* **545**, 1–13 (2012).
53. Weiss, A., Thielepape, W. & Orth, H. Intercalation into kaolinite minerals. in *Proceedings of the International Clay Conference, Jerusalem* **1**, 277–293 (1966).
54. Choudhary, V. R., Devadas, P., Kinage, A. K. & Guisnet, M. Influence of binder on the acidity and performance of H–Gallosilicate (MFI) zeolite in propane aromatization. *Appl. Catal. A Gen.* **162**, 223–233 (1997).
55. Misk, M., Joly, G., Magnoux, P., Guisnet, M. & Jullian, S. Formation of coke from propene over 5A adsorbents – influence of the binder on the coke composition, location and removal. *Microporous Mesoporous Mater.* **40**, 197–204 (2000).
56. Brindley, G. W. & Nakahira, M. Kinetics of dehydroxylation of kaolinite and halloysite. *J. Am. Ceram. Soc.* **40**, 346–350 (1957).
57. Bellotto, M., Gualtieri, A., Artioli, G. & Clark, S. M. Kinetic study of the kaolinite–mullite reaction sequence. Part I: Kaolinite dehydroxylation. *Phys. Chem. Miner.* **22**, 207–217 (1995).
58. Nakagaki, S., Benedito, F. L. & Wypych, F. Anionic iron(III) porphyrin immobilized on silanized kaolinite as catalyst for oxidation reactions. *J. Mol. Catal. A Chem.* **217**, 121–131 (2004).
59. Tironi, A., Trezza, M. A., Irassar, E. F. & Scian, A. N. Thermal Treatment of Kaolin: Effect on the Pozzolanic Activity. *Procedia Mater. Sci.* **1**, 343–350 (2012).
60. Rong, T.–J. & Xiao, J. The catalytic cracking activity of the kaolin–group minerals. *Mater. Lett.* **57**, 297–301 (2002).
61. Kube, P. *et al.* Green synthesis of propylene oxide directly from propane. (2022). doi:10.26434/CHEMRXIV–2022–2CLNW
62. Walling, C. & Clark, R. T. Reactions of primary and secondary alkoxy radicals derived from hypochlorites. *J. Am. Chem. Soc.* **96**, 4530–4534 (1974).
63. Murakami, M. & Ishida, N. β–Scission of Alkoxy Radicals in Synthetic Transformations. *Chem. Lett.* **46**, 1692–1700 (2017).
64. Blake, P. G. & Hinshelwood, C. N. The homogeneous decomposition reactions of gaseous formic acid. *Proc. R. Soc. London. Ser. A. Math. Phys. Sci.* **255**, 444–455 (1960).
65. Yu, J. & Savage, P. E. Decomposition of Formic Acid under Hydrothermal Conditions. *Ind. Eng. Chem. Res.* **37**, 2–10 (1998).
66. Bansal, K. M. & Freeman, G. R. Free–radical chain reactions in the radiation–sensitized pyrolysis of ethanol vapor. *J. Am. Chem. Soc.* **90**, 7190–7196 (1968).

Chapter 5. Conclusion and Future Directions

5.1 Summary of Work Discussed

This dissertation aimed to characterize surface structures and reactivity of oxyfunctionalized BN. Herein, we characterized oxyfunctionalized BN as a function of reaction progress to show explicit correlational relationships between BO_3 functionality, alkane/O_2 conversions, and propylene selectivity. Examining these features through catalytic studies, ATR-IR, XAS, and XPS provided strong evidence that tri-oxygenated B sites play a significant role in the activation of BN catalyzed ODHP and appear to achieve a steady state with the reaction. These observations also bridge the binary characterizations of fresh and spent material, with a systematic characterization of the active layer growth.

The interactions between IPA and oxyfunctionalized BN were investigated via catalytic decomposition in a flow-through reactor and *in-situ* DRIFTs-TPD-MS. After exposure to ODHP conditions BN developed an oxyfunctionalized surface that initially dehydrated IPA to propylene at rates nearly 18x that of fresh BN and nearly 3x that of 4 wt% V_2O_5 / SiO_2. High temperature dehydration of the oxyfunctionalized BN generated boroxyl networks represented by B-O-B units that were immediately accessible upon introduction of IPA. On this relatively dehydroxylated surface, Lewis basic bridging O^{2-} atoms may abstract protons from the alcohol to form B-OH and an adjacent isopropoxide on B in the form B-O-R. Dissociative adsorption of IPA on

dehydroxylated BO_x represented by path 2 in scheme 3.2 occurs faster than IPA reactions on hydroxylated BO_x. This decomposition pathway for IPA may account for the initial high reactivity observed by the spent material. As the reaction proceeds, increasing hydroxylation of BO_x limits pathway 2 and shifts activity primarily to pathway 1, which may only occur on hydroxylated surfaces. Increasing hydroxylation decomposes IPA via dissociative and non-dissociative mechanisms. Lewis acidic B in certain BOH sites may form B-O-R with the alcohol via water elimination. Increasing B-OH concentration weakly binds IPA to the surface via H bonding of B-OH nests. Steady-state activity on spent BN is similar, but slightly lower than fresh BN with a slight increase in dehydrogenation activity to acetone. Although slow, dehydration of adjacent BOH species was observed via the consistent production and release of water from the surface.

FA decomposition on fresh and spent BN under non-oxidative conditions was examined via catalytic and DRIFTs-TPD-MS studies. Both exhibit transient reactivity periods and converge to similar rates of FA decomposition within 1hr and favor different reaction products. While dehydration of FA to CO was the main reaction pathway observed, fresh BN exhibited an r_{CO} / r_{CO2} of ~1.25. This nearly 1:1 ratio is observed in the product selectivity for fresh BN at 20% FA conversion- 41.8% CO_2 and 58.2% CO. Spent BN exhibited a growing r_{CO} / r_{CO2} value from ~2.25 to 4.5, which was maintained at steady state. The 3.6-fold increase supports the increase

acidic character of the oxyfunctionalized surface, particularly under assumed B–OH saturation coverage. Dissociative adsorption of FA to monodentate formate species and B–OH groups was observed via DRIFTs. Initially mainly H_2O was observed as the surface dehydrates and later CO2 became the main TPD product in the decomposition of formate.

Both IPA and FA decomposition studies show that surface alkoxides were formed with differing binding energies to the surface. Terminal alkoxides were more reactive and favored C–O scission at lower temperatures, while thermally stable bridged alkoxides or strongly bound alkoxides also featured C–H scission at increased temperatures. These results are reminiscent of the work by Murakami et. al. who showed that acetaldehyde and ethylene were formed on different active sites on B_2O_3 / Al_2O_3 in ethane oxidation.[1] They further showed that acetaldehyde formation passed through a maximum with increasing B_2O_3 loading, while CO and CO_2 formation were suppressed, and ethylene formation increased linearly. The bulk oxide therefore suppresses overoxidation and favors olefin formation. IPA and FA decompositions suggest that although there are strongly bound alkoxide that may decompose to unselective products, under reaction conditions the BO_x surface can readily perform acid–base reactions to selectively achieve the olefin. The amphoteric nature of the overall borate network also allows for the stabilization of alkoxides, H–abstraction reactions via weak H–abstractors like O^{2-} and strong H–abstracters

>BO•, and H donation to less acidic alcohols. Acid –base pairs and allow for facile dissociative adsorption of several oxygenated species and incoming alkanes. These features contribute to the high selectivity and reactivity observed on BN catalysts. However, the diminished activity in the presence of BOH suggests that the slow step in regenerating more reactive sites via BOH condensation may need to be further studied.

These studies also indicate that water may play several roles within BN-catalyzed ODHP. One such role may be facile hydrolysis of B-O-B to B-OH which may have contributed to the deceleration of the IPA reaction rate. Results of IPA oxidation indicate that increased hydroxylation, which may result from interactions of water and the oxyfunctionalized surface, may contribute to surface dehydrogenation pathways for IPA. Similarly, FA results shows that surface dehydration is the initial surface reaction after the adsorption. This occurs either by the facile desorption of molecularly adsorbed H_2O or the condensation of adjacent BOH groups. In both cases, the release of H_2O is a necessary and slow step. Once water is generated, it may also participate in the reaction pathways. Although further studies are necessary to determine the exact influence of water on the system it has been shown to catalyze both dehydration and dehydrogenation of FA.[2,3] We can extend this observation to BN catalyzed ODHP, where we observed that surface reactions between water and the oxyfunctionalized surface decreased tri-coordinated oxygenated B sites under

ODHP conditions via XRS. If water transitions B sites away from homoleptic coordination environments (i.e., all three ligands attached to B are the same as is the case with BO_3) then we would expect to see slight reductions in propylene selectivity during ODHP. Indeed, we do observe the reduction in propylene selectivity in our water co-feed studies in BN catalyzed ODHP and in our recent *in-situ* XRS measurements.[4] It is also necessary to understand how water may influence surface reactions of the bound alkoxides.

These studies show how sensitive the BO_x surface is to the reaction environment. Understanding the dynamics of the oxyfunctionalized surface under reaction conditions has required a healthy mix of experimental and computational approaches. The Alexandrova group used molecular dynamics simulations of BN oxidation at 500 ºC to evidence a variety boron oxide surfaces accessible under reaction conditions and heterogeneity of electronic density for B and O atoms within varying oxides.[5] They show that the chemical potentials for B and O within the system allow for oxides like B_6O_6, B_4O_2, etc. that exist at different probabilities at room temperature compared to reaction temperatures. The interconversion of oxides at reaction temperatures suggests that there are highly dynamic and thermally accessible metastable sites that can contribute to the observed reactivity. Our recent collaboration with the Alexandrova group explored metastable BO_x sites in effort to understand the dynamic surface reactivity of the oxyfunctionalized layer beyond

thermodynamically stable BO_3 units.[4] Computational work by Zisheng Zhang of the Alexandrova group identified metastable three sites with unsaturated B–B–B units that were present at reaction temperature with >5% population where the initial O_2 adsorption on a {BB} site was calculated to be kinetically barrierless and thermodynamically favorable: : B6O3#2, B6O3#3, and B5O2#1. This resulted in the formation of peroxo-like BO_x species: >B–O–O–B<, which cleaved readily over B6O3#2 to form >BO•, reactive species. We have since been able to use these findings in tandem with our reaction studies to build a simplified microkinetic model which accounts for both surface and gas activation pathways for propane, figure 5.1. We show that this model can accurately describe the product selectivity as a function of the P_{O2} and the strength of the H-abstractors in the system. We have since made use of this microkinetic model to design high performing model boron-based catalysts for ODHP investigated in this thesis.

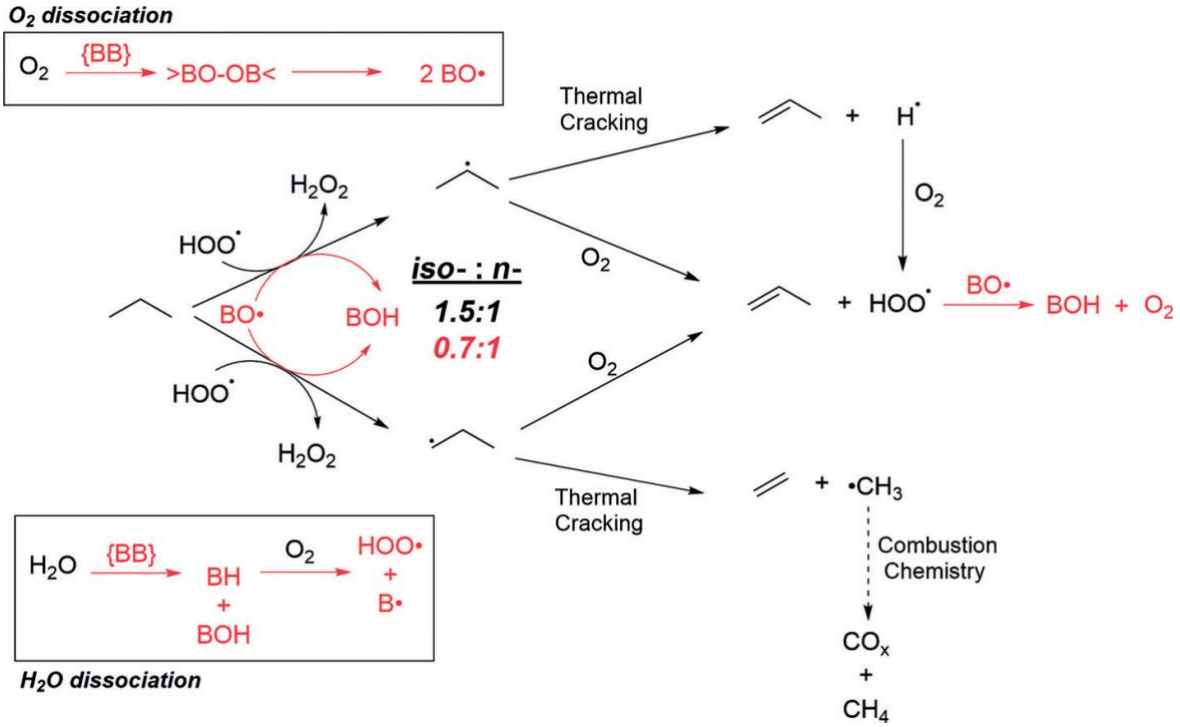

Figure 5.1. Example mixed heterogeneous–homogeneous mechanism for the partial oxidation of propane over oxyfunctionalized BN with {BB} and >BO•, proposed as relevant active species. (ref. 4)

Economical designs of an ODHP catalyst should maximize the surface availability of the identified active phase/centers on a cheaper bulk material. The low cost, high availability, and relatively high surface areas of Al_2O_3, SiO_2 and, Carbon (C) present these materials as common support selections for model supported catalysts (e.g. V / SiO_2 or V / Al_2O_3). To-date, we have examined the reactivity and stability of BO_x / SiO_2 and BO_x / activated C.[6,7] In the former case, we show that the Si–O–B bonds are easily hydrolyzed and much of the BO_x layer was leached away during the reaction. The synthesized set of BO_x / SiO_2 materials was useful in extracting requirements for an active boron-based catalyst, we showed that the reduced selectivity we observed was a direct result of BO_x-derived reactive intermediates

interacting unfavorable with the Si–OH / Si–O–Si surface. In direct contrast, we showed that BO_x / activated C materials were highly active and produced competitive product selectivities as BN. BO_x / activated C did not leach BO_x appreciably and exhibited excellent stability relative to BN. We were able to show that BO_x could be used to protect the carbon support from combustion and enable the use of a cheap material to carry the active phase. We applied many of the same principles to the early design of the 3D printed monoliths.

Our initial study on a variety of borides and boron containing crystal structures showed little to no correlation between reactivity and surface area. We later concluded that the more relevant parameter was having enough oxygenated boron sites present that could initiate radical oxidation pathways that may propagate through the catalyst bed volume. The volcano–like correlation between the concentration of BN within a fixed bed volume and the rate of propane activation, suggests that too much BN also provided termination sites for radicals within the system. Therefore, the relevant optimization parameters become stabilizing small quantities of highly dispersed and stably anchored BO_x in a catalyst bed conducive to homogeneous reactivity (i.e., increased void fraction). By combining the cheap clay kaolinite with oxyfunctionalized BN throughout a 3D printed monolith design, we achieved a structured bed with great thermal conductivity, and a void fraction much higher than the packed bed equivalent. [4,8,9] Preliminary data discuss here shows that

these 3D printed BN monoliths can achieve similar kinetics, catalytic performance, and competitive (even higher) olefin selectivities. Most importantly, we demonstrate we can significantly increase the $r_{propylene}$ / $r_{ethylene}$ ratio by optimizing the catalyst design for increased homogeneous activity.

5.2 Questions and Future Directions

Much of our work has been optimizing boron-based catalysts for partial alkane oxidation. As a group we have examined C_1–C_4 alkanes and a variety of conditions. However, we still have remaining questions for boron-based ODHP materials like:

1. Can we achieve competitive olefin yields if we stabilize miniscule amounts of boron oxyhydroxide as initiators and optimize homogeneous radical oxidation pathways?
2. What are the pathways relevant for oxygenate formation and can these also be optimized via boron-based material studies?
3. Why is there a negative correlation between propane conversion and reaction rate for BN-catalyzed ODHP?
4. Can boron-based materials be explored for other selective oxidative reactions? (e.g., Formic acid decomposition for H_2 generation)

Our recent comparative technoeconomic analysis for the production of propylene from BN-catalyzed ODHP revealed that this technology is not yet financially competitive with the Uhde, DOW (UoP), or Lummus PDH technologies. The main

pain point was the downstream separation of unreacted propane from propylene for the feed recycle in the operating cost. Increasing propane conversion and propylene yield is of course the desired route to overcome this operating expenditure. However, in lieu of this, regulatory interventions may significantly change this economic assessment. For example, CO_2 taxes, which have been widely considered as a market-based approach in climate change mitigation, would significantly alter the operating costs for the PDH processes which generate CO_2 through intense energy consumption for high temperature processes, regeneration cycles including but not limited to moving solid belts and multiple reactors in series, and low-pressure operations to drive PDH conversion. In this context, the proposed 45% energy reduction possible with ODHP could turn this technology from being reasonably profitable to economically competitive. Additionally, ODHP does not need to be a stand-alone process. For example, Uhde implemented oxydehydrogenation processes downstream from the conventional PDH reactor in an effort to reduce energy consumption of the STAR process once they acquired it. Similarly, we can imagine that precious metals and corrosive metals may also be subject to additional regulatory friction. It is then necessary to develop nascent ODHP technologies with non-metal materials like BN. While boron-based ODHP has yet to match the performance or economic viability of PDH, these studies on BN and have revitalized ODHP studies with a new class of non-metal boron catalysts. The discovery of a stable, active, and highly selective boron materials have contributed significantly to

the field of ODHP including but not limited to an array of high level, creative, and robust characterization techniques for non-crystalline dynamic oxidic surfaces. This research has spurred useful collaboration between kineticists, advanced X-ray research scientists, theoreticians, and solid-state NMR experts.

5.6 References

1. Murakami, Y., Otsuka, K., Wada, Y. & Moikawa, A. Partial Oxidation of Ethane over Boron Oxide Added Catalysts. *Chem. Lett.* 545–548 (1989).
2. Columbia, M. R. & Thiel, P. A. The interaction of formic acid with transition metal surfaces, studied in ultrahigh vacuum. *J. Electroanal. Chem.* **369**, 1–14 (1994).
3. Yu, J. & Savage, P. E. Decomposition of Formic Acid under Hydrothermal Conditions. *Ind. Eng. Chem. Res.* **37**, 2–10 (1998).
4. Venegas, J. M. *et al.* Why Boron Nitride is such a Selective Catalyst for the Oxidative Dehydrogenation of Propane. *Angew. Chemie Int. Ed.* **59**, 16527–16535 (2020).
5. Zhang, Z., Jimenez-Izal, E., Hermans, I. & Alexandrova, A. N. Dynamic Phase Diagram of Catalytic Surface of Hexagonal Boron Nitride under Conditions of Oxidative Dehydrogenation of Propane. *J. Phys. Chem. Lett.* **10**, 20–25 (2019).
6. Mark, L. O. *et al.* Highly Selective Carbon-Supported Boron for Oxidative Dehydrogenation of Propane. *ChemCatChem* **13**, 3611–3618 (2021).
7. Love, A. M. *et al.* Synthesis and Characterization of Silica-Supported Boron Oxide Catalysts for the Oxidative Dehydrogenation of Propane. *J. Phys. Chem. C* **123**, 27000–27011 (2019).
8. Steinfeldt, N., Buyevskaya, O. V, Wolf, D. & Baerns, M. Comparative Studies of the Oxidative Dehydrogenation of Propane in Micro-Channels Reactor Module and Fixed-Bed Reactor. in *Natural Gas Conversion VI* (eds. Iglesia, E., Spivey, J. J. & Fleisch, T. H. B. T.-S. in S. S. and C.) **136**, 185–190 (Elsevier, 2001).
9. Schwarz, O., Duong, P.-Q., Schäfer, G. & Schomäcker, R. Development of a microstructured reactor for heterogeneously catalyzed gas phase reactions: Part I. Reactor fabrication and catalytic coatings. *Chem. Eng. J.* **145**, 420–428 (2009).

Appendix A – Experimental Methods

A.1 Materials

h-BN powders were purchased from Sigma Aldrich (99.5% purity). Catalyst pellets were generated via hydraulic press (12 mm ID stainless steel die) using the following pressure program 5 tons (hold 30 sec), 7 tons (hold 90 sec). Pellets were crushed and sieved to 600-425 μm. Pellet surface areas were on average 7 m^2 g^{-1} as confirmed by N_2 physisorption experiments. Reagent grade (>99.5%) isopropanol and formic acid were purchased from Sigma Aldrich. Quartz chips were purchased from Pyromatics. Ultra-high purity (UHP) grade He, Ar, O_2, and N_2 were purchased from Airgas. Research grade Propane was purchased from Matheson Tri-Gas Supply. 4 wt% V/SiO_2 catalysts were synthesized via incipient wetness using a previously reported.[1] Kaolinite was purchased from Millipore Sigma.

A.2 Catalytic Testing

Catalytic reactions were carried out in a Microactivity Effi Microreactor (PID Eng. & Tech) fit with 3 EL Flow Bronkhort Mass Flow controllers which individually controlled the delivery of N_2, O_2, and C_3H_8 to the catalyst bed. The desired amount of catalyst was loaded into a quartz reactor tube (12 mm O.D. x 8 mm I.D. x 36 cm) packed with quartz chips such that the catalyst bed was centered between two quartz wool plugs. A thermocouple (k-type) sat in the center of the catalyst bed. The reactor tube was placed into a split tube furnace within a hot box heated to 160 ºC for all

experiments. Reactive gas mixture was fed top-down through the reactor tube. In a typical ODH run, the furnace was heated to 550 ºC under 30 mL_n min^{-1} N_2 and 10 mL_n min^{-1} O_2 and held under these conditions for at least 1hr after the temperature stabilized. The catalyst was then brough to the desired temperature for reaction testing. Typically, the gas mixture was held at 30% C_3H_8, 15% O_2, and 55% N_2 and the total flow rate was changed between 20 and 120 mL_n min^{-1}, unless otherwise stated. Sample was treated under these conditions until steady state was achieved. Less than 1% conversion was observed under these conditions at 500 ºC in a blank quartz reactor tube packed with quartz chips. Once contacted with the catalyst bed, the reaction effluent was fed to a thermoelectrically cooled condensing unit maintained at -2ºC, which was emptied periodically to avoid accumulation of condensed liquid. Dried effluent was then analyzed via on-line gas chromatography (GC Shimadzu 2010) fit with parallel lines: Hayesep QBond, RT-QBond, and Mol Sieve 5A lines to a TCD and RTX-1 (or GS-Gaspro) lines to an FID. He (UHP) was used as the carrier gas. N_2 was used as an internal standard for all experiments and an average of 5 GC measurements were taken per data point (e.g., conversion, selectivity, reaction rate, etc.) with an average standard deviation < 1%. All carbon balance closed within 3% for all experiments.

Saturated vapor delivery was carried out using a saturator sitting in a bath of acetone or water to bring the saturator to the desired temperature. Dry gas mixtures were

bubbled through the saturator held at the desired temperature and atmospheric pressure to deliver the vapor feed to the reactor. All 1/8" stainless steel gas lines to and from the reactor were heated to ~110 ºC to prevent physisorption of vapors and any other liquids.

A.3 Characterization

Diffuse Reflectance Infrared Fourier Transform Spectroscopic (DRIFTs) and Attenuated Total Reflectance IR (ATR-IR) measurements were performed via Alpha Bruker Vertex 70 liquid nitrogen cooled MCT detector. Typically, 256 scans were averaged for spectra recorded between 800-4000 cm^{-1} using a 4 cm^{-1} resolution. In a typical DRIFTs experiment, 5 mg of catalyst were finely ground and loaded into an *in-situ* DRIFTs cell. The sample was then pretreated at 600 ºC (20 ºC min^{-1}) in 40 mL_n $min^{-1}$of 20% O_2 in Ar for 1 hr to clean the surface of contaminants. The sample was then cooled to 20 ºC prior to adsorption. All effluent was analyzed via on-line mass spectrometry (Extrel Core Mass Spectrometer) which was calibrated via various standards using the Questor5 software package. The relevant m/z fragmentation matrix was generated with specific detection m/z for each species with minimal relative interference and standard deviation and whole fragmentation patterns for each species were used to assure proper identification. Vapor delivery was carried out via saturation of gas mixture to the DRIFTs cell.

Xray Photoelectron Spectroscopy (XPS) measurements were done via Thermo Scientific XPS (micro-focused monochromated Al K-alpha X-ray source) with a flood gun to reduce surface charging. Samples conditions were 10^{-7} mbar pressure and room temperature. C 1s, O 1s, B 1s, N 1s, Si 1s, and Al 2p regions were scanned using a 50 ev pass energy, a 50 ms dwell time, a 400 μm spot size, and a 0.2 ev energy step size. The number of scans per element was adjusted to improved signal-to-noise. Elemental surface compositions, peak integrations, and peak deconvolutions were done via Avantage (Thermo Scientific) Software package.

A.4 References

1. Love, A. M. *et al.* Elucidation of Anchoring and Restructuring Steps during Synthesis of Silica-Supported Vanadium Oxide Catalysts. *Chem. Mater.* **28**, 5495-5504 (2016).

Appendix B – Supporting Information for Chapter 2

Table B.1. Two-level full experimental design for isobutane with corresponding t and p-values.

Terms	Process Variable / units	Low / -1	High / +1	t-value	*p*-value
1	Temperature / ºC	400	500	0.29	0.785
2	Feed Flowrate / mL_n min^{-1}	20	80	-0.54	0.615
3	P_{alkane} / atm	0.10	0.40	1.3	0.252
4	P_{O2} / atm	0.02	0.20	0.82	0.448
5	Temperature*Flowrate			-0.9	0.407
6	Temperature*P_{alkane}			0.07	0.946
7	Temperature*P_{O2}			0.38	0.718
8	Flowrate*P_{alkane}			-0.34	0.749
9	Flowrate*P_{O2}			-0.06	0.957
10	P_{alkane}*P_{O2}			0.91	0.403

Table B.2. Two-level ½ fractional design for methane and ethane.

Factor	Process Variable / units	Low / -1	High / +1
1	Alkane Identity	methane	ethane
2	Temperature / ºC	400	600
3	Feed Flowrate / mL_n min^{-1}	20	80
4	P_{alkane} / atm	0.10	0.40

Table B.3. Two-level ½ fractional design for methane and propane.

Factor	Process Variable / units	Low / -1	High / +1
1	Alkane Identity	methane	propane
2	Temperature / ºC	400	600
3	Feed Flowrate / mL_n min^{-1}	20	80
4	P_{alkane} / atm	0.10	0.40

Table B.4. Two-level ½ fractional design for ethane and propane.

Factor	Process Variable / units	Low / -1	High / +1
1	Alkane Identity	ethane	propane
2	Temperature / ºC	400	600
3	Feed Flowrate / mL_n min^{-1}	20	80
4	P_{alkane} / atm	0.10	0.40

Table B.5. Two-level ½ fractional design for ethane and isobutane.

Factor	Process Variable / units	Low / -1	High / +1
1	Alkane Identity	ethane	isobutane
2	Temperature / ºC	400	600
3	Feed Flowrate / mL_n min^{-1}	20	80
4	P_{alkane} / atm	0.10	0.40

Table B.6. Two-level ½ fractional design for propane and isobutane.

Factor	Process Variable / units	Low / -1	High / +1
1	Alkane Identity	propane	isobutane
2	Temperature / ºC	400	600
3	Feed Flowrate / mL_n min^{-1}	20	80
4	P_{alkane} / atm	0.10	0.40

Table B.7. *p*-values for various alkane pairing across experiments. $p < 0.05$ means term has significant impact on BN oxyfunctionalization.

Term	methane / ethane	methane/ propane	methane/ isobutane	ethane/ propane	ethane/ isobutane	propane/ isobutane
Alkane Identity	0.464	0.799	0.035	0.924	0.57	0.601
P_{alkane} / atm	0.528	0.675	0.289	0.703	0.482	0.495
Feed Flowrate / mL_n min^{-1}	0.51	0.597	0.163	0.488	0.544	0.489
Temperature / ºC	0.437	0.846	0.025	0.681	0.607	0.628
P_{alkane} * Feed Flowrate	0.436	0.865	0.025	0.613	0.25	0.356
P_{alkane} * Temperature	0.486	0.462	0.471	0.732	0.452	0.463

Table B.8. *t*-values for various alkane pairing across experiments. $-2 > t < 2$ means term has significant impact on BN oxyfunctionalization.

Term	methane / ethane	methane /propane	methane /isobutane	ethane / propane	ethane / isobutane	propane / isobutane
Alkane identity	0.184	0.799	1.4338	-0.213	1.037	-3.12
P_{alkane} / atm	0.316	0.675	-0.1612	-0.892	-1.37	-4.38
Feed flowrate / mL_n min^{-1}	0.414	0.597	-0.3013	1.843	1.127	4.46
Temperature / ºC	-0.139	0.846	-2.0313	0.972	-0.92	2.84
P_{alkane} * Feed flowrate	-0.121	0.865	-2.0137	-1.233	-3.125	-6.89
P_{alkane} * Temperature	0.636	0.462	0.0863	-0.793	-1.508	-4.84

Table B.9. 2–way interaction terms corresponding t and p–values for single terms for methane and isobutane DoE.

2-way interactions	T-value	*p*-value
Alkane Identity * P_{alkane}	1.61	0.138
Alkane Identity * P_{O2}	0.97	0.354
Alkane Identity * F_{total}	0.93	0.372
Alkane Identity * *T*	-2.62	0.026
Alkane Identity * *TOS*	0.51	0.619
P_{alkane} * P_{O2}	-0.10	0.925
P_{alkane} * F_{total}	-0.20	0.844
P_{alkane} * *T*	-2.19	0.054
P_{alkane} * *TOS*	-0.37	0.720
P_{O2} * F_{total}	-0.82	0.430
P_{O2} * *T*	-1.01	0.336
P_{O2} * *TOS*	-0..56	0.589
F_{total} * *T*	-1.31	0.219
F_{total} * *TOS*	0.12	0.904
T * *TOS*	-0.48	0.641

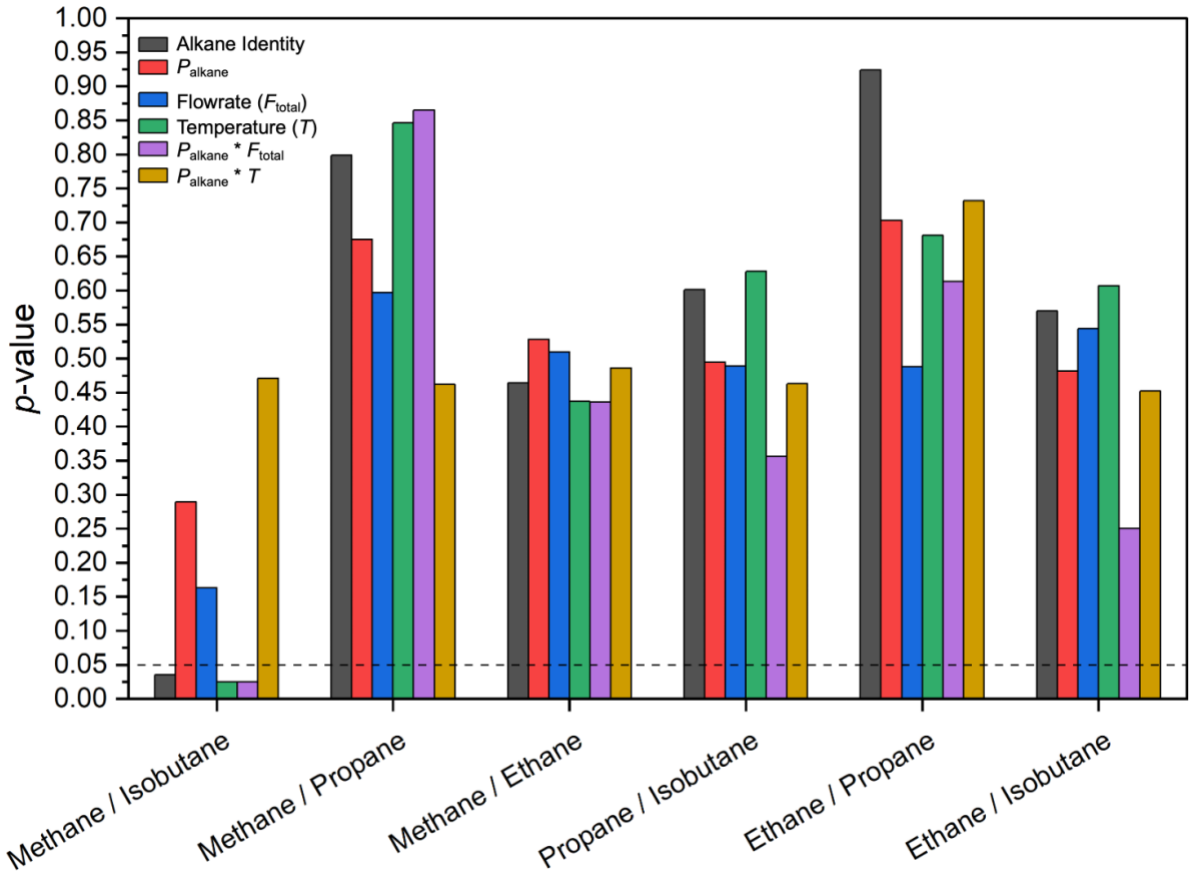

Figure B.1. Aggregated calculated t and p-values for single and 2-way interaction effect on oxyfunctionalization from ANOVA of 2-level $\frac{1}{2}$ fractional experimental design with pairwise alkane comparisons. 50 mg of BN were independently tested in random experimental order and examined via XPS.

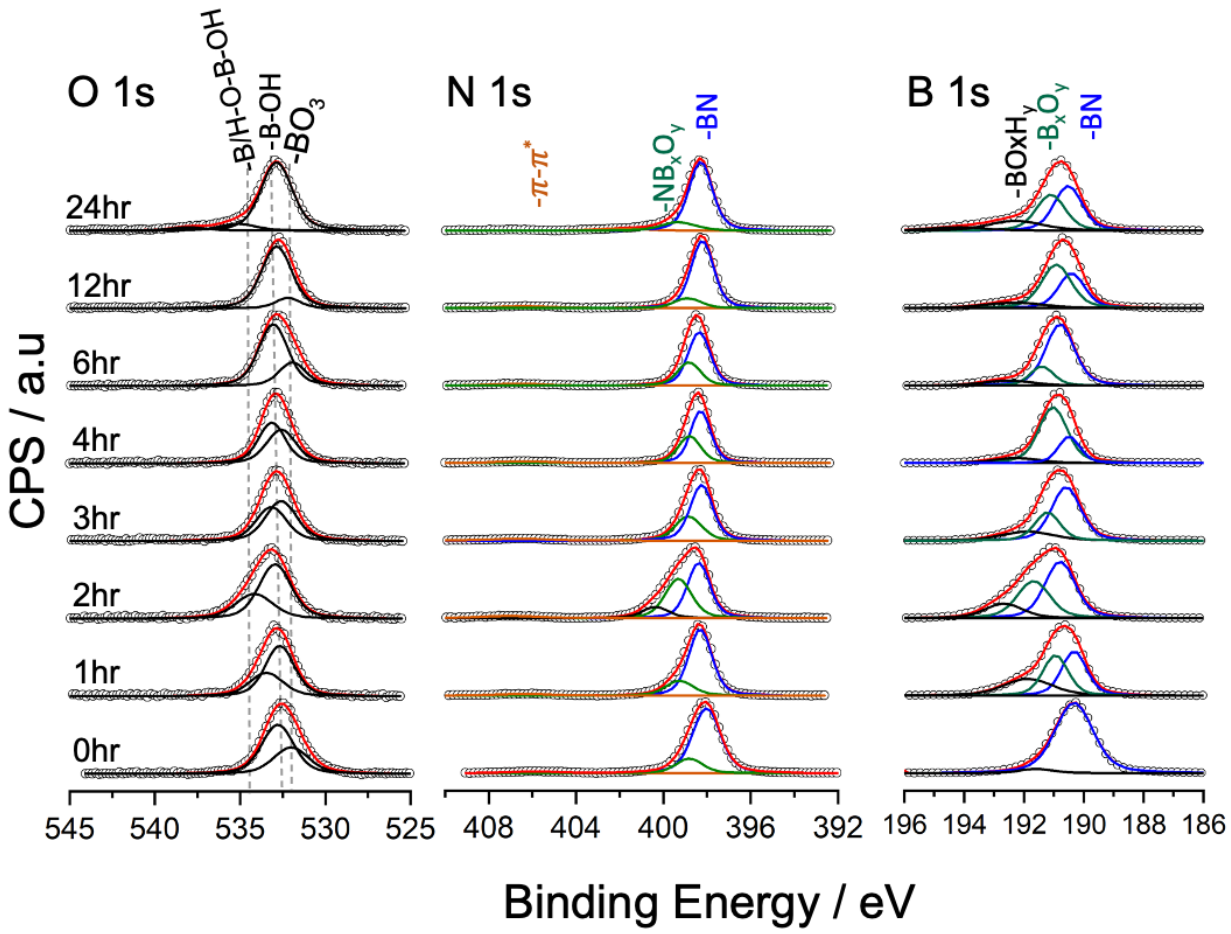

Figure B.2. Deconvolution of XPS peaks for O 1s, N 1s, and B 1s regions for all BN samples treated as a function of time on stream. BN samples independently treated under the following conditions: T= 550 ºC, F_{tot} = 80 mL_n min^{-1}, P_{tot} = 0.3 atm C_3H_8, 0.15 atm O_2, 0.55 atm N_2. Deconvolution technique outlined in Appendix A.

Appendix C – Supporting Information for Chapter 3

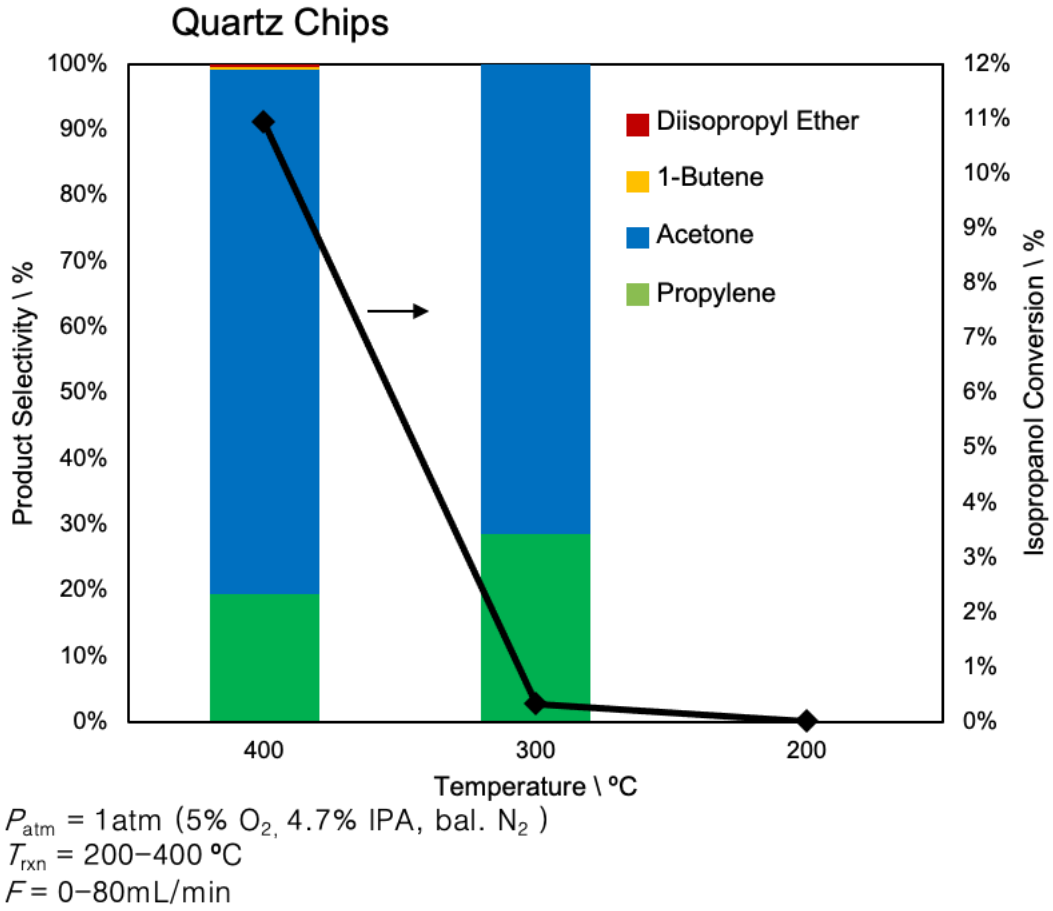

Figure C.1. Isopropanol decomposition on quartz chips as a function of reaction temperature. Conversion (right y–axis, black boxes) and product selectivities (left y–axis, stacked bar graph) are shown. Note, thermal decomposition of IPA favors dehydrogenation products.[11]

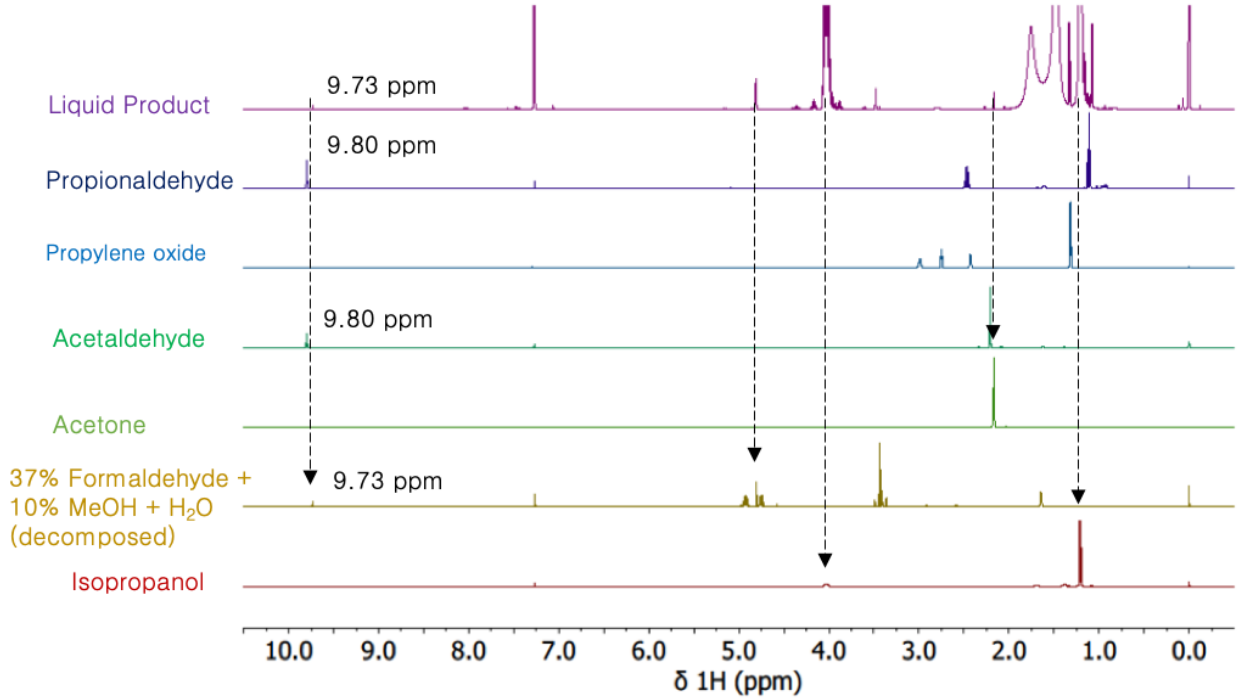

Figure C.2. Qualitative representation of ^{1}H NMR of condenser fluid (Liquid Product) post flow through reactions of isopropanol over spent BN. NMR spectra for oxygenate standards are subsequently plotted and dashed lines indicate overlap of protons environments. Feed was 5% O_2 / 4.7% IPA / bal. N_2., T = 350 ºC.

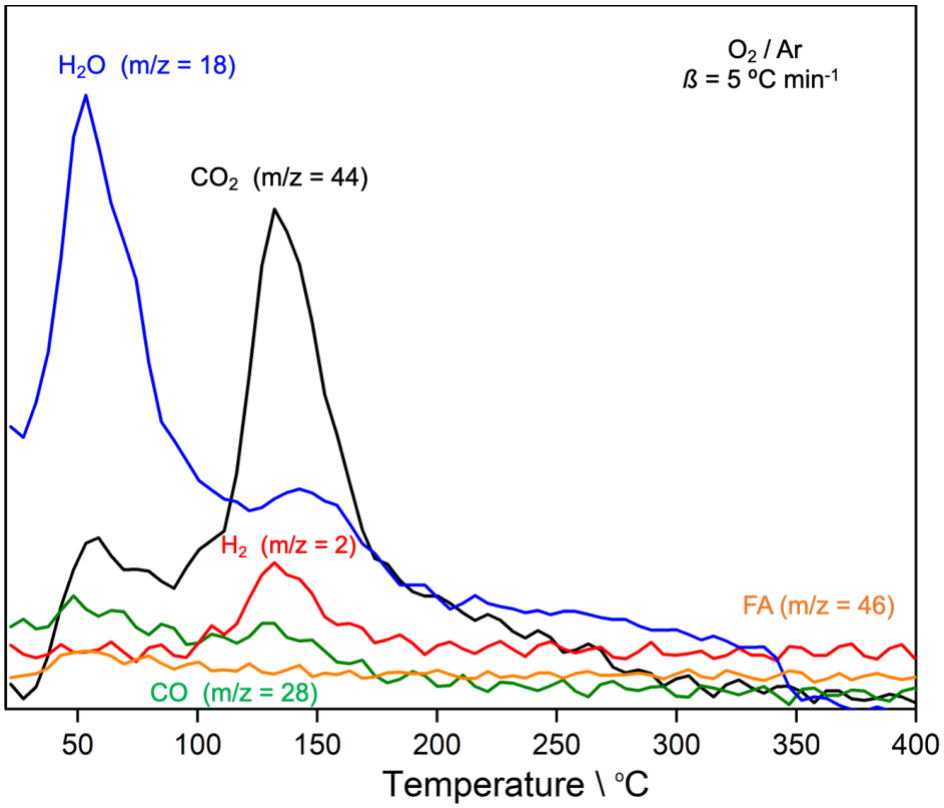

Figure C.3. MS signals for temperature programmed desorption of FA adsorbed on dehydrated spent BN. TPD was examined from 20 to 400ºC at 5ºC min^{-1} under oxidative conditions. 20% O_2 / Ar. No major changes were observed, but the TPD curve does shift to lower temperatures.

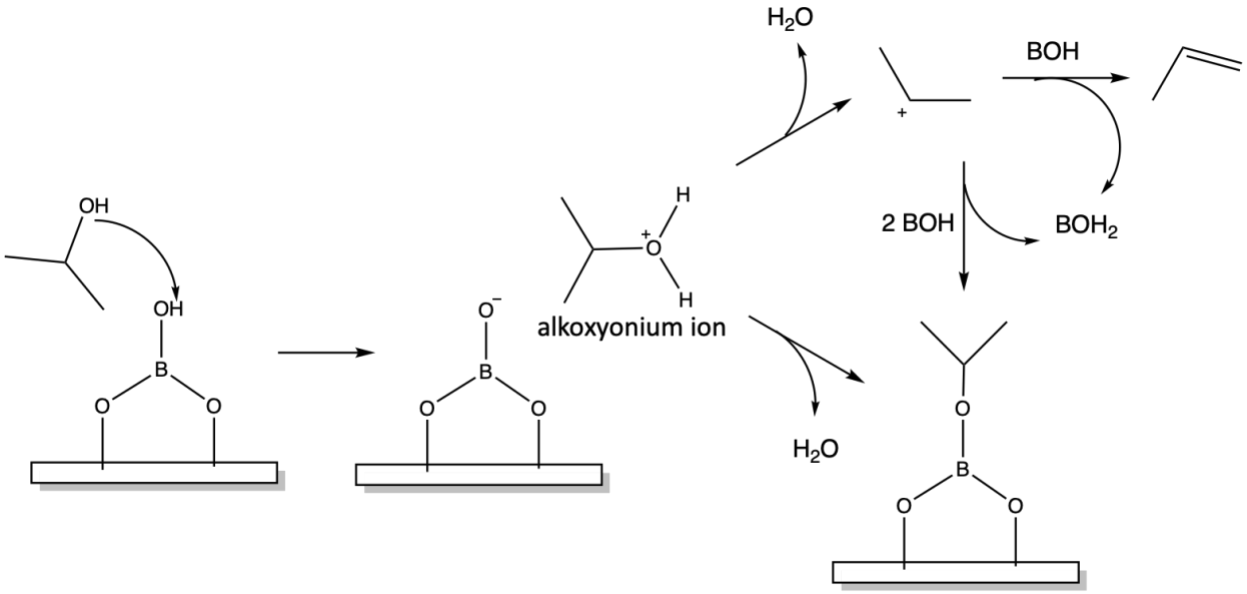

Scheme C.4. Hypothesized reaction pathways for IPA on BOH group where the relative acidities of both groups may drive the reaction via H-donation from BOH to IPA and pass the reaction mechanism through an alkoxyonium ion intermediate.

C.3 References

1. Baraton, M. I., Merle, T., Quintard, P. & Lorenzelli, V. Surface activity of a boron nitride powder: a vibrational study. *Langmuir* **9**, 1486–1491 (1993).
2. Love, A. M. *et al.* Synthesis and Characterization of Silica-Supported Boron Oxide Catalysts for the Oxidative Dehydrogenation of Propane. *J. Phys. Chem. C* **123**, 27000–27011 (2019).
3. Zhang, C. C., Gao, X. & Yilmaz, B. Development of FTIR Spectroscopy Methodology for Characterization of Boron Species in FCC Catalysts. *Catalysts* **10**, (2020).
4. Gautam, C., Yadav, A. K. & Singh, A. K. A Review on Infrared Spectroscopy of Borate Glasses with Effects of Different Additives. *ISRN Ceram.* **2012**, 428497 (2012).
5. Barakat, C., Gravejat, P., Guaitella, O., Thevenet, F. & Rousseau, A. Oxidation of isopropanol and acetone adsorbed on TiO2 under plasma generated ozone flow: Gas phase and adsorbed species monitoring. *Appl. Catal. B Environ.* **147**, 302–313 (2014).
6. Hussein, G. A. M. & Gates, B. C. Surface and Catalytic Properties of Yttrium Oxide: Evidence from Infrared Spectroscopy. *J. Catal.* **176**, 395–404 (1998).
7. Rossi, P. F., Busca, G., Lorenzelli, V., Saur, O. & Lavalley, J. C. Microcalorimetric and FT-IR spectroscopic study of the adsorption of isopropyl alcohol and hexafluoroisopropyl alcohol on titanium dioxide. *Langmuir* **3**, 52–58 (1987).
8. Bensitel, M., Moraver, V., Lamotte, J., Saur, O. & Lavalley, J.-C. Infrared study of alcohols adsorption on zirconium oxide: reactivity of alkoxy species towards CO2. *Spectrochim. Acta Part A Mol. Spectrosc.* **43**, 1487–1491 (1987).
9. Hussein, G. A. M., Sheppard, N., Zaki, M. I. & Fahim, R. B. Infrared spectroscopic studies of the reactions of alcohols over group IVB metal oxide catalysts. Part 1.—Propan-2-ol over TiO2, ZrO2 and HfO2. *J. Chem. Soc. Faraday Trans. 1 Phys. Chem. Condens. Phases* **85**, 1723–1741 (1989).
10. Vannice, M. A., Erley, W. & Ibach, H. A RAIRS and HREELS study of isopropyl alcohol on Pt(111). *Surf. Sci.* **254**, 12–20 (1991).
11. Kulkarni, D. & Wachs, I. E. Isopropanol oxidation by pure metal oxide catalysts: number of active surface sites and turnover frequencies. *Appl. Catal. A Gen.* **237**, 121–137 (2002).